Thermodynamics of Lithium Battery Materials

Hans J. Seifert
Elke Schuster, Maren Lepple, Damian Cupid, Peter Franke, Carlos Ziebert

Karlsruhe Institute of Technology (KIT)

Institute for Applied Materials – Applied Materials Physics (IAM-AWP)

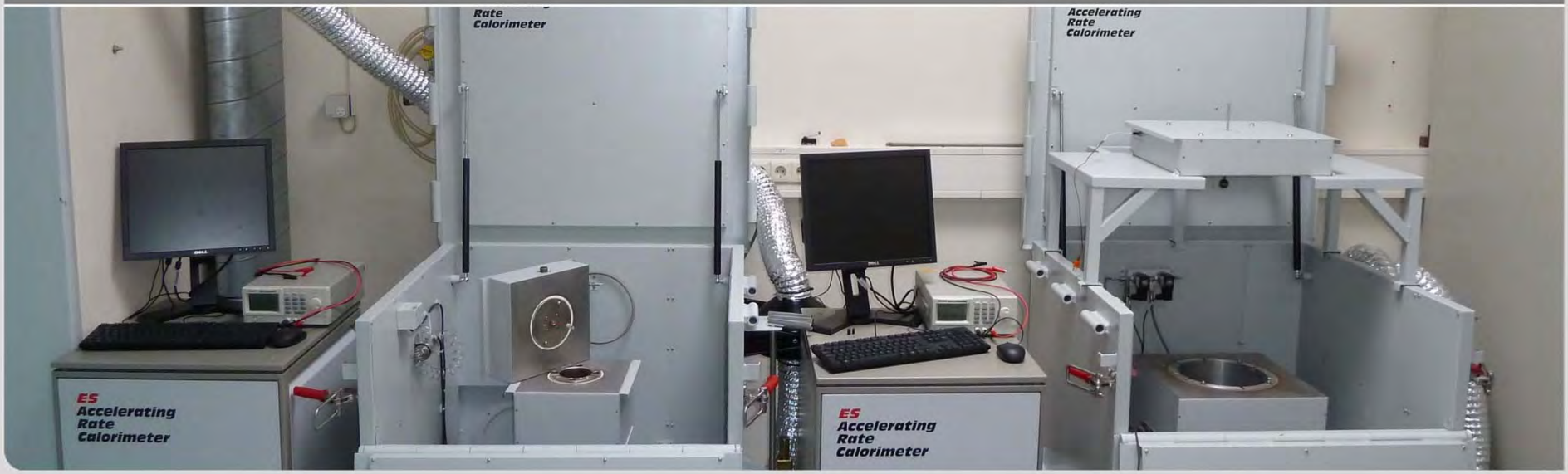

Thermodynamics of Lithium Battery Materials

- **Introduction**
- **Why battery thermodynamics and phase diagrams?**
  Calculation of voltages, …
- **Calorimetry of lithium ion batteries**
  Isothermal and adiabatic calorimetry
- **Li – Mn – O and Li – Fe – P – O materials systems**

Gunnar Eriksson Symposium 2012

Electric vehicles - some examples

Mini E
(L.A., NY, Berlin; BMW / Vattenfall)
Operating range 250 km

Smart electric drive
(London, Berlin; Daimler / RWE)
Operating range 135 km

Electric vehicles - some examples

i MiEV, Mitsubishi

Capacity of Battery: 16 kWh (200kg)
150 km operating range

Per single cell: Energy density 218 Wh/l and
Specific energy 109 Wh/kg; Specific power 550 W/kg
Total of 176 Cells in Battery System

Karlsruhe Institute of Technology

WeNDeLIB

SPP1473 DFG

IAM

Institute for Applied Materials

Energy stored in 100 kg of best commercial batteries good enough for just 100 km operating range

Batteries for Electric Vehicles have to be optimized to high energy density (kWh), save thermal behavior and cycle life

Energy density (Wh/l) and specific energy (Wh/kg) determine for a given operating range the volume and mass of battery

Battery technology spider chart (USABC) for electrical vehicles (EV)

Specific Power
Discharge: 300 W/kg

Operating temperature:
-40 to +50°C

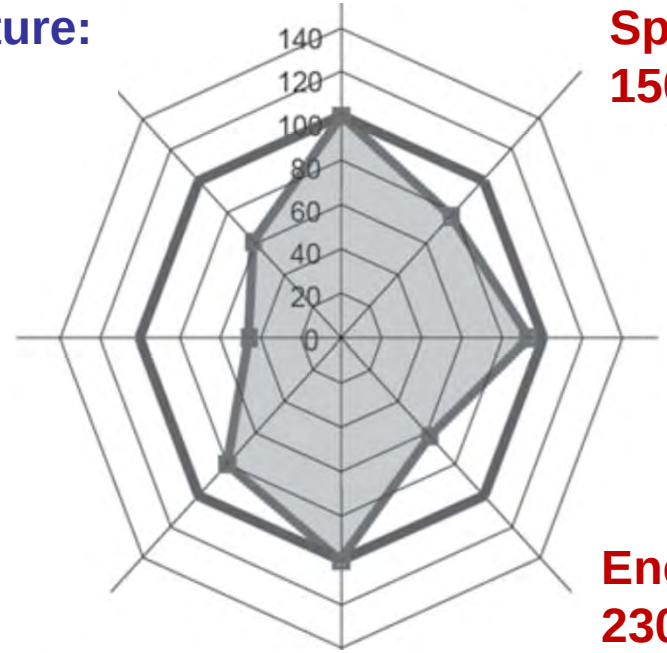

Specific Energy at C/3:
150 Wh/kg

Selling price at
10k/Jahr: 150$/kWh

Power density:
460 W/l

Calendar life:
10 years

Energy density at C/3:
230 Wh/l

Cycle life at
80% DOD: 1000 Cycles

Sources:
(1) D. Howell, Energy Storage Research and Development, Annual Progress Report 2006 (Washington, D.C.: Office of FreedomCAR and Vehicle Technologies, U.S. Department of Energy, 2007)
(2) FreedomCAR and Fuel Partnership and United States Advanced Battery Consortium (USABC), Electrochemical Energy Storage Technical Team Technology Development Roadmap (Southfield, MI: USCAR, 2006)

Why Battery Thermodynamics and Phase Diagrams?

Thermodynamics and phase diagrams govern battery performance

Thermal management of batteries (Heat dissipation and temperature distribution)

Battery safety (thermal runaway)

Structural changes in active materials

Surface energies (nano-micro)

Synthesis of complex ceramic materials

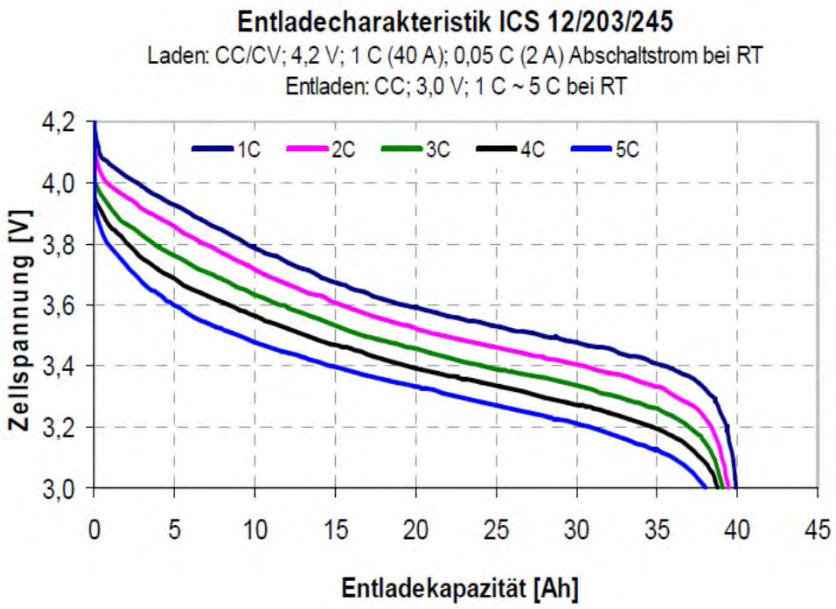

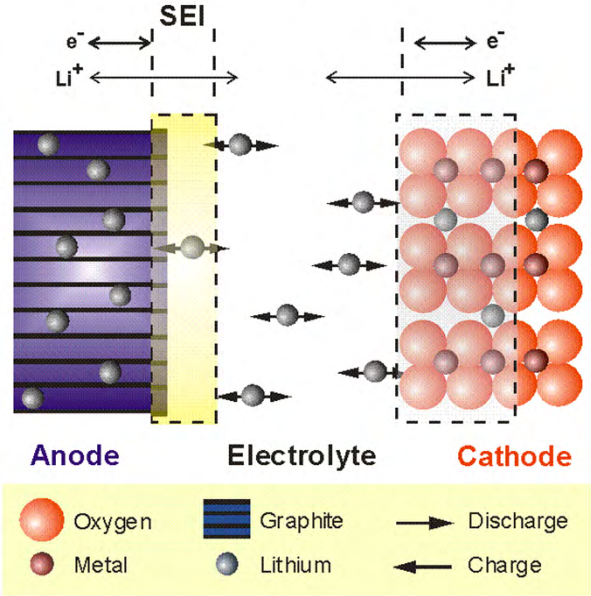

Lithium Ion Batteries – Operation

$$Li_xC_n \underset{C}{\overset{D}{\rightleftharpoons}} C_n + xLi^+ + xe^- \qquad Li_{1-x}MO_2 + xe^- + xLi^+ \underset{C}{\overset{D}{\rightleftharpoons}} LiMO_2$$

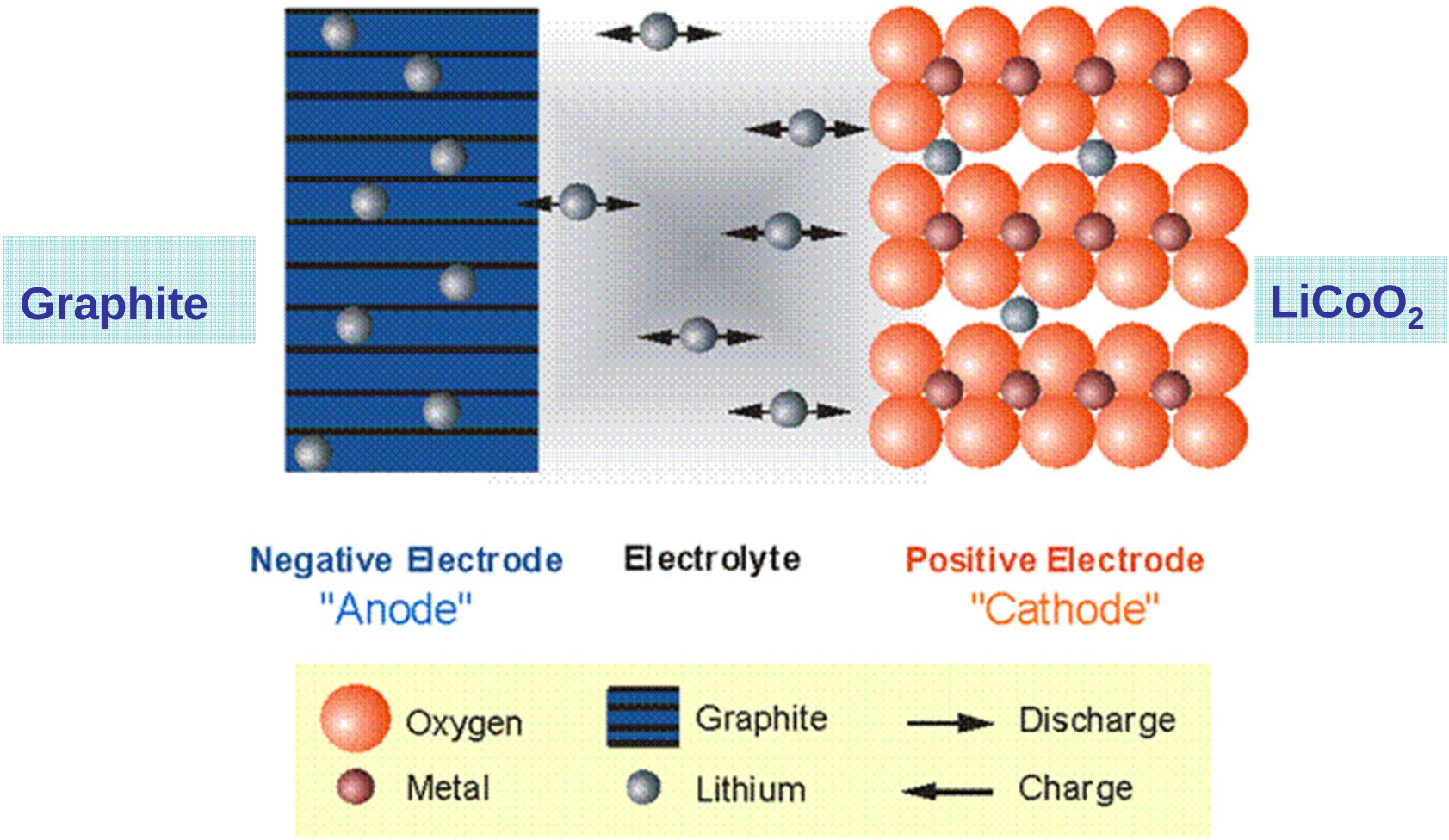

Presently: Anode: graphitic C; Electrolyte: $LiPF_6$ in organic carbonate solvents; Cathode: Co-based $LiMO_2$

Anode and Cathode Materials: State-of-the-Art

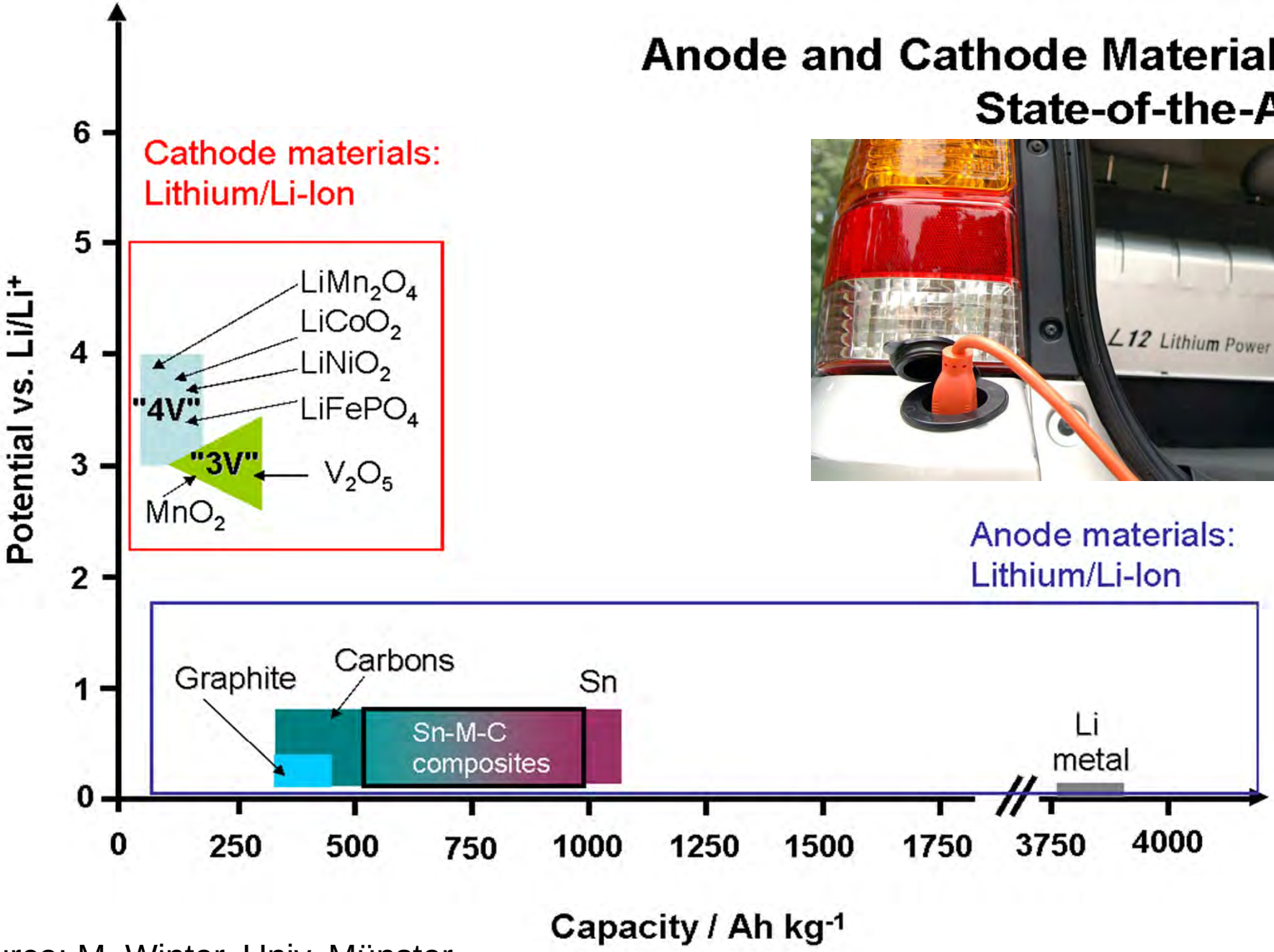

Source: M. Winter, Univ. Münster

German Research Foundation, Priority Programme 1473
Materials with New Design for Improved Lithium Ion Batteries - WeNDeLIB

DFG Schwerpunktprogramm 1473, Kick-Off-Treffen,
Werkstoffe mit neuem Design für verbesserteLithium-Ionen-Batterien - WeNDeLIB

Started in October 2010

Program Commission:

Hans Jürgen Seifert	Karlsruher Institut für Technologie (Chair)
Rainer Schmid-Fetzer	Technische Universität Clausthal (Co-Chair)
Martin Winter	Universität Münster (Co-Chair)
Nicola Hüsing	Universität Salzburg
Andreas Gutsch	Li-Tec, Kamenz, now with KIT
Bengt Hallstedt	RWTH Aachen
Ingo Steinbach	ICAMS, Bochum

International Member:

Alexandra Navrotsky	University of California, Davis

13 joint projects (36 projects in total) + coordinator project

German Research Foundation, Priority Programme 1473
Materials with New Design for Improved Lithium Ion Batteries - WeNDeLIB

Vision of this priority program:

Coupling of materials thermodynamics and kinetics and modelling of materials design for innovative lithium ion batteries

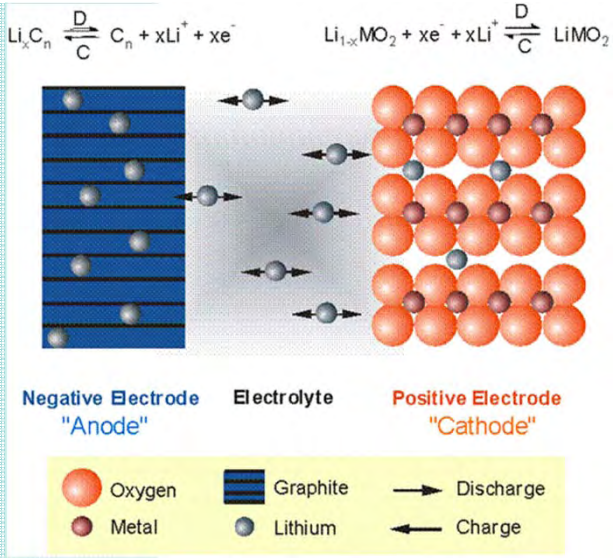

Ideal case:

Complete design of battery before the experimental work or processing starts in the lab or in industrial operation

Still a long way to go - We introduce a new *interdisciplinary* concept for LiB (no international program to be compared with this approach)

- Scientific Focus -

Interdisciplinary Work – Correlation of:

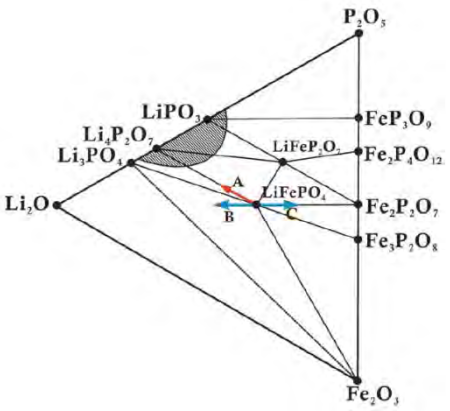

Materials
- Thermodynamics,
- Constitution,
- Kinetics

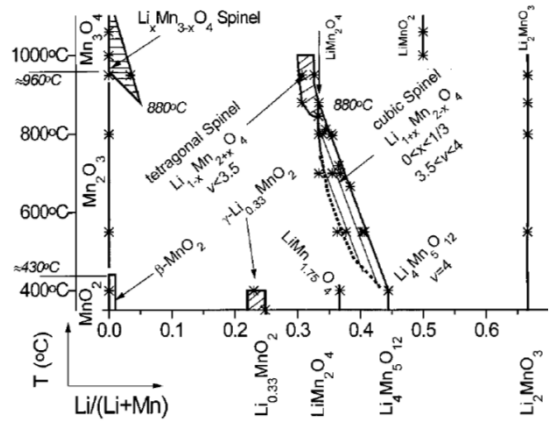

Crystal chemistry,
Microstructure,
Innovative Materials
Synthesis

Electrochemical performance and safety of cells / batteries

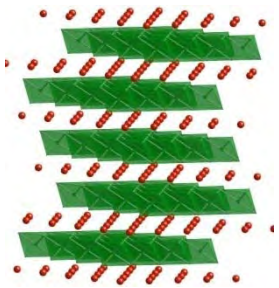

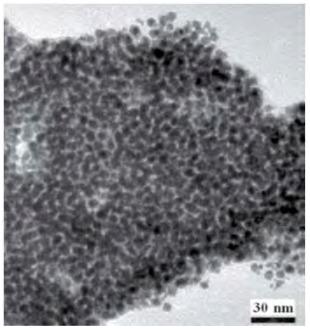

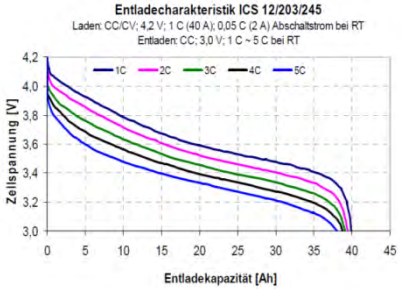

Approach by electrochemical cell reaction equations

Write reaction as

$$x\,A + A_y\,R = A_{y+x}\,R$$

ΔG_r° = Gibbs free energy change due to the reaction

$$= \Sigma \Delta G_f^\circ(\text{products}) - \Sigma \Delta G_f^\circ(\text{reactants})$$

This can be related to the cell voltage

$$\Delta G_r^\circ = -\,z\,q\,E$$

z = charge number carried by ions in electrolyte
q = elementary charge per particle
E = externally measurable cell voltage

Approach by electrochemical cell reaction equations

If ΔG_r° has units of energy/mol, then

$$\Delta G_r^\circ = -z F E$$

F = charge per mol = 96,500 Coulombs/mol

Approach by phase diagrams

Coulometric Titration of Li Into Al at 400°C

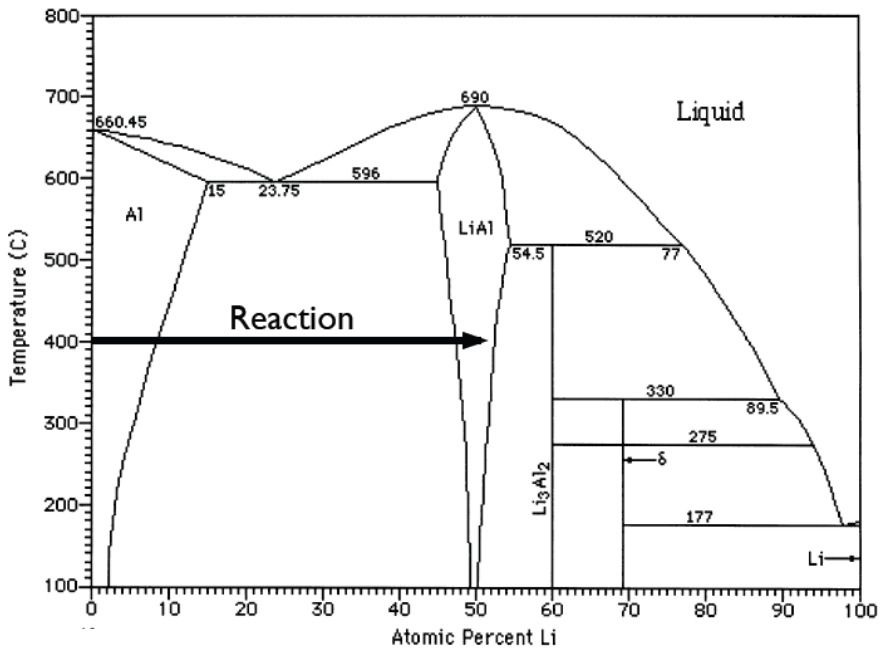

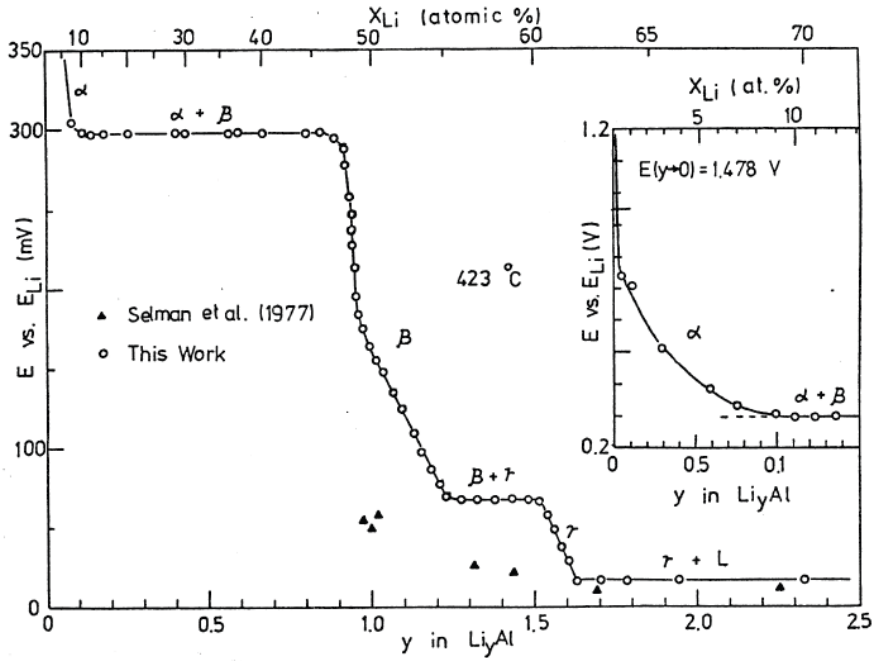

Al **Li**

y in Li_yAl

Measured Using LiCl-KCl as a Molten Salt Electrolyte

C.J. Wen, B.A. Boukamp, R.A. Huggins, W. Weppner, J. Electrochem. Soc. 126, 2258 (1979)

Electrochemical conversion mechanism

$$M^{n+}X_m + n \cdot e^- + n \cdot Li^+ \longleftrightarrow M^0 + n \cdot Li^+ X_{m/n}$$

X = O, N, F, S, P

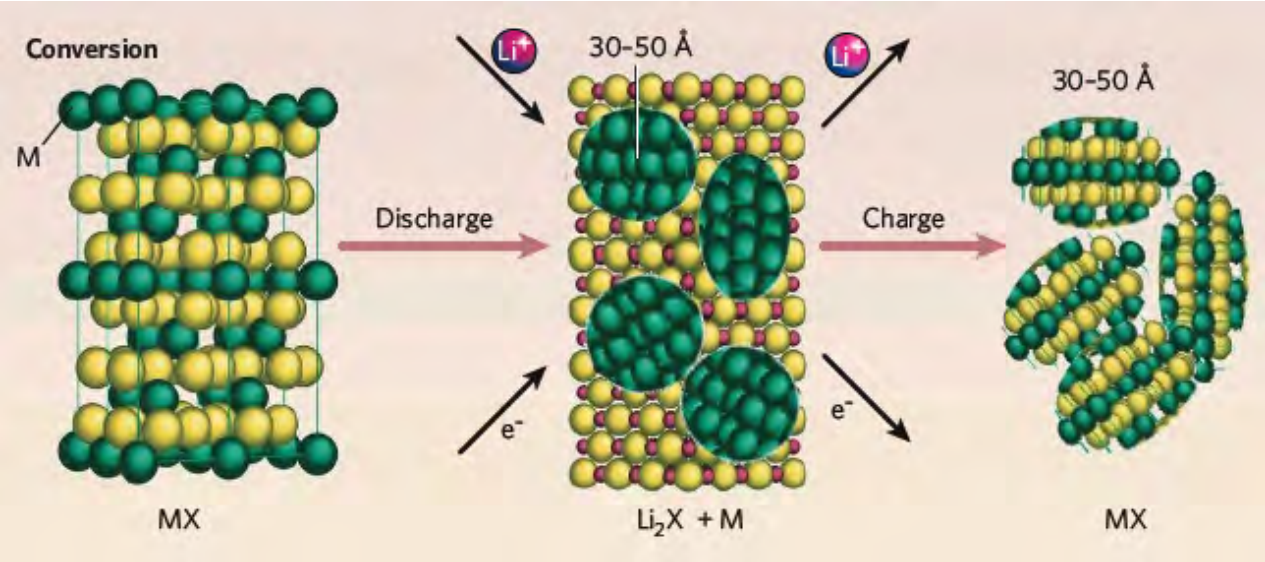

M. Armand et al., Nature, 2008, 451:652-657

$$CuO + 2 \cdot e^- + 2 \cdot Li^+ \longleftrightarrow Cu^0 + Li_2O$$

- Cu-Fe-O electrodes for LIB exhibit
  - Fe-oxides: high theoretical capacity
  - Cu-oxides: cycling stability

Calculated Li-Cu-O system (CALPHAD result); isothermal section

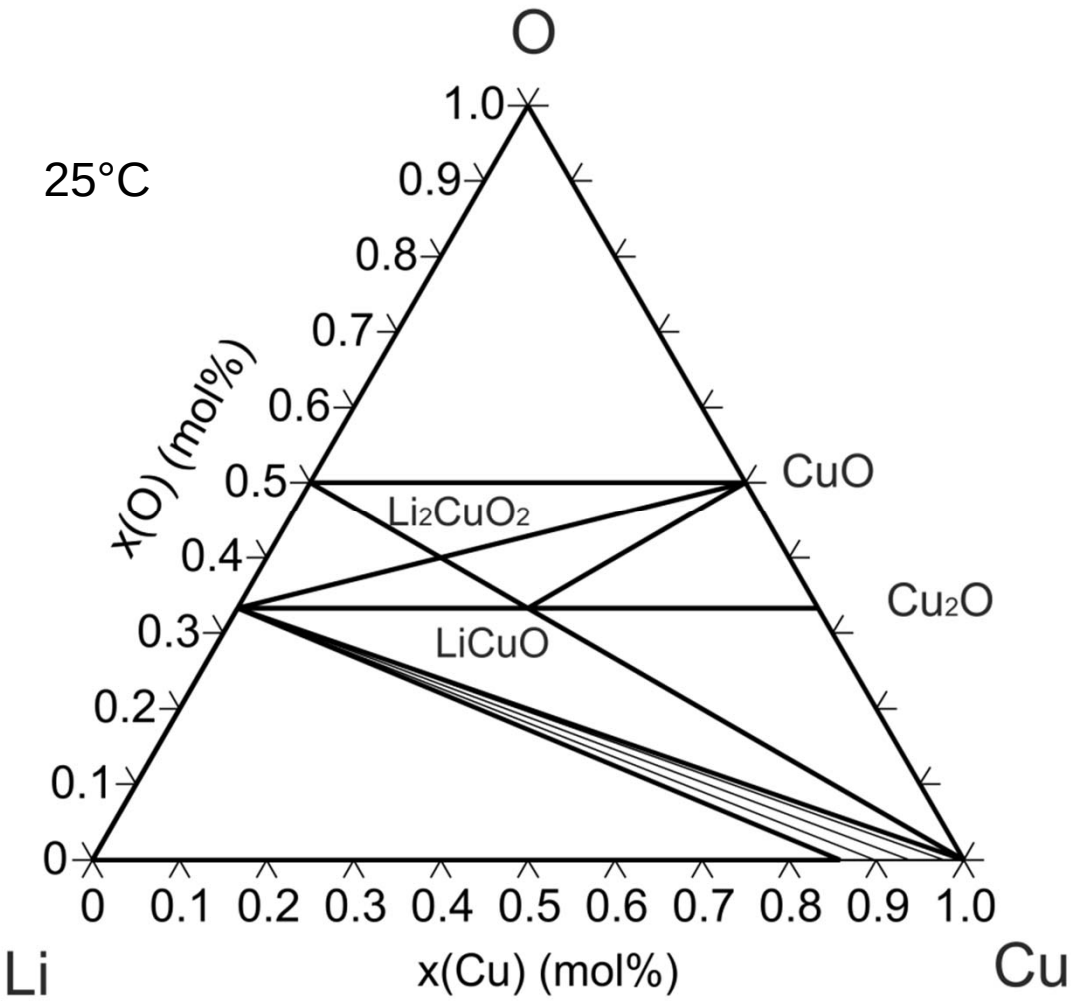

Calculated Li-Cu-O System, equilibrium voltages

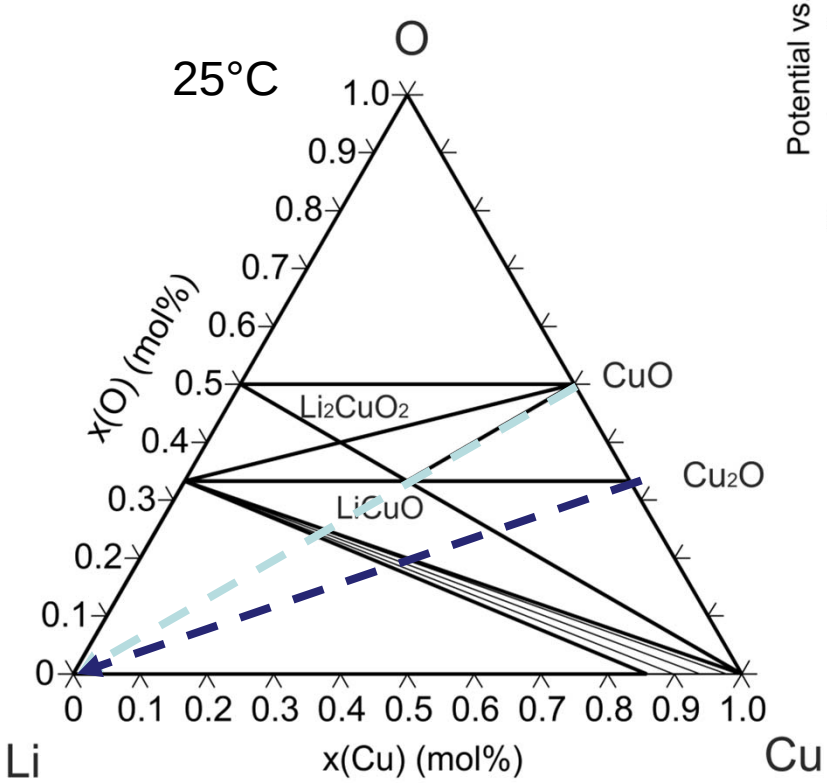

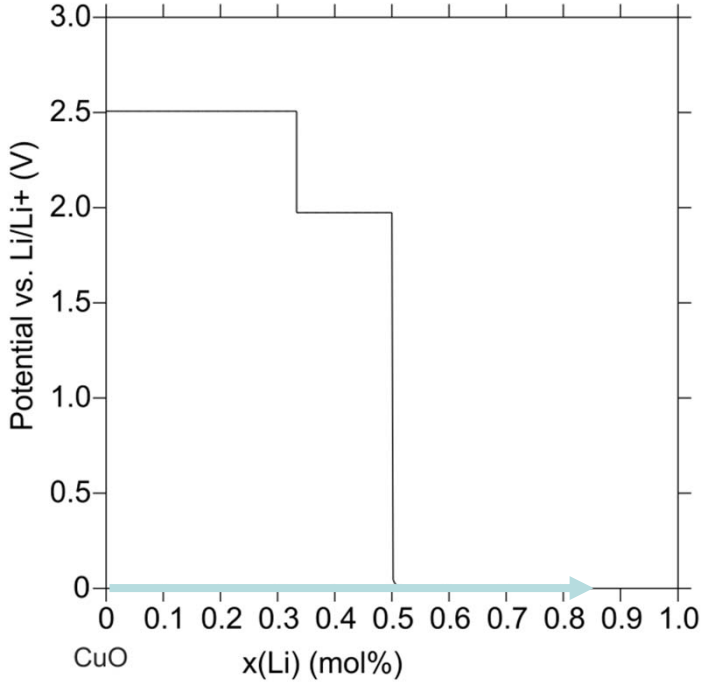

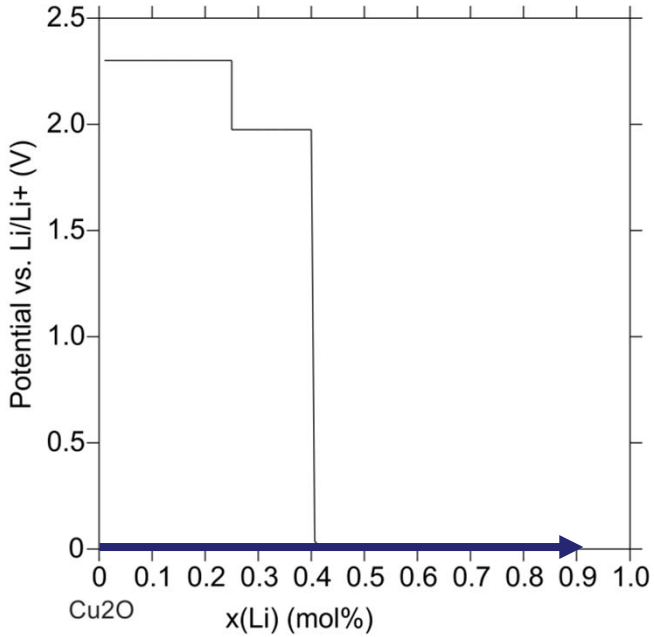

More relationships Thermodynamics - Phase Diagrams - Electrochemistry

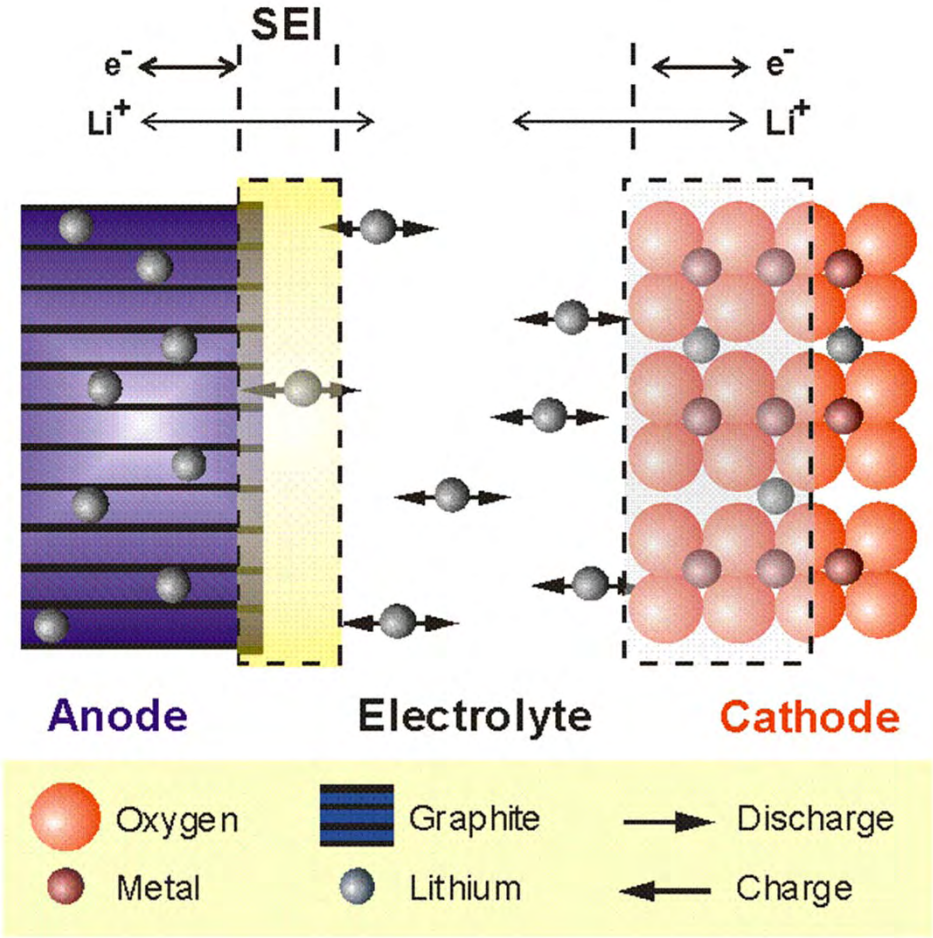

$$Li_x AN + CA \xrightarrow{\text{discharge}} AN + Li_x CA$$

More relationships Thermodynamics - Phase Diagrams - Electrochemistry

Full lithium ion cell discharge reaction

$$Li_x AN + CA \xrightarrow{\text{discharge}} AN + Li_x CA$$

Free energy of the full reaction is:

$$\Delta G(x,T) = -n \cdot F \cdot E_0(x,T)$$

Free energy of the full reaction can be written:

$$\Delta G(x,T) = -\Delta H(x,T) - T\Delta S(x,T)$$

Neglecting T-dependence:

$$\Delta G_0(x,T) = -\Delta H(x) - T\Delta S(x)$$

Combining equations:

$$\Delta S(x) = F\left(\left.\frac{\partial E_0(x,T)}{\partial T}\right|_x\right) \quad \Delta H(x) = F\left(-E_0(x,T) + T\left.\frac{\partial E_0(x,T)}{\partial T}\right|_x\right)$$

$E_0(x,T)$	**Open circuit voltage**
n	**Charge number (n=1 for Li^+)**
F	**Faraday constant**
ΔH, ΔS	**Heat and entropy of reaction**
$\left.\frac{\partial E_0(x,T)}{\partial T}\right\|_x$	**Temperature slope of $E_0(x,T)$**

In-situ technique “entropymetry” and phase diagrams

OCV
for one specific temperature

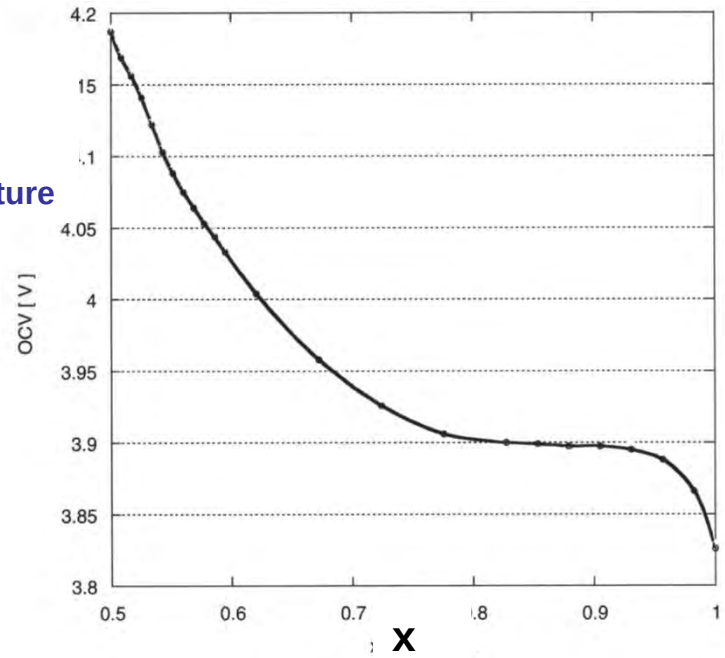

Open circuit voltage of Li_xCoO_2

ΔS

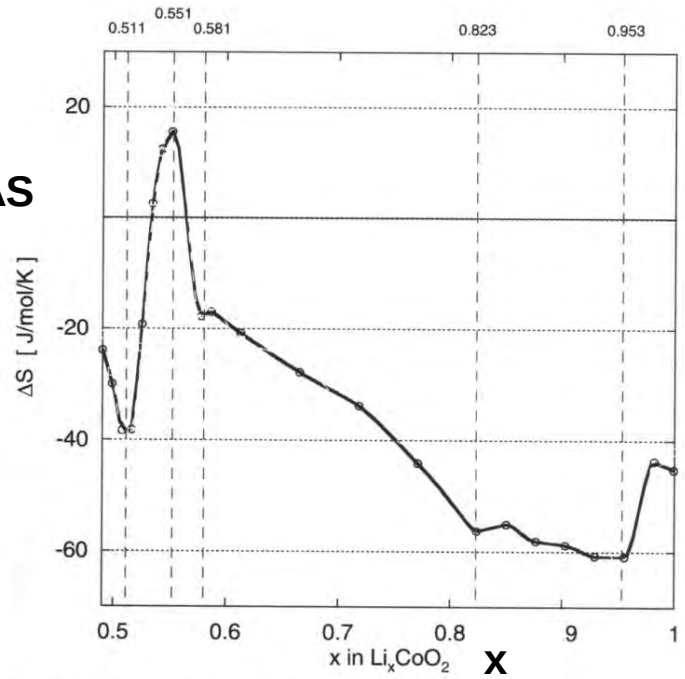

Entropy of Li intercalation in Li_xCoO_2

Note: Half cells measured

$$\overline{\Delta S}\Big|_0^1 = F\left(\int_0^1 \frac{\partial E_0(y,T)}{\partial T}\Big|_y dy\right)$$

Li_xCoO_2 Phase diagram

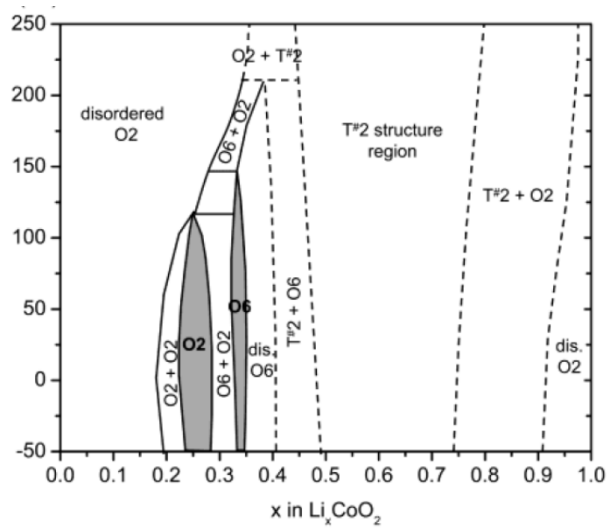

Yazami et al. in Lithium Ion Rechargeable Batteries, WILEY-VCH (2010)

Reversible and irreversible heat during cell reaction

$$Q_r = T\Delta S \frac{I}{nF}$$

Reversible heat generation

with

$$\Delta S(x) = F\left(\left. \frac{\partial E_0(x,T)}{\partial T} \right|_x \right)$$

$$Q_{irr} = -I^2 R_i$$

Irreversible heat generation

$$Q = Q_r + Q_{irr}$$

Total heat generation

+ side reactions

40Ah pouch cell

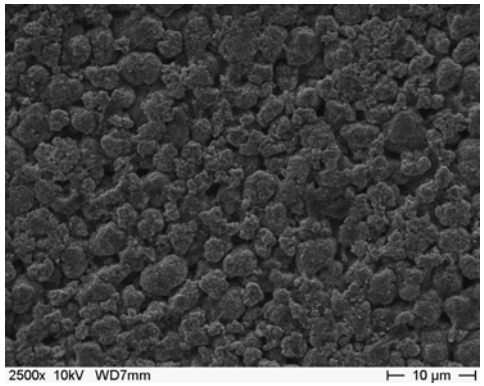

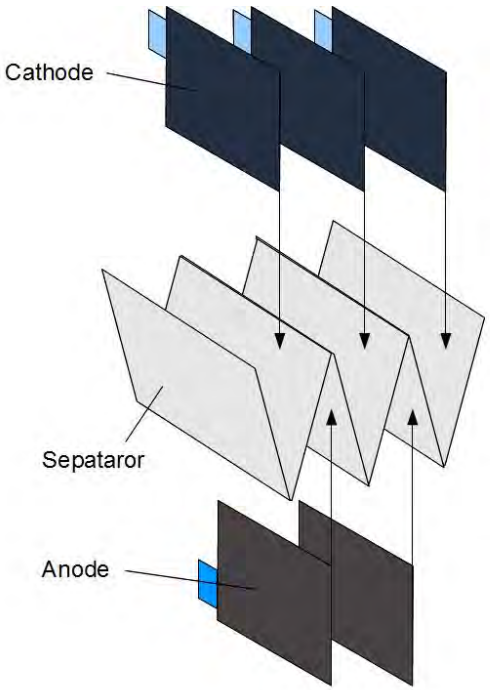

Cathode material:
$Li(Ni_{1/3}Mn_{1/3}Co_{1/3})O_2$
→ NMC

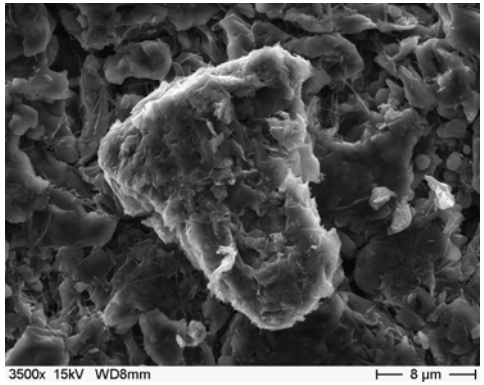

Anode material:
→ graphite

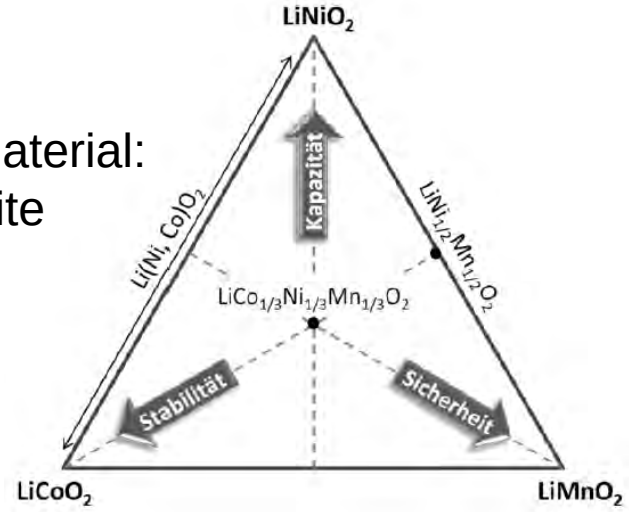

B. Ketterer, U. Karl, D. Möst, S. Ulrich, Wissenschaftliche Berichte FZKA 7503 (2009)

40Ah cell with eight thermocouples measured in Accelerating Rate Calorimeter (ARC)

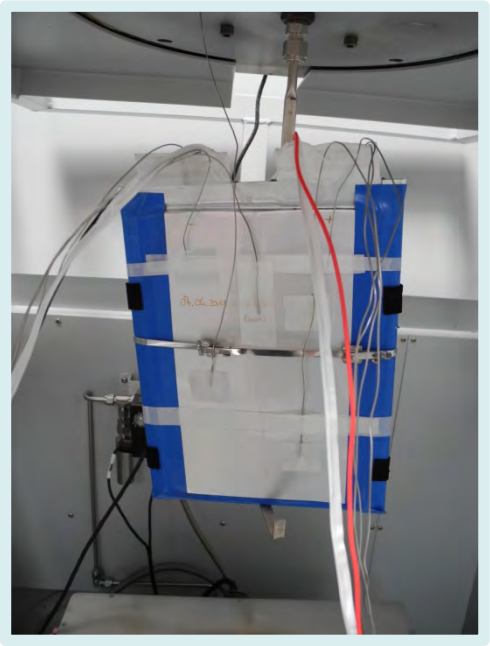

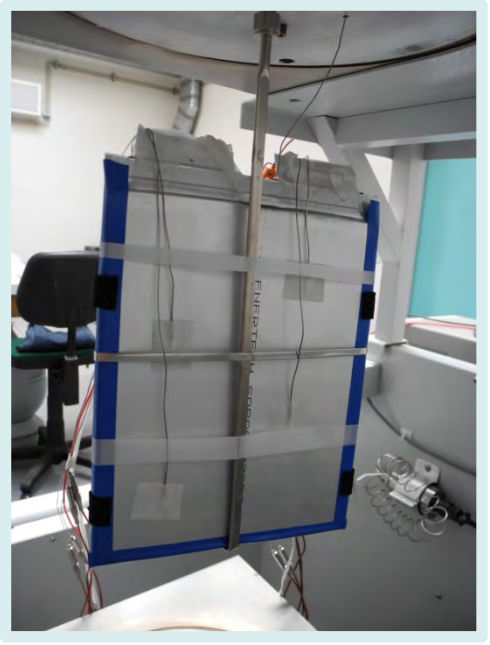

Isothermal cycling of a 40Ah pouch cell

Discharge parameter:

- method: constant current (CC)
- U_{min} = 3,0V
- I = 5A → C/8-rate

Charge parameter:

- method: constant current, constant voltage (CCCV)
- U_{max} = 4,1V
- I = 5A → C/8-rate
- I_{min} = 0.5A

at room temperature

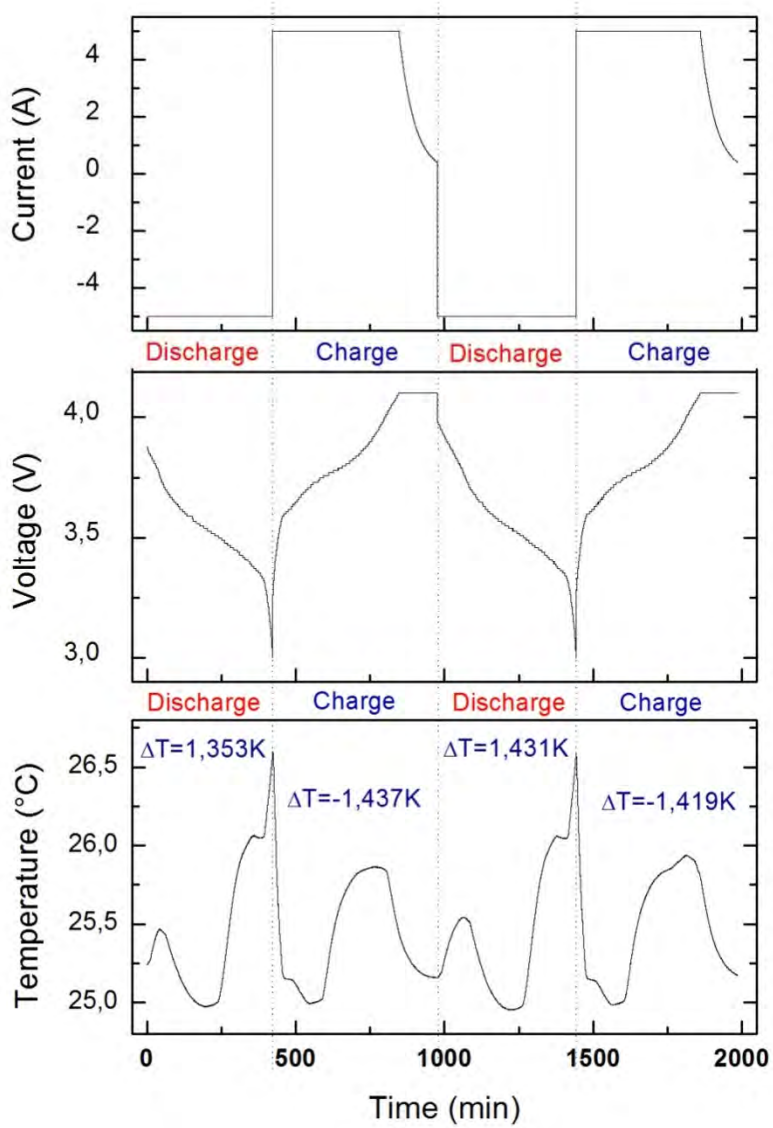

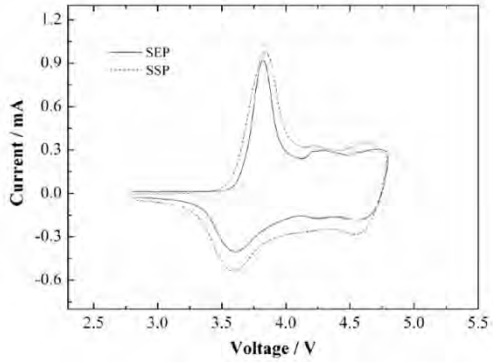

temperature coefficient

$$\left(\frac{\delta E}{\delta T}\right) < 0$$

Procedure like in:

H.-B. Ren, et. al., Int. J. Electrochem. Sci. 6, p. 727 – 738 (2011)

A.K. Shukla, T.P. Kumar, Current Sci. 94, p. 314-331 (2008)

Temperature measurements on a 40Ah pouch cell

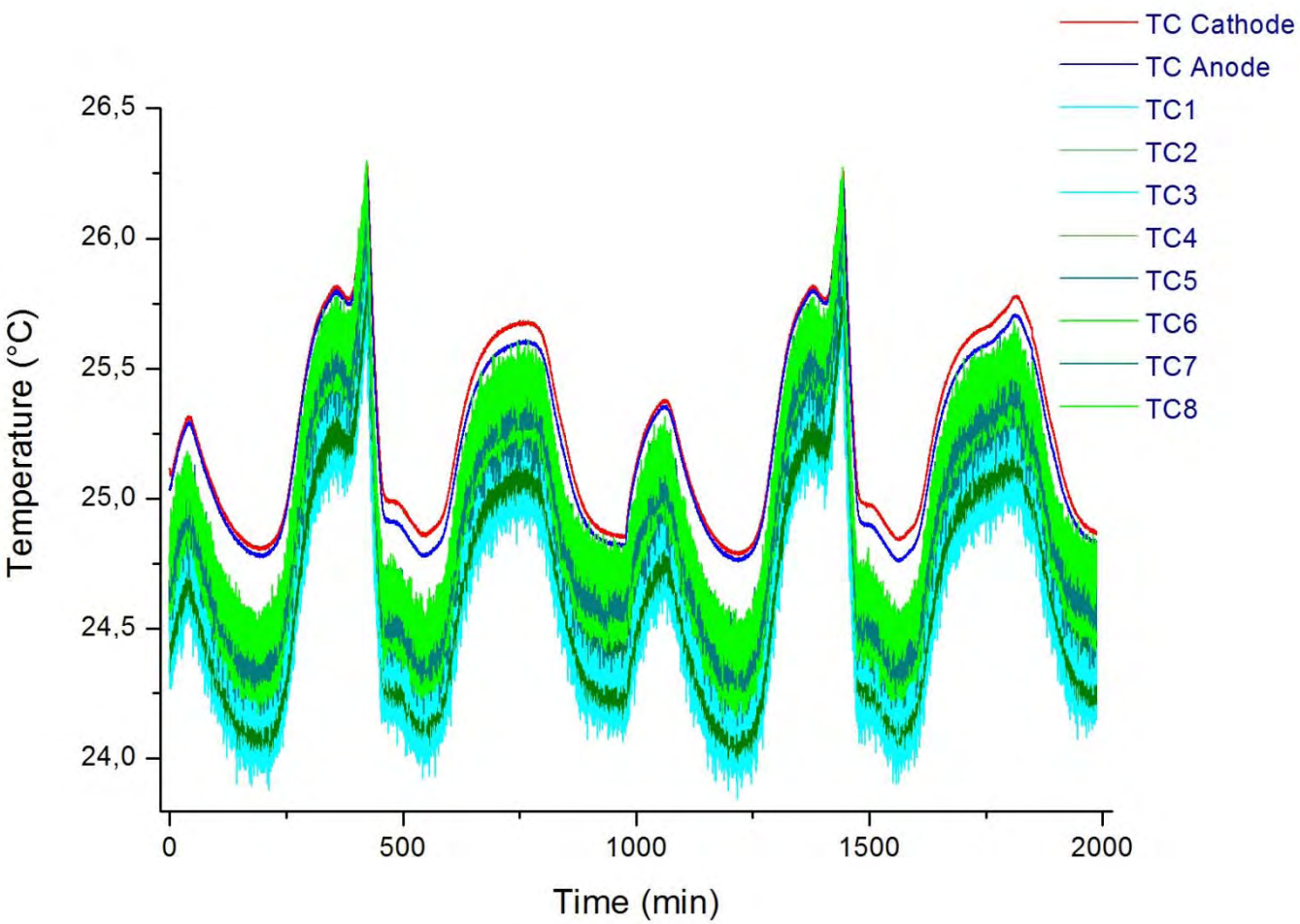

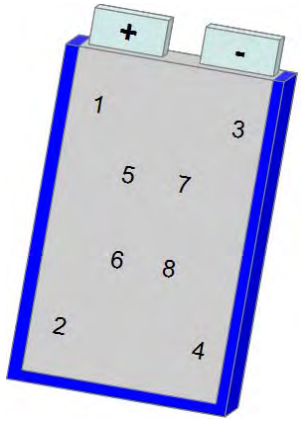

Adiabatic cycling of a 40Ah pouch cell

Discharge parameter:

- method: constant current (CC)
- U_{min} = 3,0V
- I = 5A → C/8-rate

Charge parameter:

- method: constant current, constant voltage (CCCV)
- U_{max} = 4,1V
- I = 5A → C/8-rate
- I_{min} = 0.5A

at room temperature

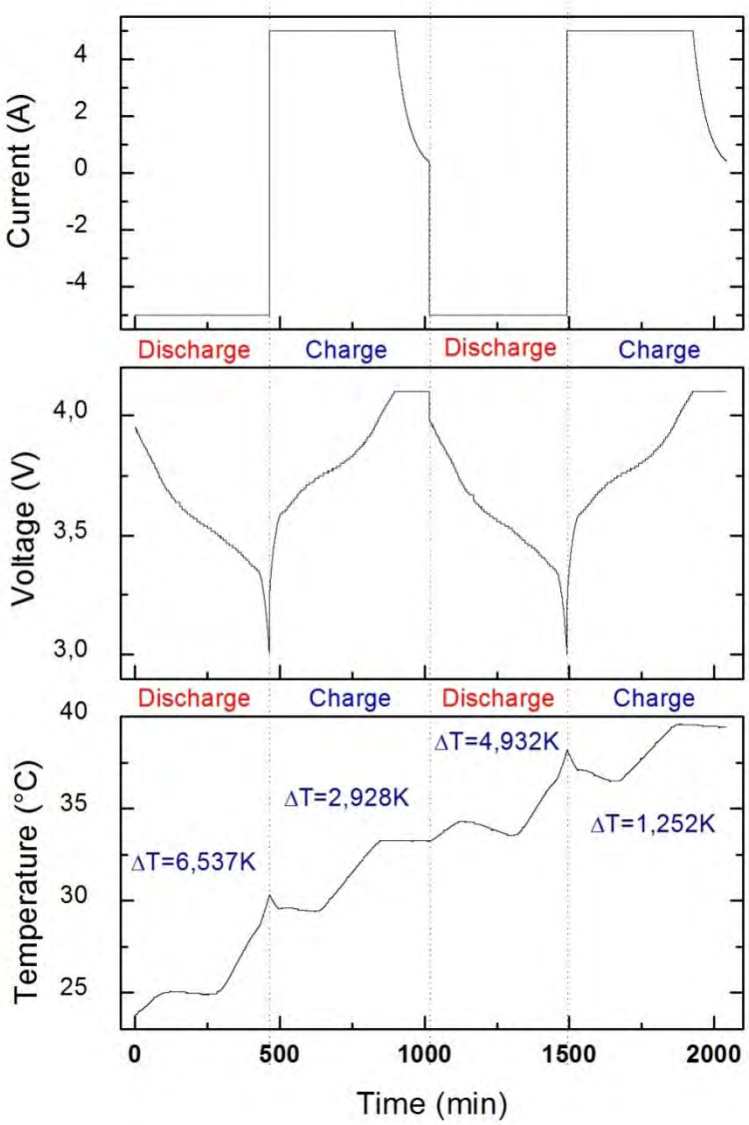

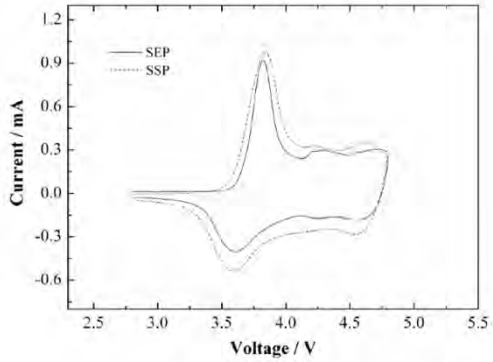

temperature coefficient

$$\left(\frac{\delta E}{\delta T}\right) < 0$$

Procedure like in:

H.-B. Ren, et. al., Int. J. Electrochem. Sci. 6, p. 727 – 738 (2011)

A.K. Shukla, T.P. Kumar, Current Sci. 94, p. 314-331 (2008)

Temperature measurements on a 40Ah pouch cell

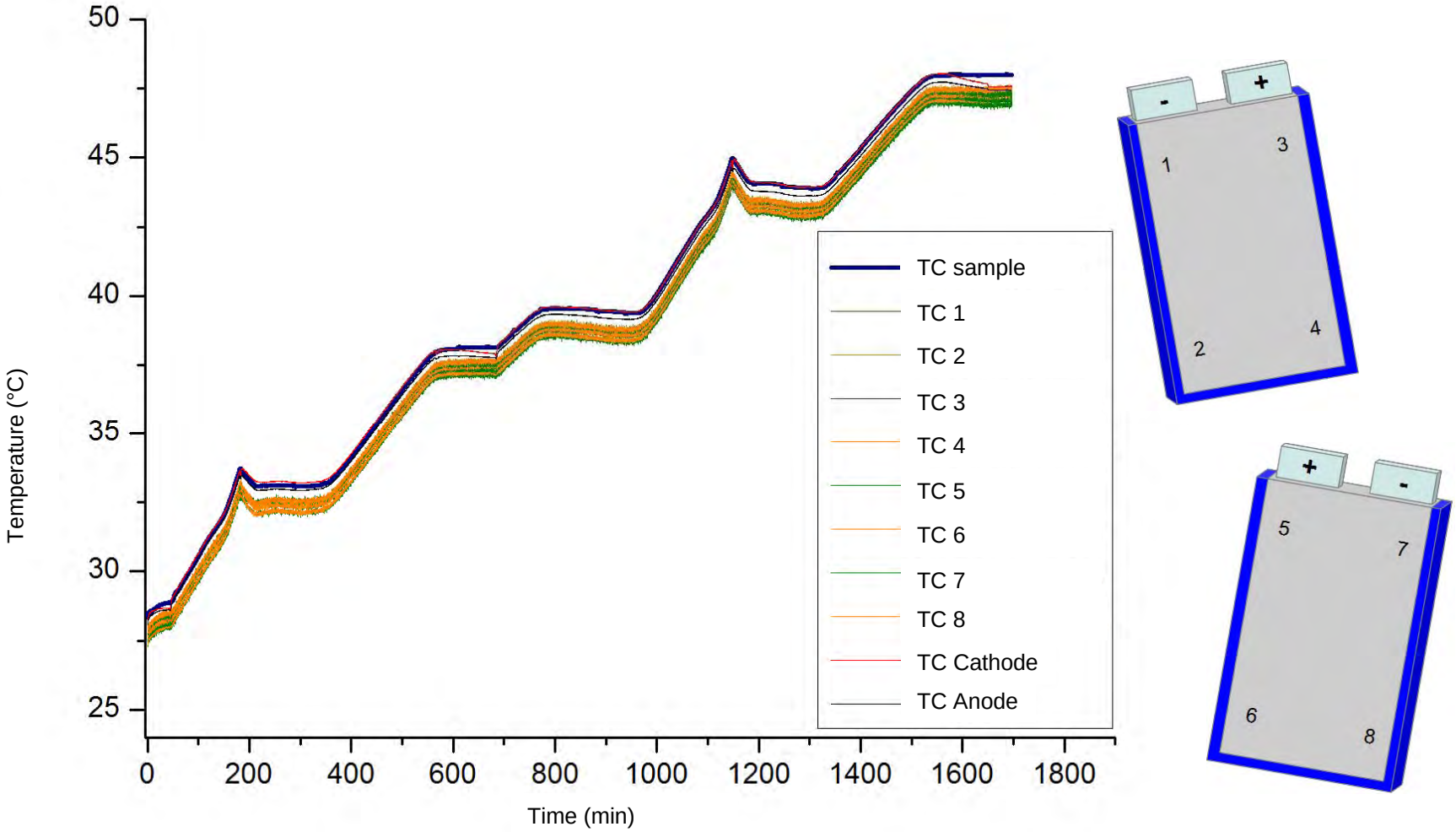

Li-Mn-O System

Thermodynamically stable phases in the Li-Mn-O system.

Stoichiometric	$LiMn_2O_4$ (c)
Cation-mixed	$Li_{1+x}Mn_{2-x}O_4$ (c); $0 < x \leq 1/3$
	$Li_4Mn_5O_{12}$
Mn-rich	$Li_{1-x}Mn_{2+x}O_4$ (t); $0 < x < \sim 0.1$
Mn-deficient	$Li_1Mn_{2-x}O_4$ (c); $x = 1/4$

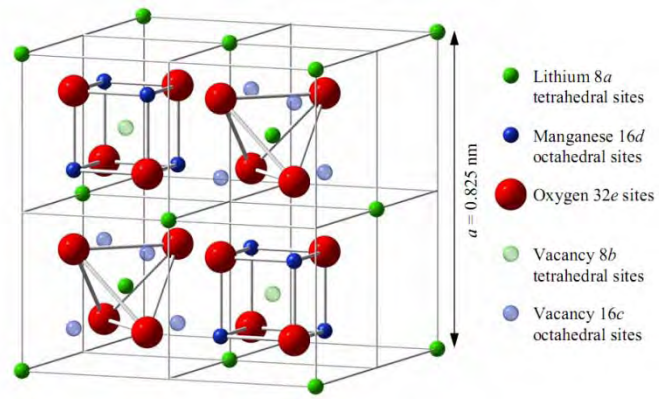

Thermodynamically unstable phases in the Li-Mn-O system.

De-lithiated	$Li_{1-y}Mn_2O_4$
Lithiated	$Li_2Mn_2O_4$ (t)
Oxygen-deficient	$Li_{1+x}Mn_{2-x}O_{4-\delta}$; $\delta >> 0$
Mn-deficient	$LiMn_{2-x}O_4$ (c); $0 < x < 1/4$
Oxygen-rich	$Li_2Mn_4O_9$ (c)
Cation-deficient	$Li_{1-x}Mn_{2-y}O_4$ (c)

Li-Mn-O System

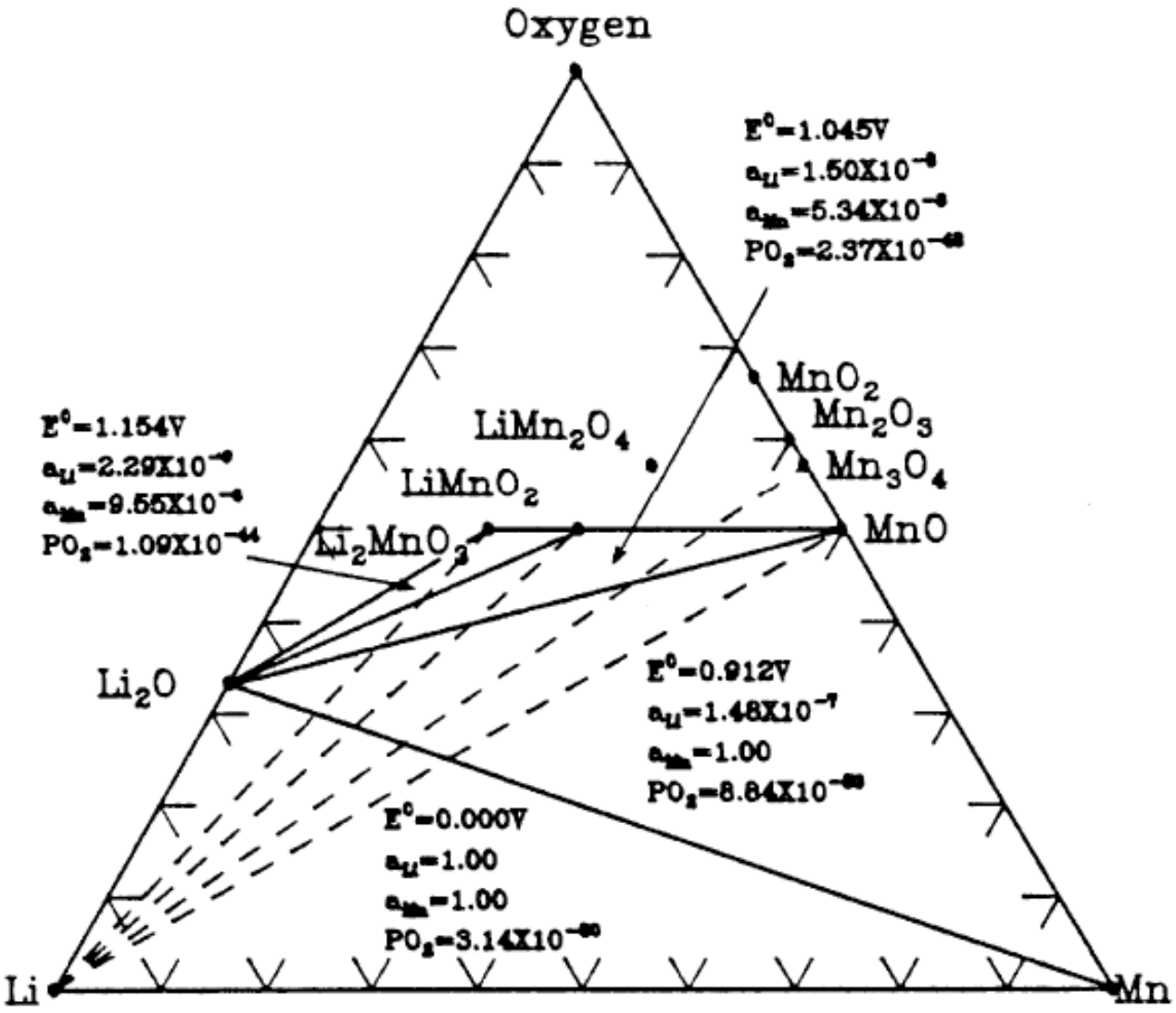

R. Huggins, Advanced Batteries, Springer 2011

Li-Mn-O System

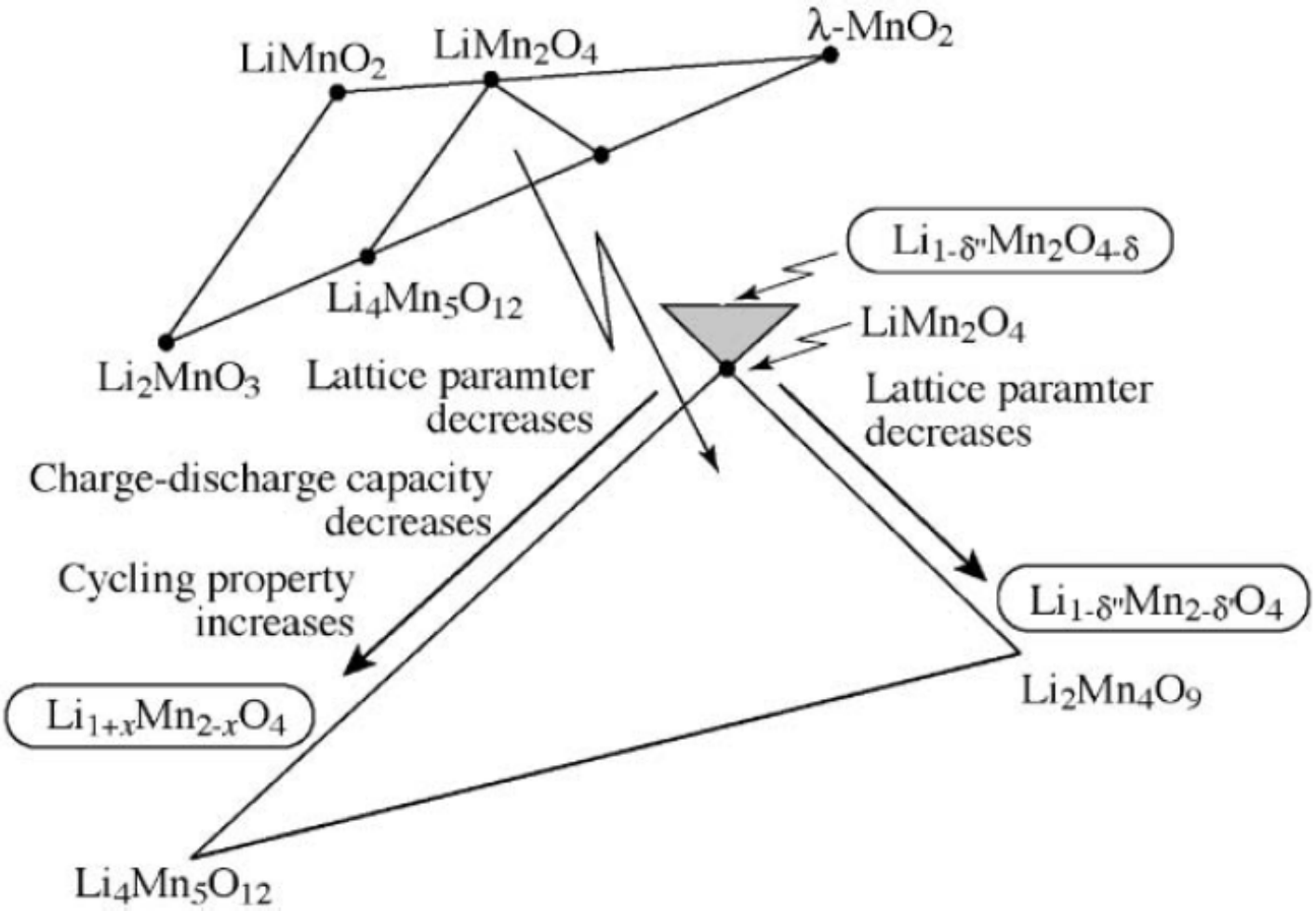

Phase relationships in the system $LiMnO_2$ – Li_2MnO_3 - λ-MnO_2 and subsystem $LiMn_2O_4$ - $Li_4Mn_5O_{12}$ – $Li_2Mn_4O_9$ (Yonemura et al. 2004).

Li-Mn-O System

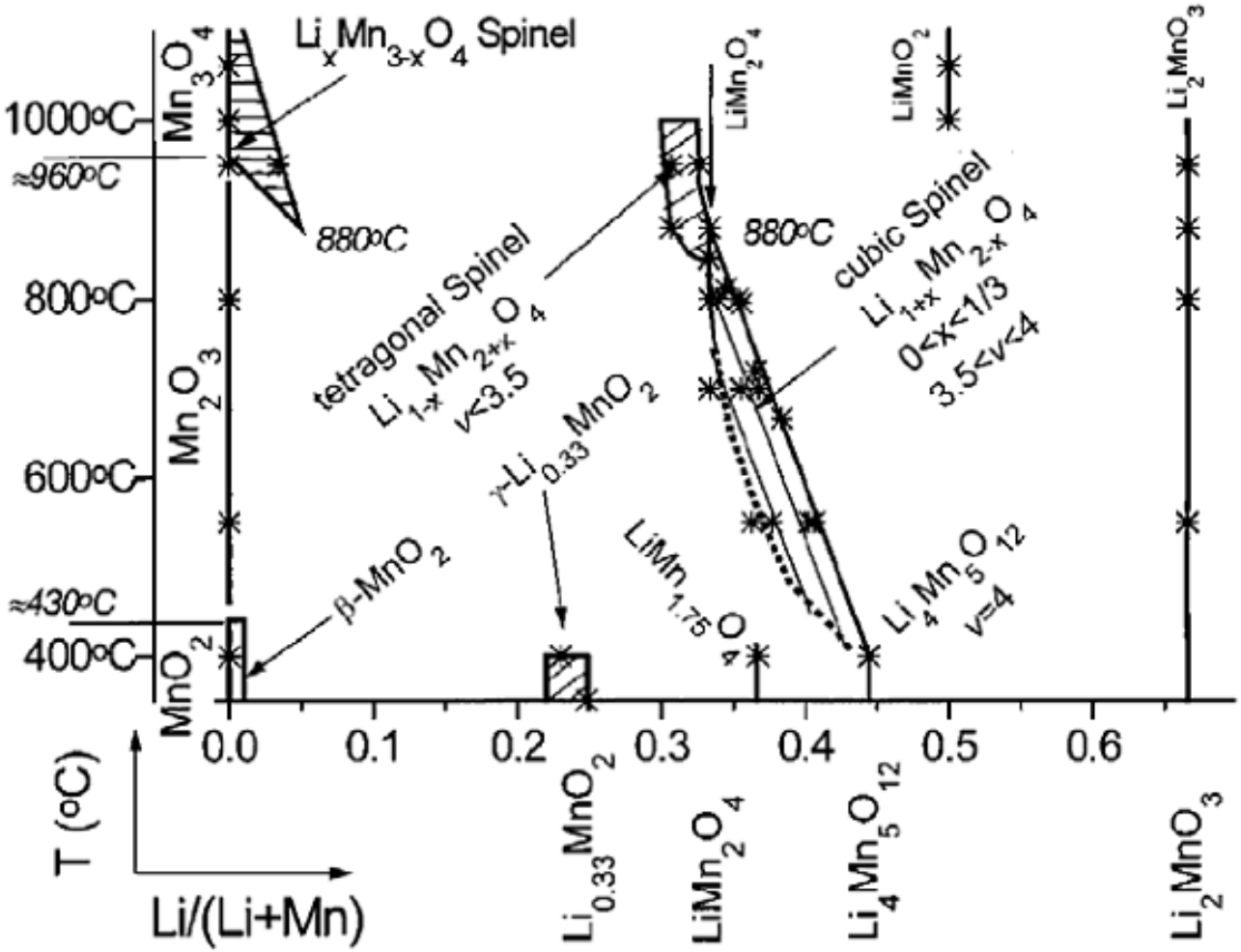

[1999 Pau]

- Samples prepared using the solid state method
- Phase diagram investigated at pO_2=0.21 atm

[1999 Pau] *Chem. Mater.*, 11 (1999), 3065-3079.

Li-Mn-O System

$p(O_2)$=0.21 atm

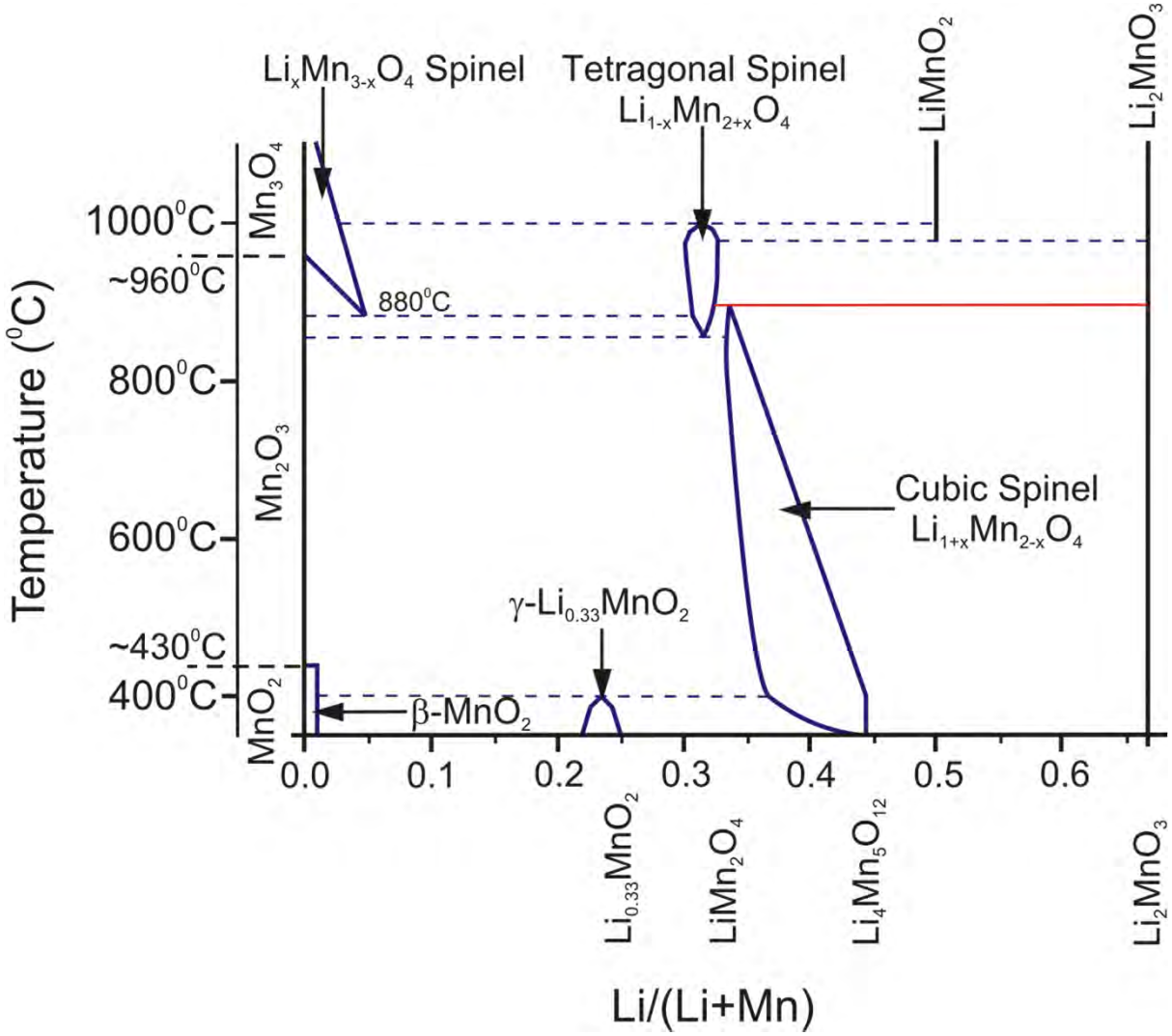

$$LiMn_2O_4 \leftrightarrow zLi_2MnO_3 + Li_{1-2z}Mn_{2-z}O_{4-3z-y}(tet) + (y/2)O_2$$

Li-Mn-O System

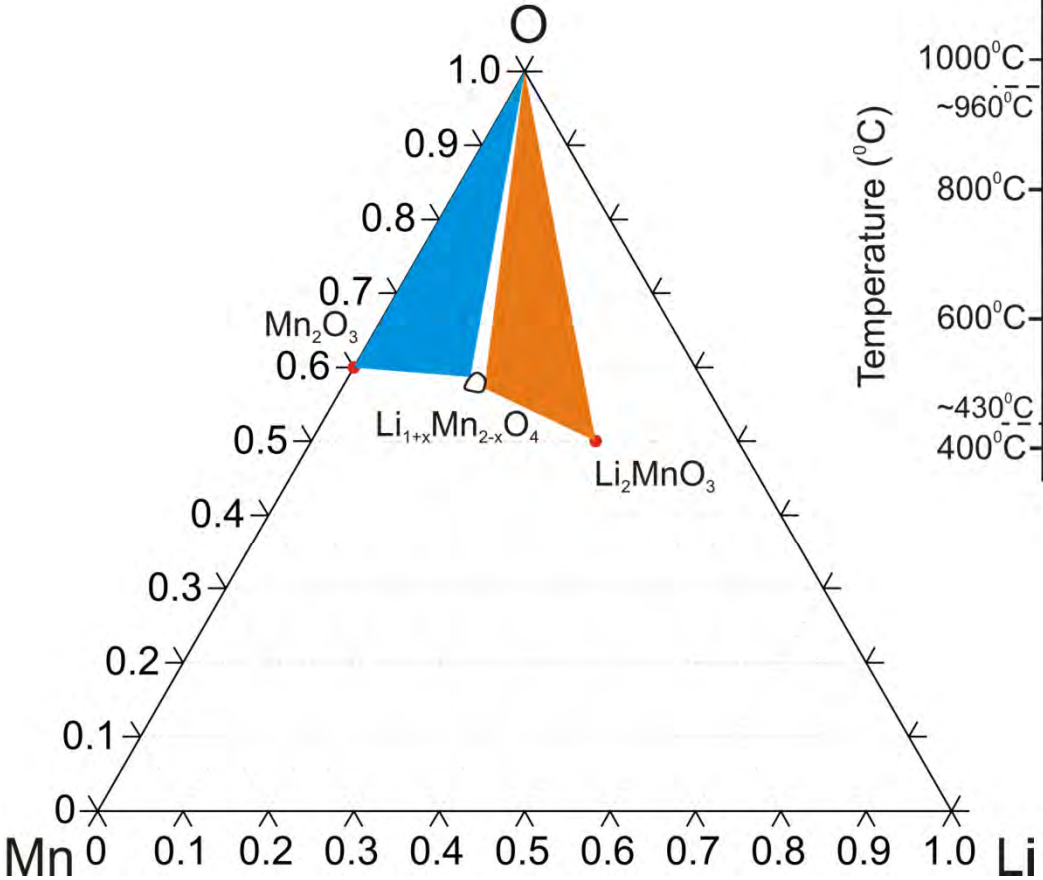

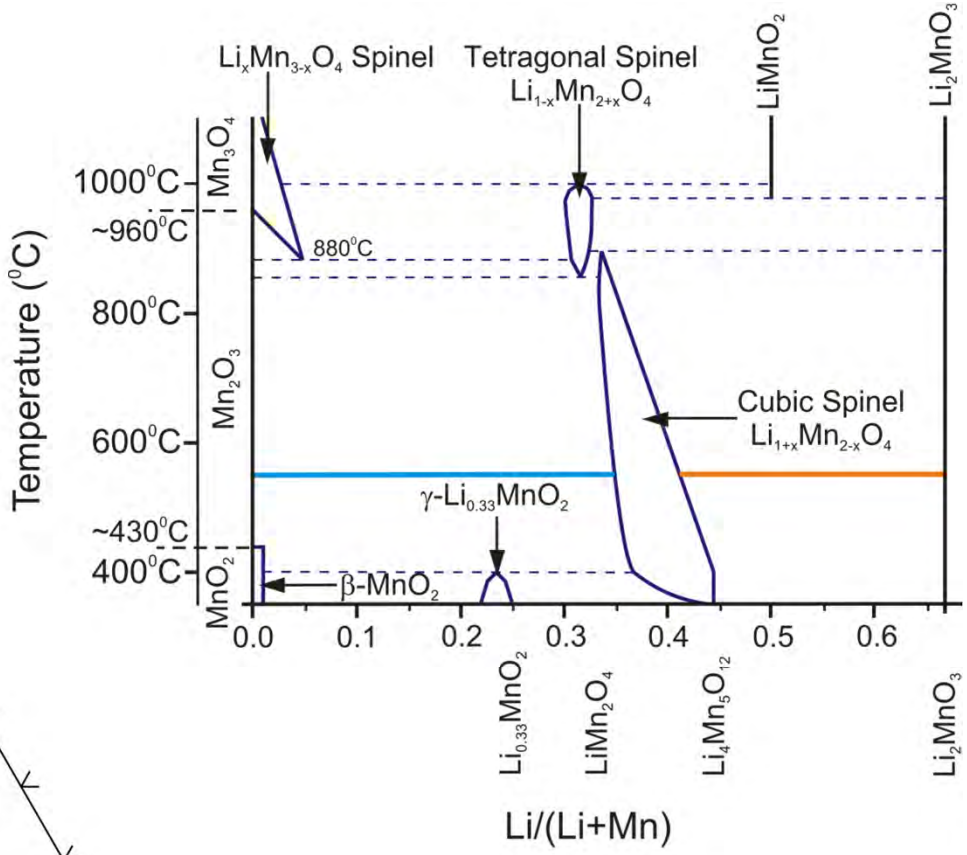

Li-Mn-O System

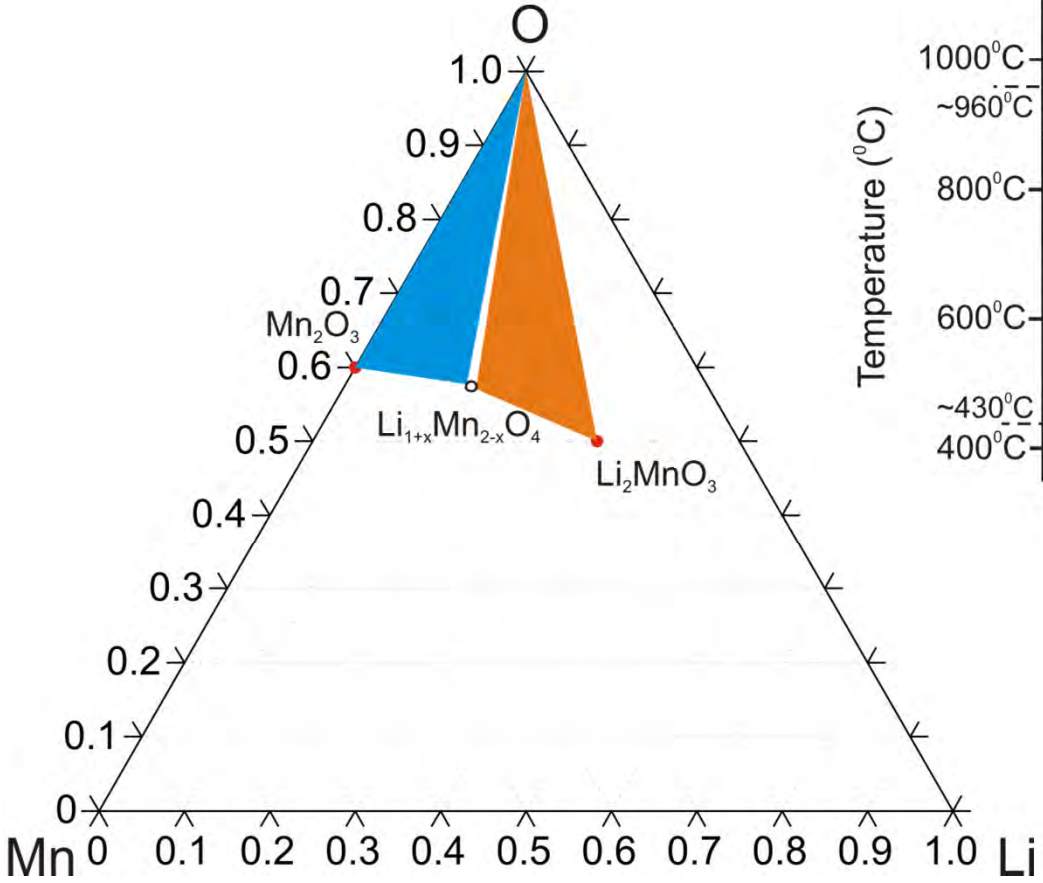

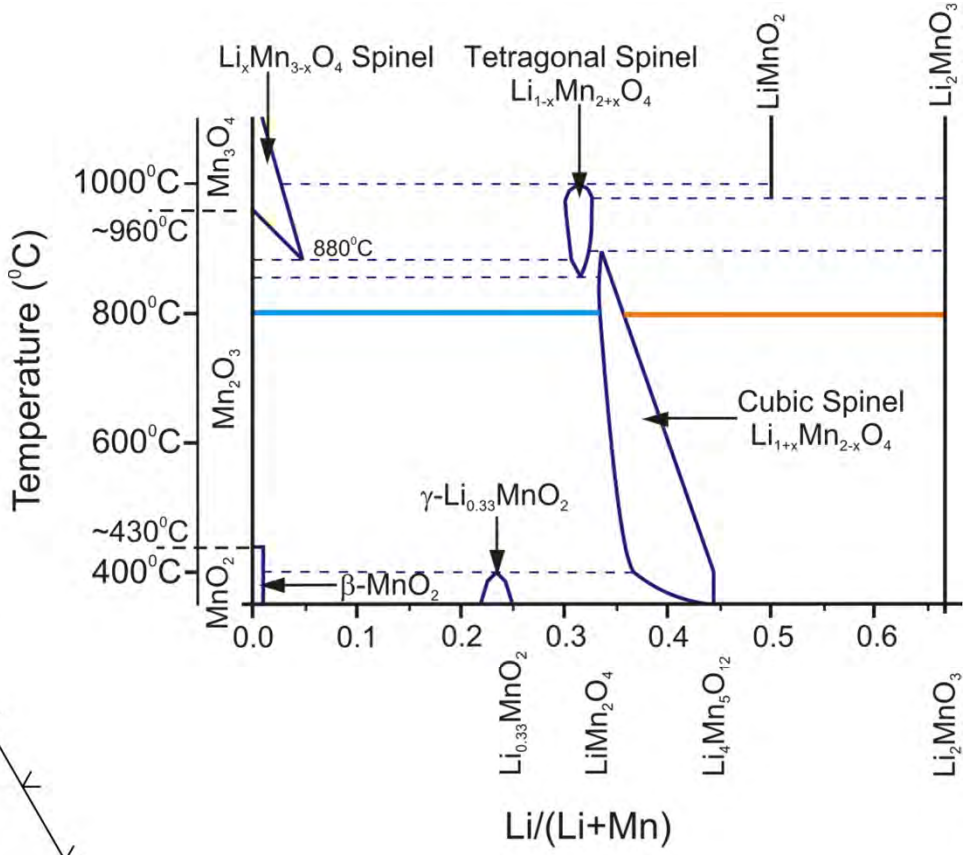

Li-Mn-O System

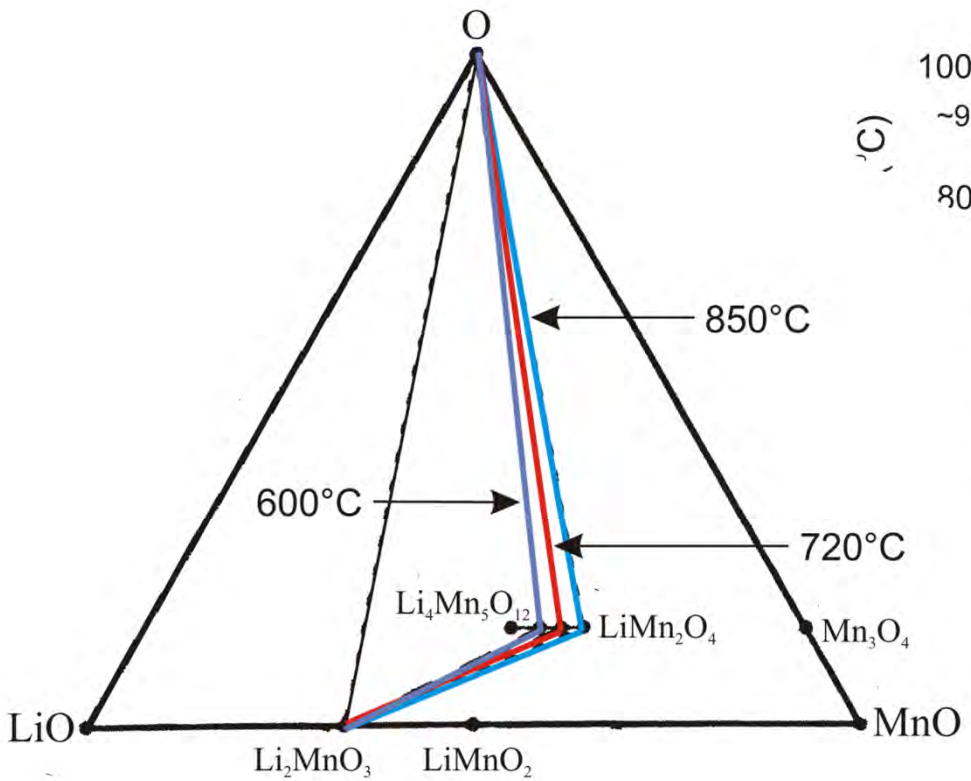

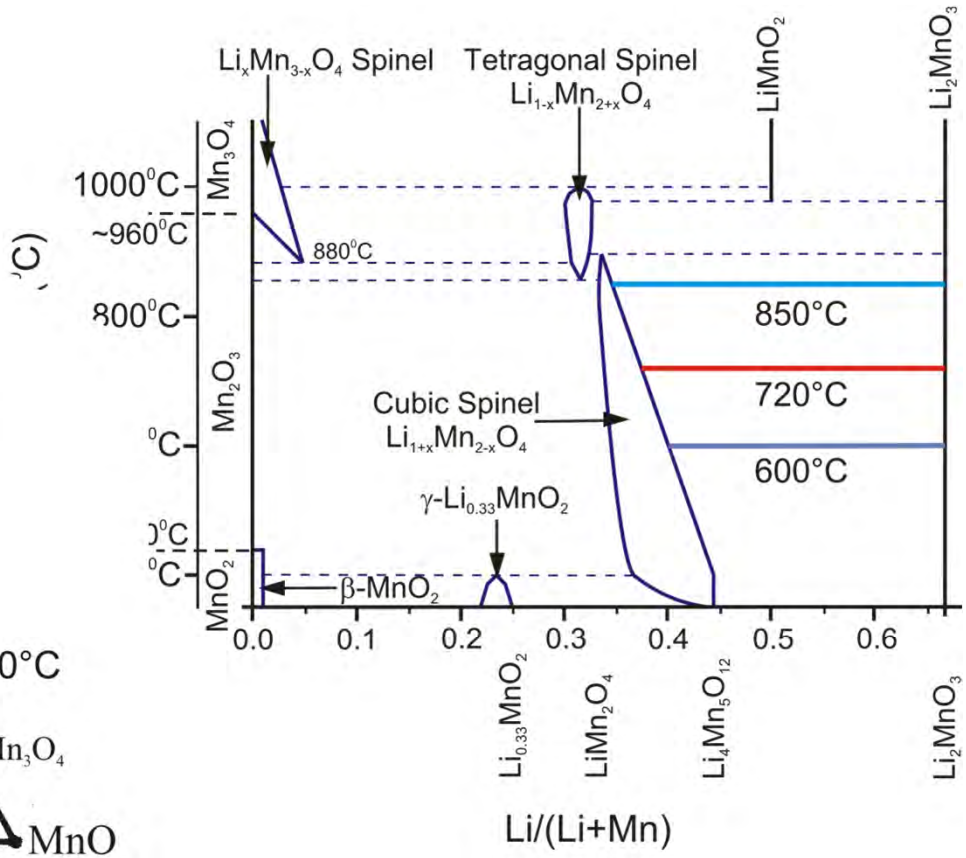

[1996Gao] Gao and Dahn, *J. Electrochem. Soc.*, 143(6), 1783-1788, 1996

Li-Mn-O System

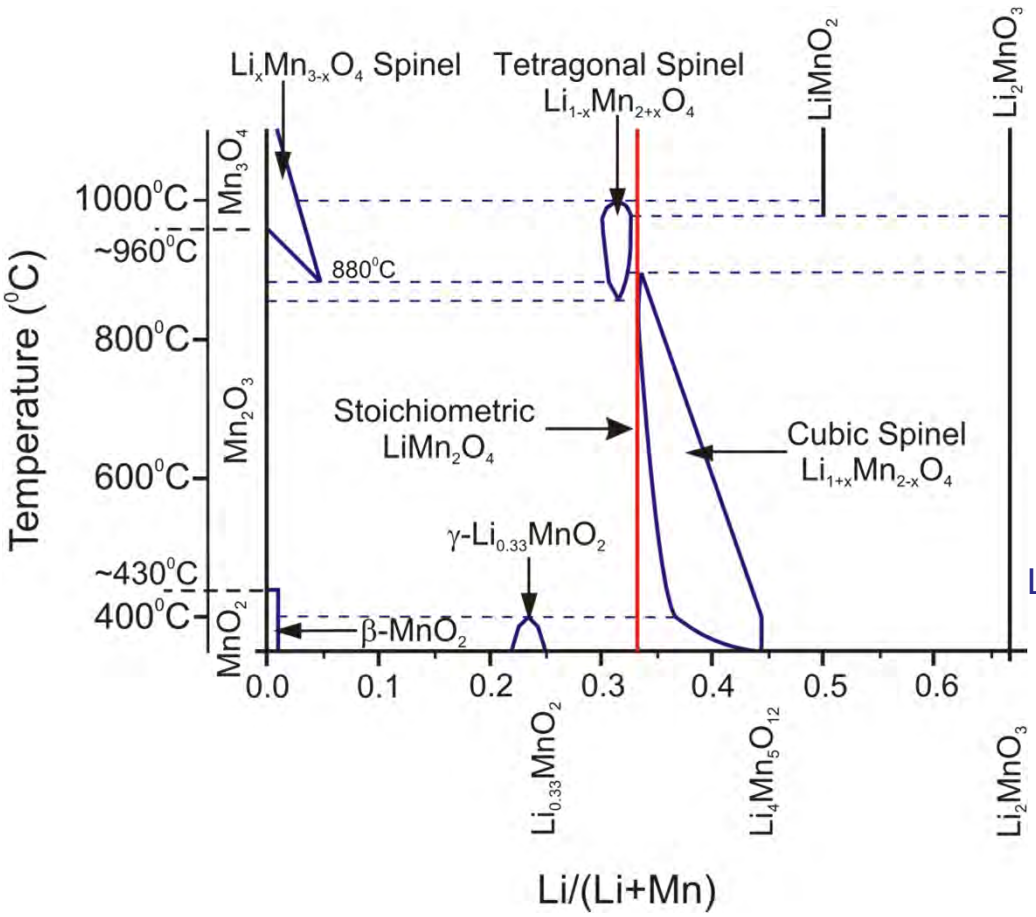

$LiMnO_2 + Li_xMn_{3-x}O_4$

↓

$LiMnO_2 + Li_xMn_{3-x}O_4 + Li_{1-x}Mn_{2+x}O_4$*(tet)*

↓

$LiMnO_2 + Li_{1-x}Mn_{2+x}O_4$*(tet)*

↓

$LiMnO_2 + Li_{1-x}Mn_{2+x}O_4$*(tet)* $+ Li_2MnO_3$

↓

$Li_{1-x}Mn_{2+x}O_4$*(tet)* $+ Li_2MnO_3$

↓

$Li_{1-x}Mn_{2+x}O_4$*(tet)* $+ Li_{1+x}Mn_{2-x}O_4$*(cub)* $+ Li_2MnO_3$

↓

$Li_{1-x}Mn_{2+x}O_4$*(tet)* $+ Li_{1+x}Mn_{2-x}O_4$*(cub)*

↓

$Li_{1-x}Mn_{2+x}O_4$*(tet)* $+ Li_{1+x}Mn_{2-x}O_4$*(cub)* $+ Mn_2O_3$

↓

$Li_{1+x}Mn_{2-x}O_4$*(cub)* $+ Mn_2O_3$

Enthalpy of Drop Solution of $Li_{1+x}Mn_{2-x}O_{4-\delta}$

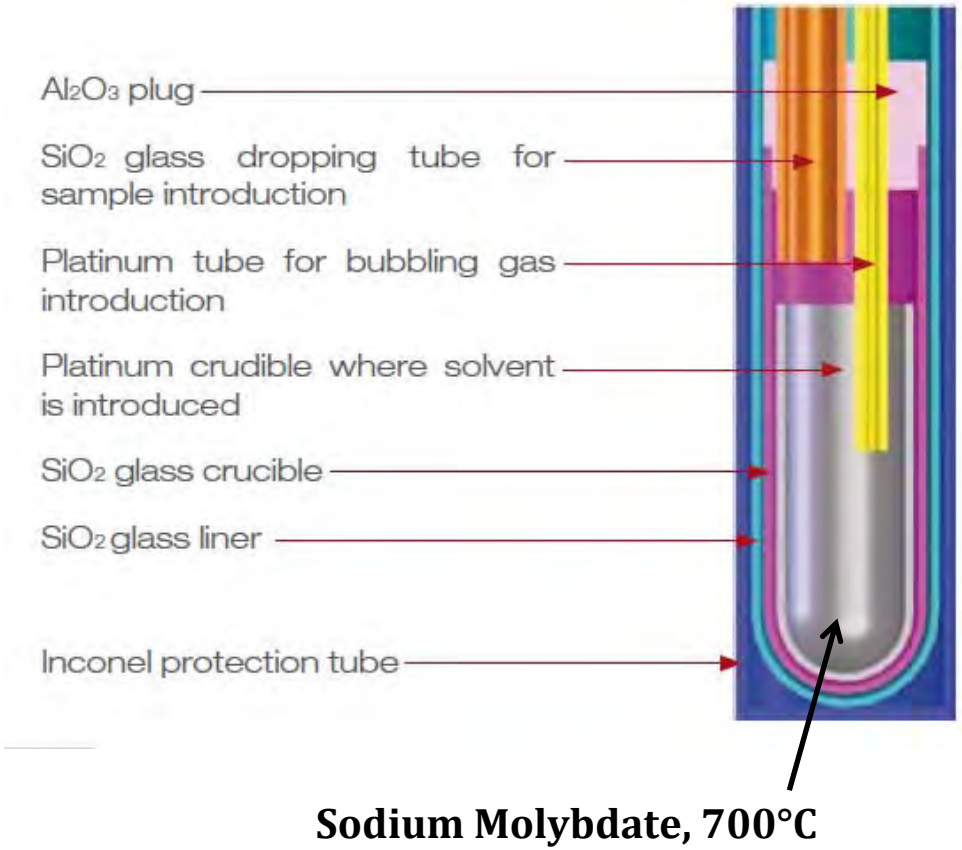

AlexSys, SETARAM

High Temperature Calvet Calorimeter

Enthalpy of Drop Solution of $Li_{1+x}Mn_{2-x}O_{4-\delta}$

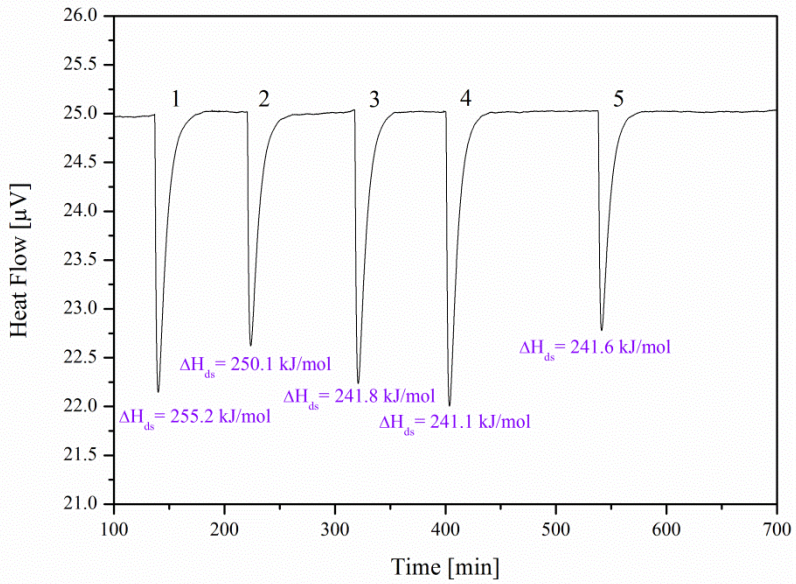

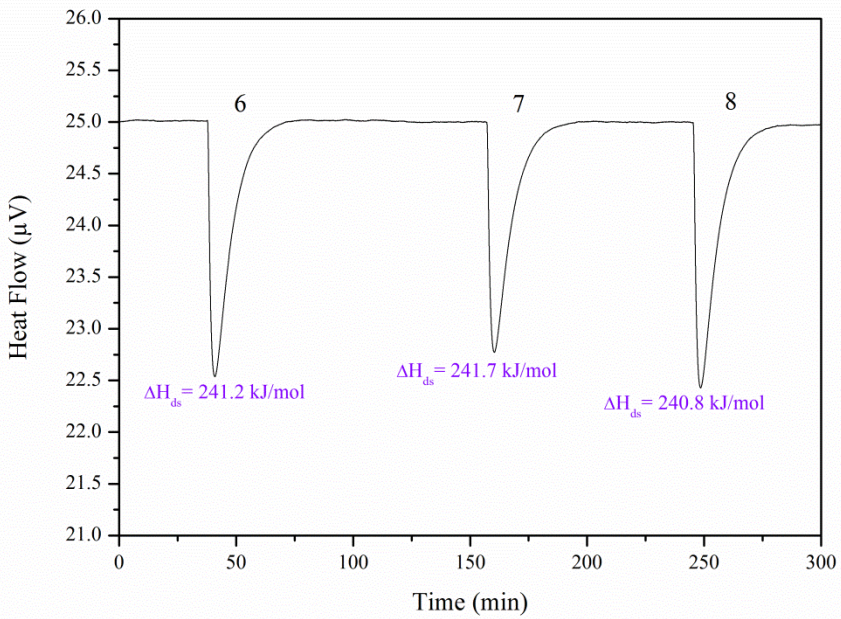

Sample Number	DROP 1	DROP 2	DROP 3	DROP 4	DROP 5	DROP 6	DROP 7	DROP 8
Date	08. Mai	08. Mai	08. Mai	08. Mai	08. Mai	09. Mai	09. Mai	09. Mai
Mass pellet (mg)	*6,00*	*5,14*	*6,10*	*6,62*	*4,85*	*5,35*	*4,83*	*5,59*
T(room) (°C)	*23,90*	*24,10*	*24,20*	*24,10*	*24,20*	*24,50*	*24,30*	*24,20*
T(cal.) (°C)	700,40	700,40	700,40	700,40	700,40	700,40	700,40	700,40
Formula weight (g/mol)	180,815	180,815	180,815	180,815	180,815	180,815	180,815	180,815
Moles of LiMn2O4 (mol)	0,0000332	0,0000284	0,0000337	0,0000366	0,0000268	0,0000296	0,0000267	0,0000309
Peak Area [µV.s]	1832,4170	1538,5640	1765,6030	1910,2030	1402,3320	1544,6110	1397,2290	1611,2630
Calibration factor from Al_2O_3 calibration[J/µV.s]	**0,00462077**	**0,00462077**	**0,00462077**	**0,00462077**	**0,00462077**	**0,00462077**	**0,00462077**	**0,00462077**
Measured Heat Effect (kJ/mol)	**255,1652**	**250,0926**	**241,8308**	**241,0849**	**241,5781**	**241,2203**	**241,6957**	**240,8258**
Accepted Measurement	0	0	1	1	1	1	1	1

Commercial cathode materials

Olivine structure

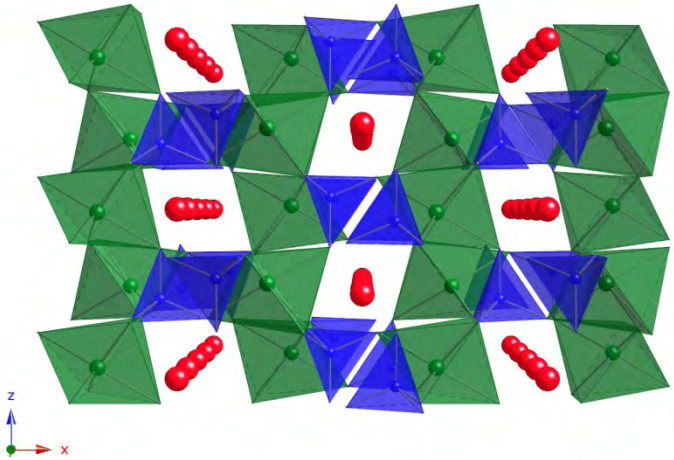

Layered structure

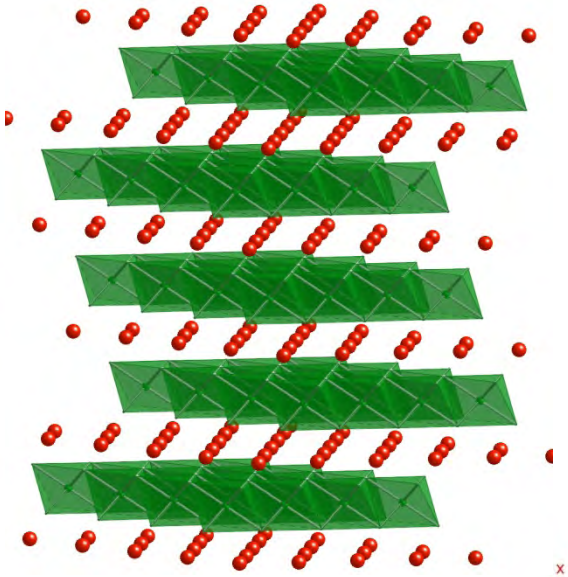

Spinel structure

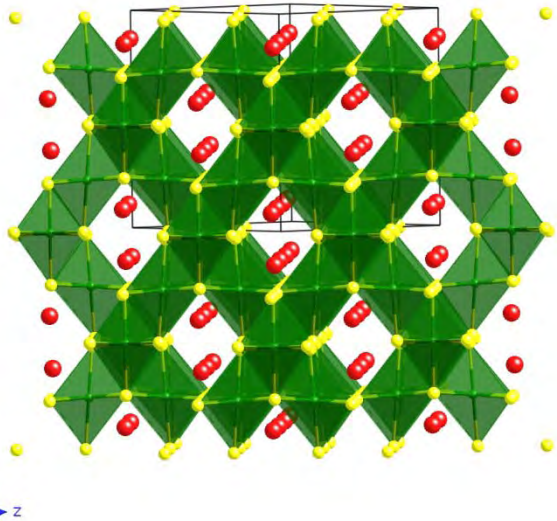

$LiCoO_2$: ≈ 160 mAh/g

$LiFePO_4$: ≈ 160 mAh/g

$LiMn_2O_4$: ≈ 100 mAh/g

Gravimetrical energy densities (capacities)

Li-Fe-P-O System

$LiFePO_4$ - Stable phase?

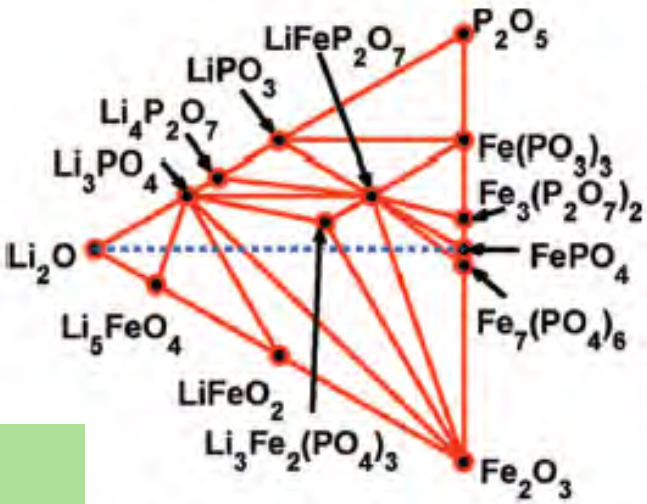

(a) $\mu_{O_2} = -10.50\ eV$, $Fe_7(PO_4)_6$ appears

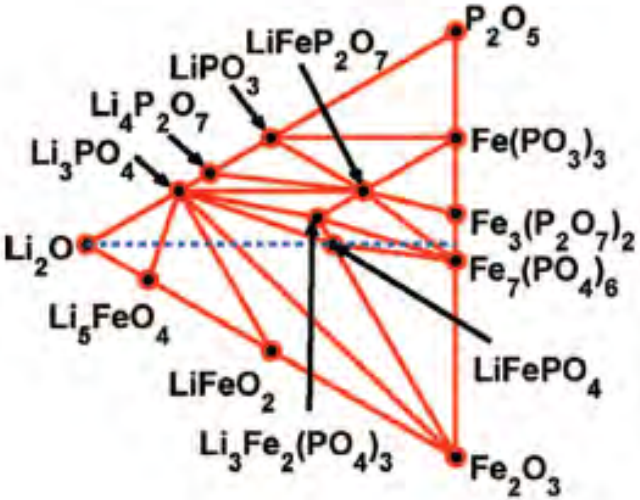

(b) $\mu_{O_2} = -11.52\ eV$, $LiFePO_4$ appears

Figure 2. Phase diagrams at less reducing environments.

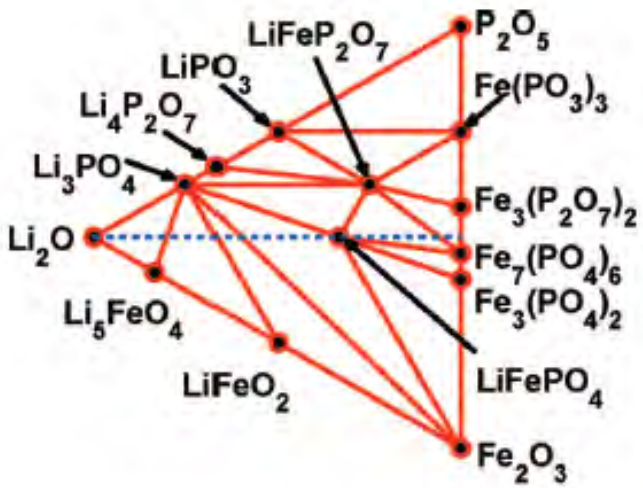

(a) $\mu_{O_2} = -11.74\ eV$, $Li_3Fe_2(PO_4)_3$ disappears

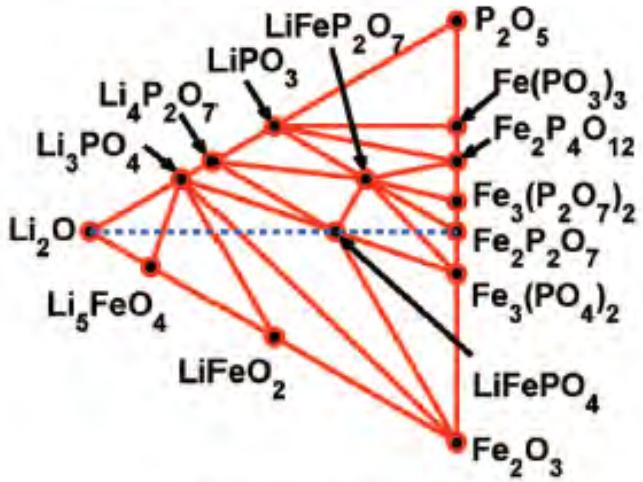

(b) $\mu_{O_2} = -12.38\ eV$, $Fe_2P_2O_7$ appears

Figure 3. Phase diagrams at more reducing environments.

Ong et al. (2008)

Li-Fe-P-O System

$LiFePO_4$ - Stable phase?

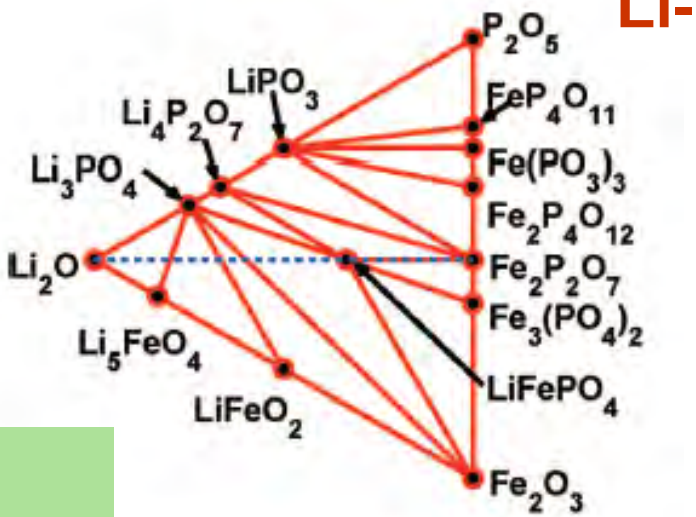

(a) $\mu_{O_2} = -13.08\ eV$, $LiFeP_2O_7$ disappears

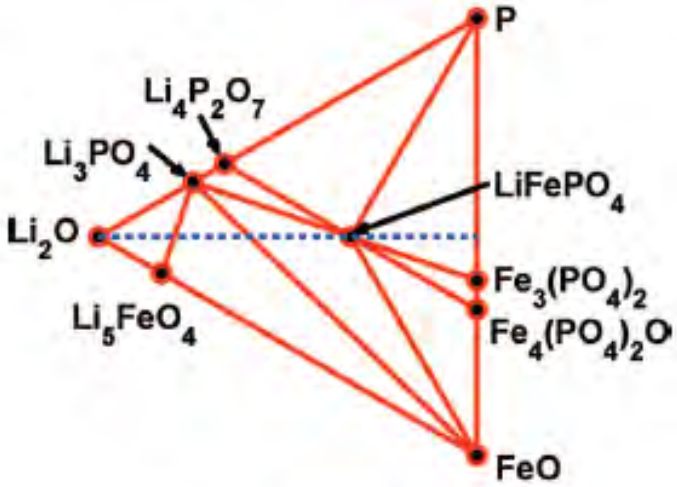

(b) $\mu_{O_2} = -16.08\ eV$, $Fe_2P_2O_7$ disappears

Figure 4. Phase diagrams at highly reducing environments.

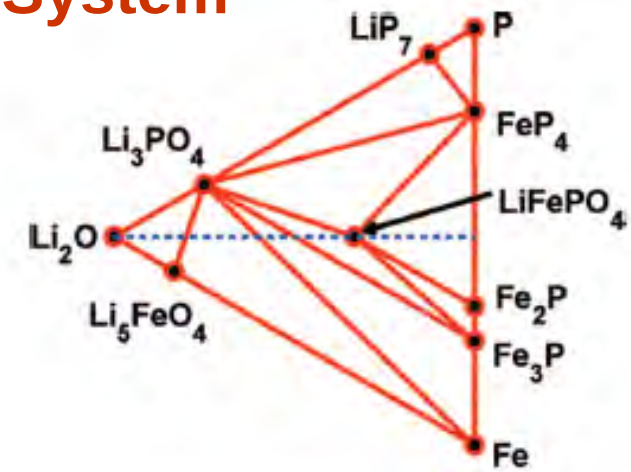

(a) $\mu_{O_2} = -16.70\ eV$, $Fe_3(PO_4)_2$ disappears

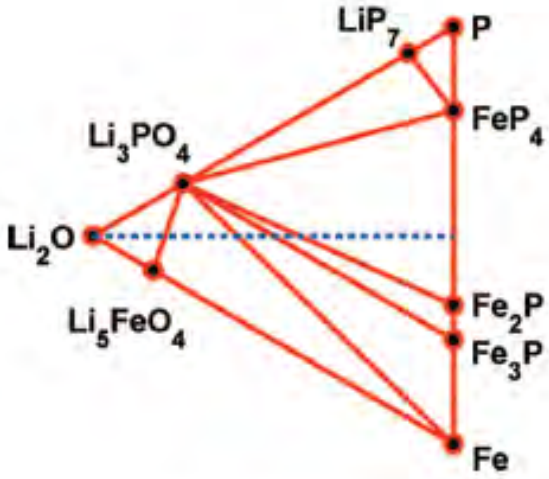

(b) $\mu_{O_2} = -16.74eV$, $LiFePO_4$ disappears

Figure 5. Phase diagrams at extremely reducing environments.

Ong et al. (2008)

Li-Fe-P-O System

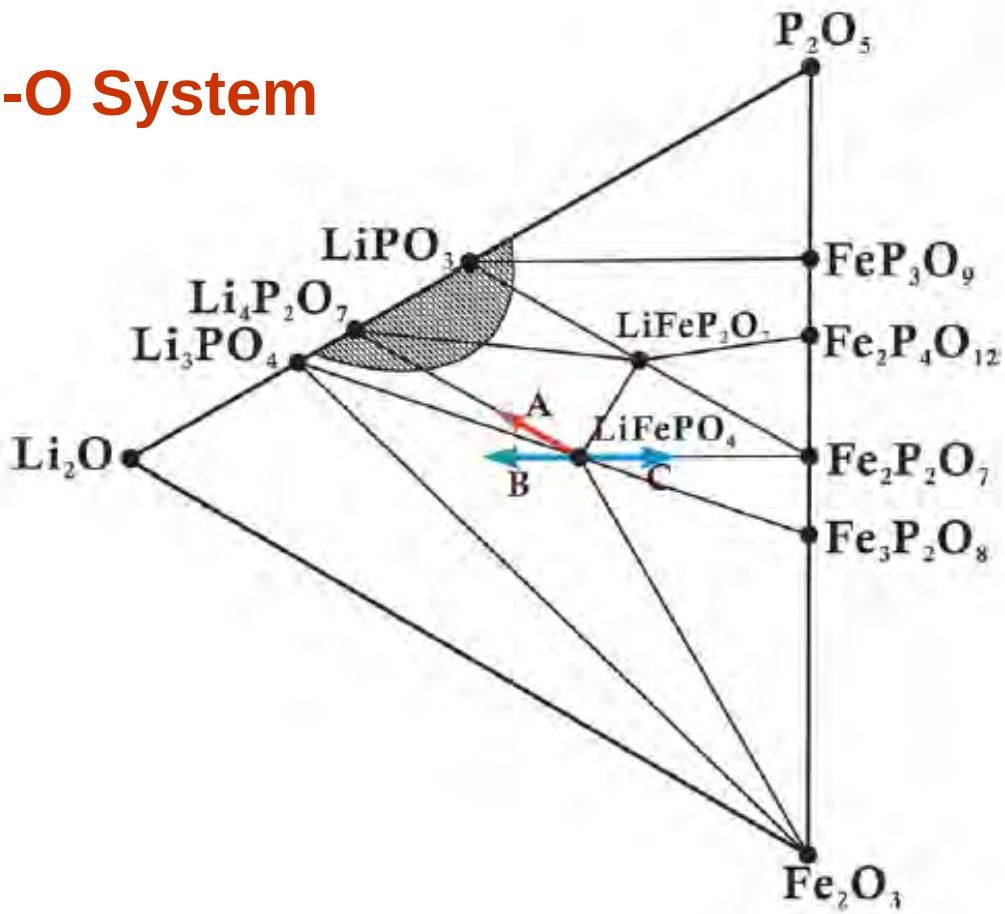

Figure S1. **Calculated Li-Fe-P ternary phase diagram equilibrated with an oxygen potential under reducing conditions.** The 'A' arrow indicates off-stoichiometry induced in the samples described in this Letter. The 'B' and 'C' arrow respectively indicate the more common one-to-one Fe/P deficiency and lithium deficiency. The shaded area in phase diagram indicates relevant coating compositions.

Kang and Ceder (2009)

Thermodynamics of Lithium Battery Materials

- Materials Thermodynamics, Phase Diagrams and Electrochemistry to be simultaneously investigated
- Fundamental for electrochemical cell performance, understanding of thermal and safety behavior and for preparation of cathode materials
- Thermodynamics and phase diagrams even for the most important systems e.g. Li-Co-O, Li-Mn-O and Li-Fe-P-O to be investigated in more detail

Li-Mn-O System

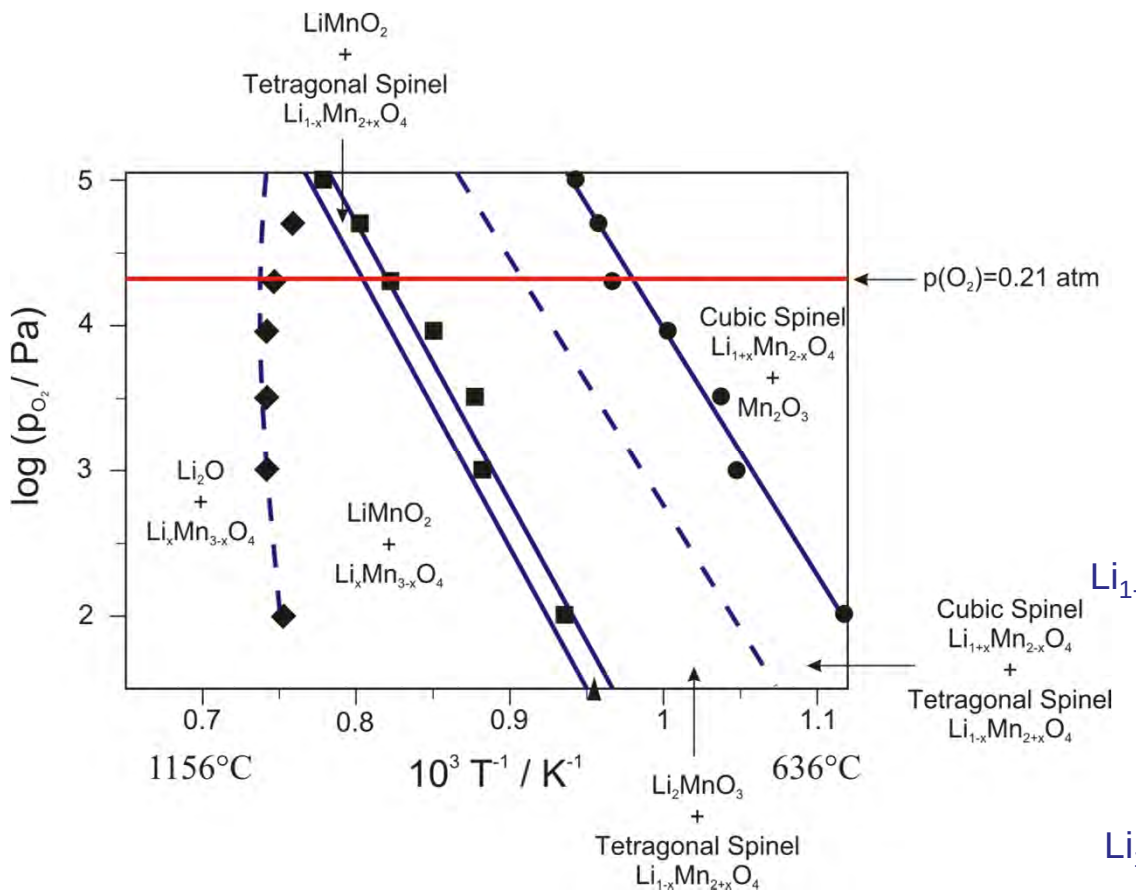

$LiMnO_2 + Li_xMn_{3-x}O_4$

↓

$LiMnO_2 + Li_xMn_{3-x}O_4 + Li_{1-x}Mn_{2+x}O_4$*(tet)*

↓

$LiMnO_2 + Li_{1-x}Mn_{2+x}O_4$*(tet)*

↓

$LiMnO_2 + Li_{1-x}Mn_{2+x}O_4$*(tet)* $+ Li_2MnO_3$

↓

$Li_{1-x}Mn_{2+x}O_4$*(tet)* $+ Li_2MnO_3$

↓

$Li_{1-x}Mn_{2+x}O_4$*(tet)* $+ Li_{1+x}Mn_{2-x}O_4$*(cub)* $+ Li_2MnO_3$

↓

$Li_{1-x}Mn_{2+x}O_4$*(tet)* $+ Li_{1+x}Mn_{2-x}O_4$*(cub)*

↓

$Li_{1-x}Mn_{2+x}O_4$*(tet)* $+ Li_{1+x}Mn_{2-x}O_4$*(cub)* $+ Mn_2O_3$

↓

$Li_{1+x}Mn_{2-x}O_4$*(cub)* $+ Mn_2O_3$

Li-Ni-Mn-Co-O System

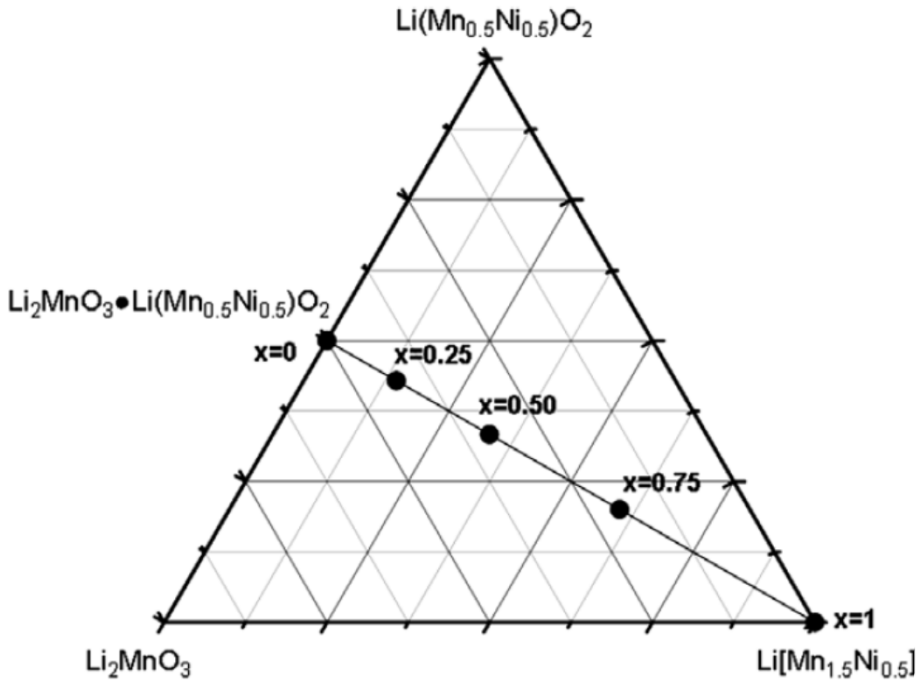

Phase compositions in the $Li[Mn_{1.5}Ni_{0.5}]O_4$-Li_2MnO_3- $Li[Mn_{0.5}Ni_{0.5}]O_4$ system (Park 2007).

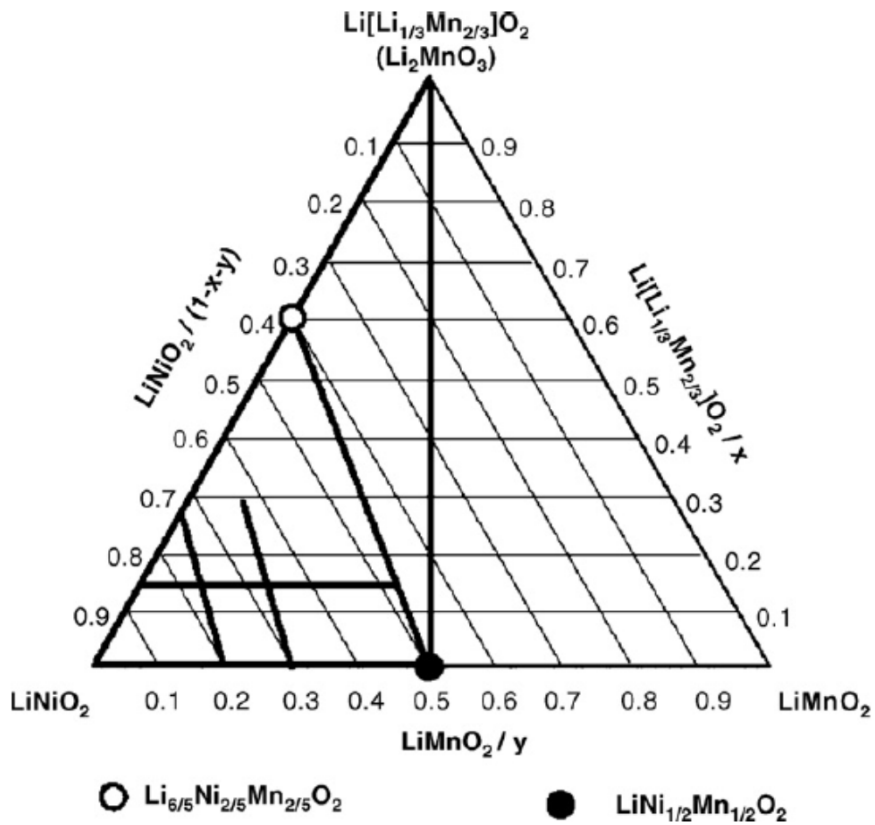

Composition triangle in the system $LiNiO_2$–$LiMnO_2$–$Li[Li_{1/3}Mn_{2/3}]O_2$. Bold lines represent the compositions which have been reported as single phase via a high temperature solid state reaction Zhang et al. (2008).

Li-Ni-Mn-Co-O System

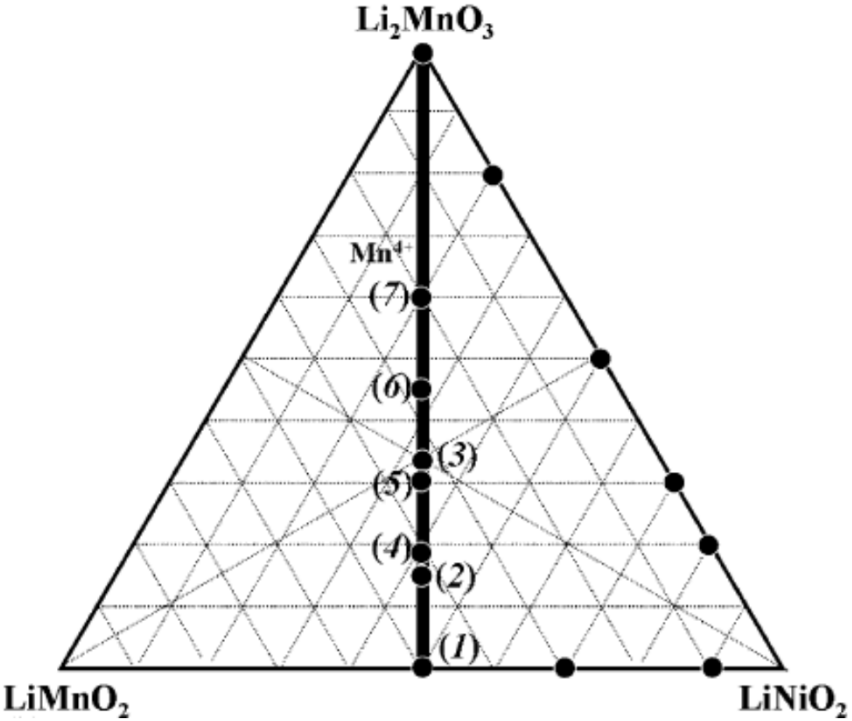

Triangle system Li_2MnO_3-$LiMnO_2$-$LiNiO_2$ (Park 2005).
Bold line indicates Mn oxidation state of +4.

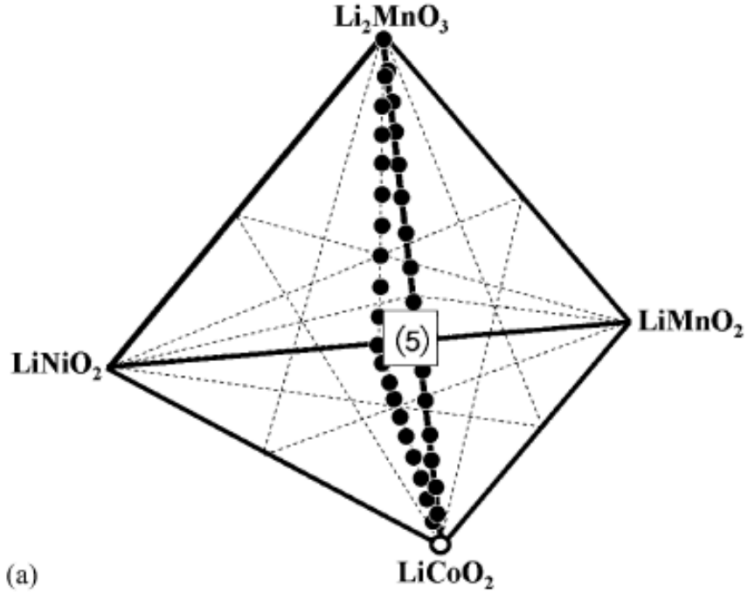

$LiMnO_2$-$LiCoO_2$-$LiNiO_2$-Li_2MnO_3 phase diagram,
b) Section $LiNi_{1/2}Mn_{1/2}O_2$-$LiCoO_2$-Li_2MnO_3

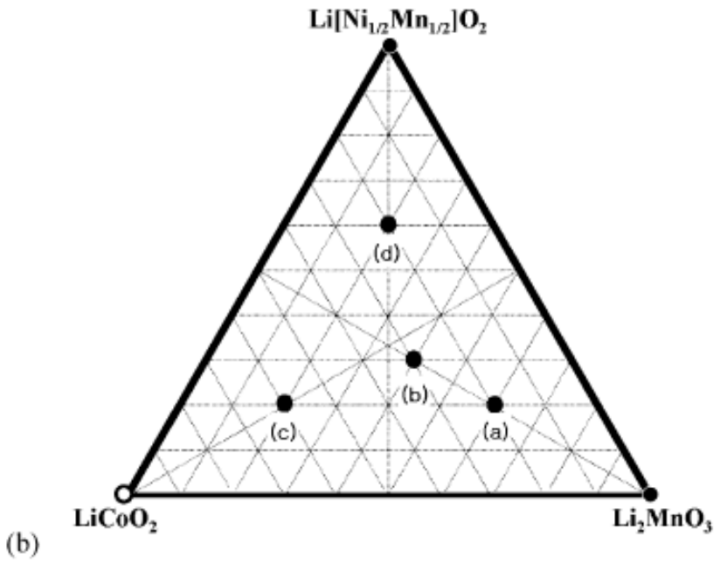

Li-Mn-O System

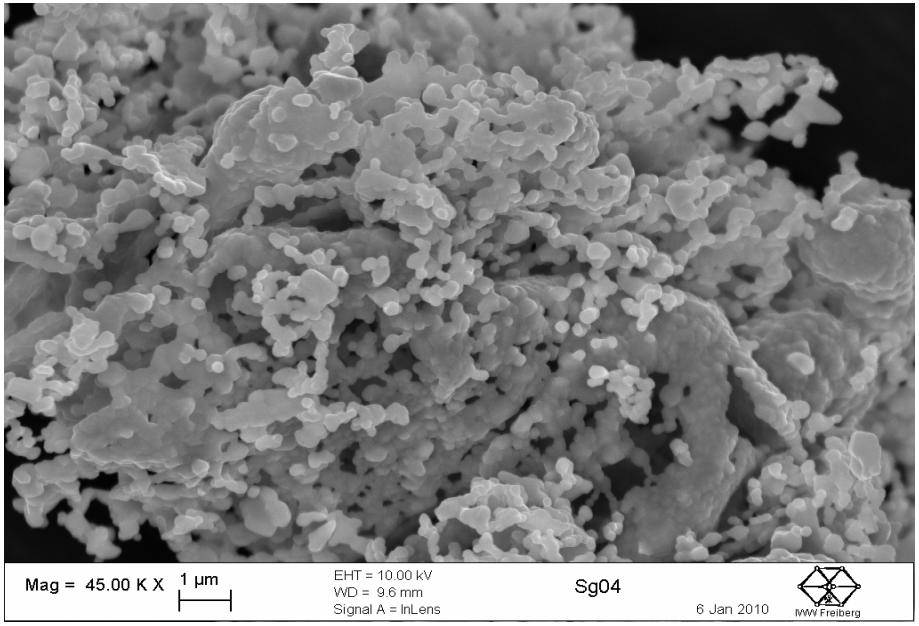

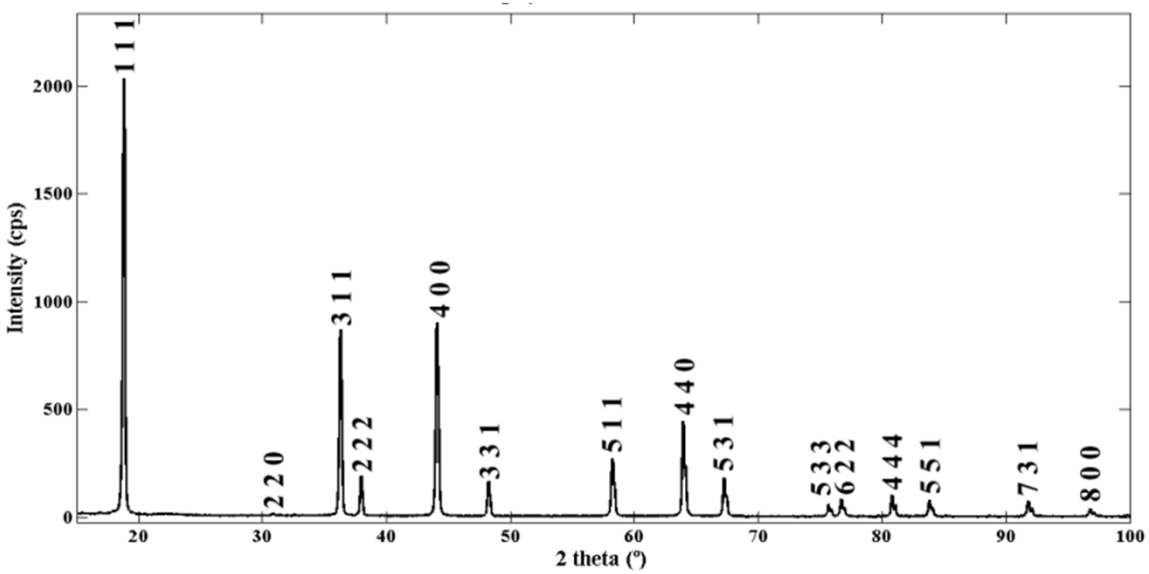

Li-Mn-O System

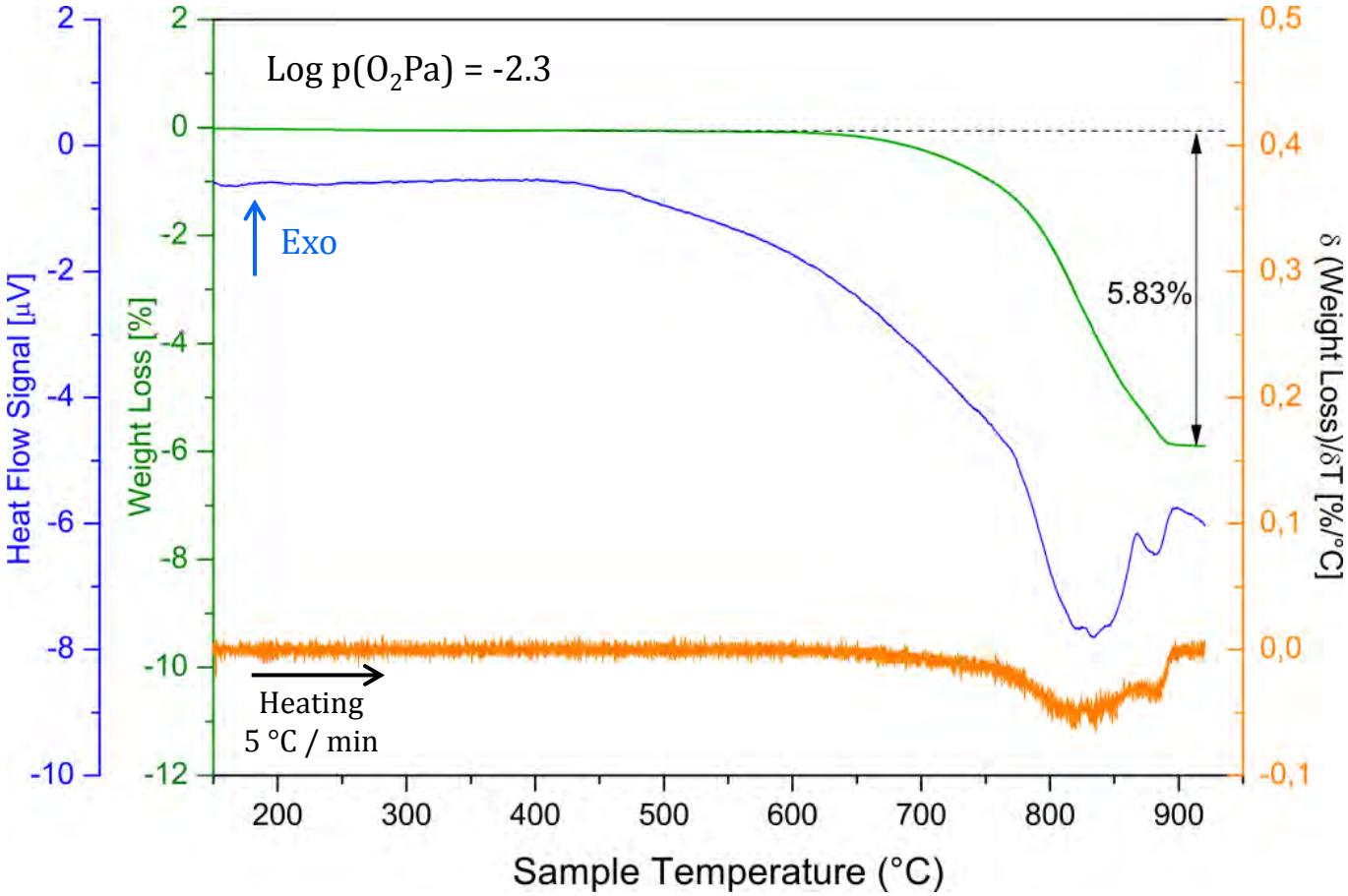

$$3LiMn_2O_4 \leftrightarrow 3LiMnO_2 + Mn_3O_4 + O_2$$

5.89% theoretical weight loss

Li-Mn-O System

- Reaction of stoichiometric $LiMn_2O_4$ at $Log(pO_2)$=-2.3 not indicated in the critically evaluated potential diagram for stoichiometric $LiMn_2O_4$

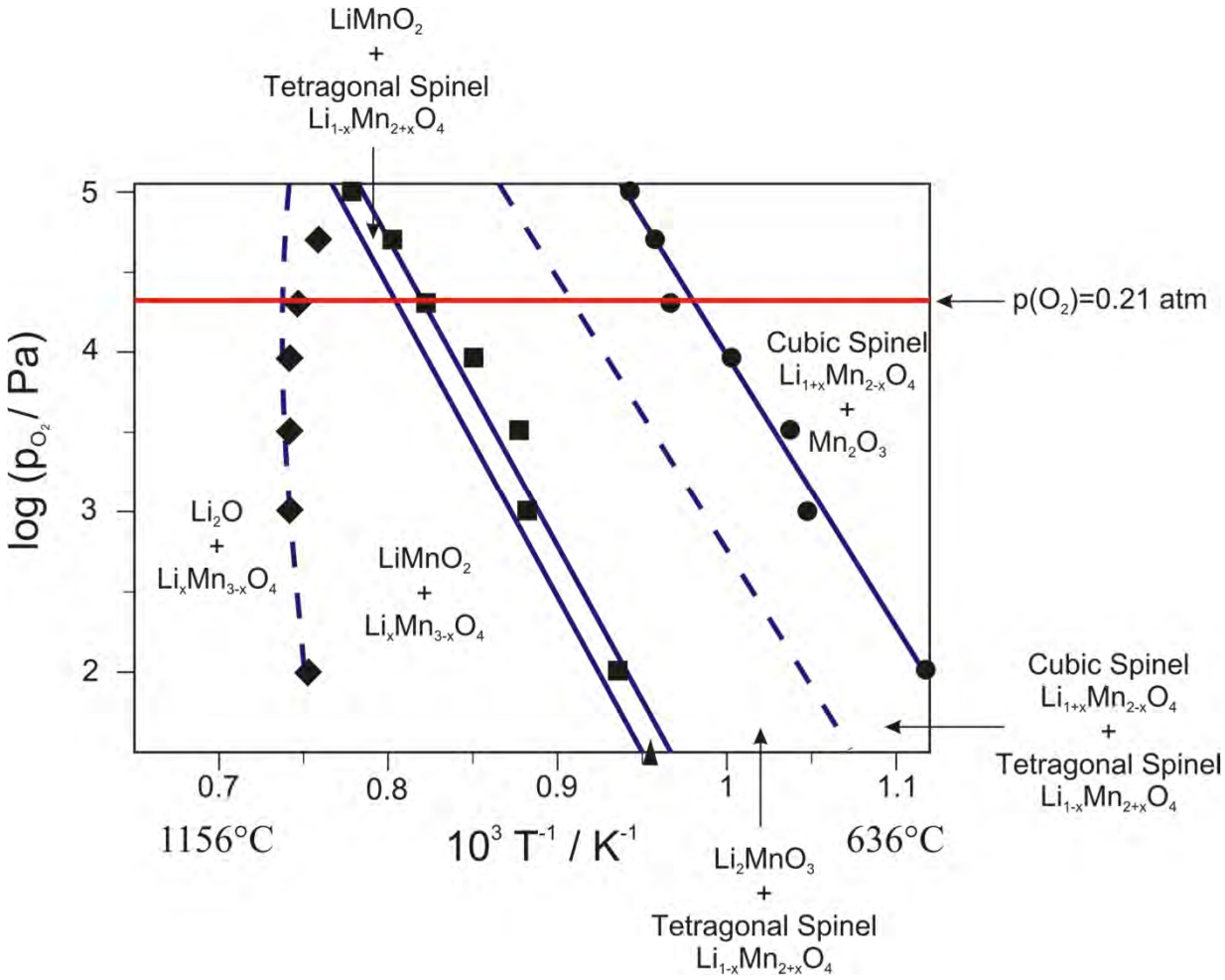

Li-Mn-O System

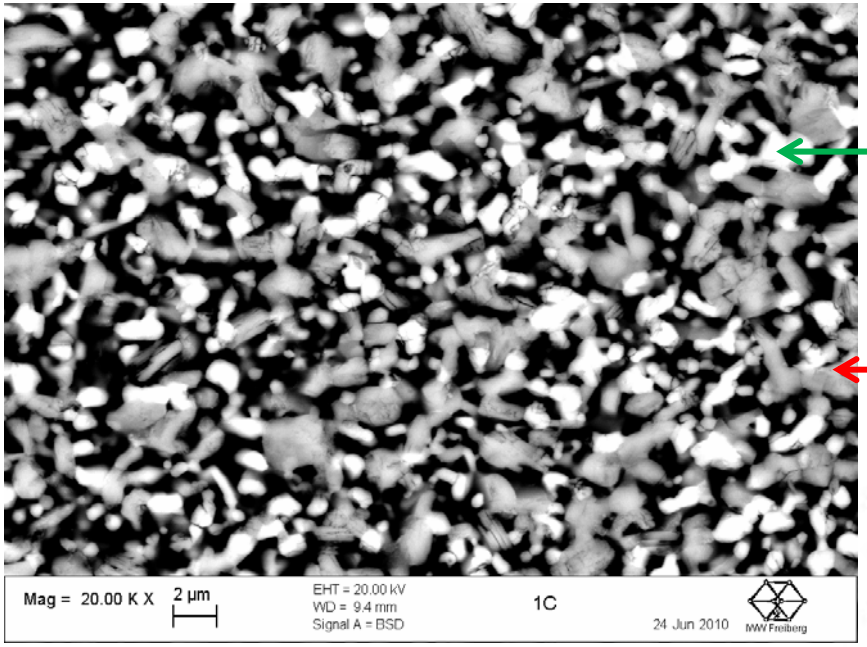

Mn_3O_4

$LiMnO_2$

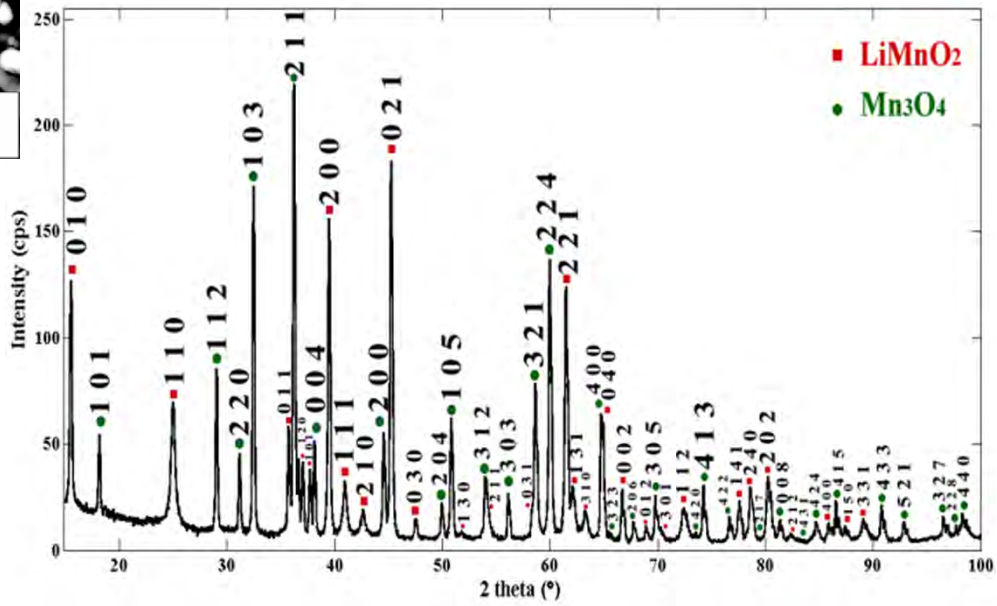

$$3LiMn_2O_4 \leftrightarrow 3LiMnO_2 + Mn_3O_4 + O_2$$

Li-Mn-O System

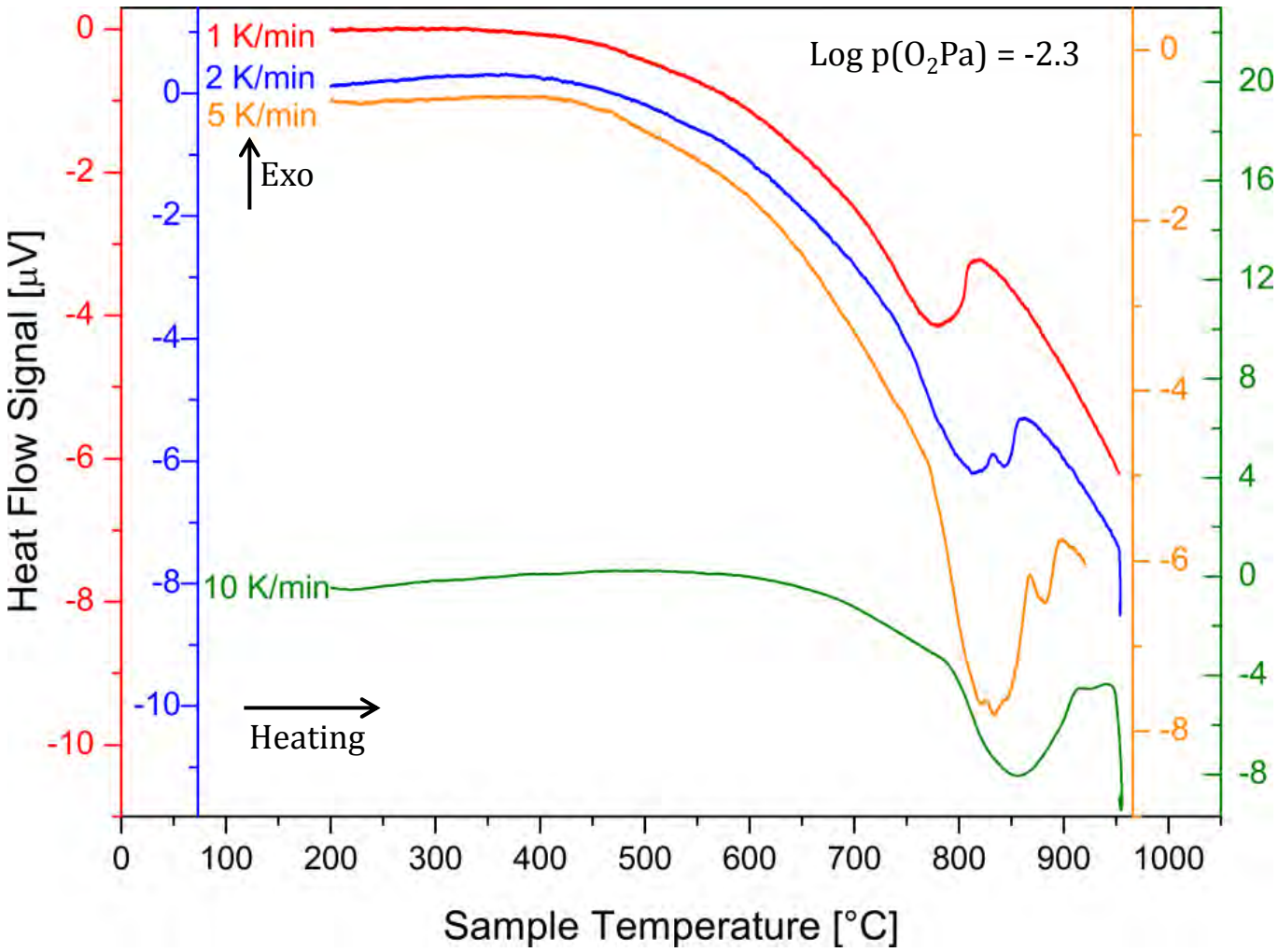

$$3LiMn_2O_4 \leftrightarrow 3LiMnO_2 + Mn_3O_4 + O_2$$

Li-Mn-O System

- Reaction temperature determined as first deviation of the 1st derivative of weight loss from baseline
- Reaction temperature at $\log(pO_2)$=-2.3 is 541.5°C

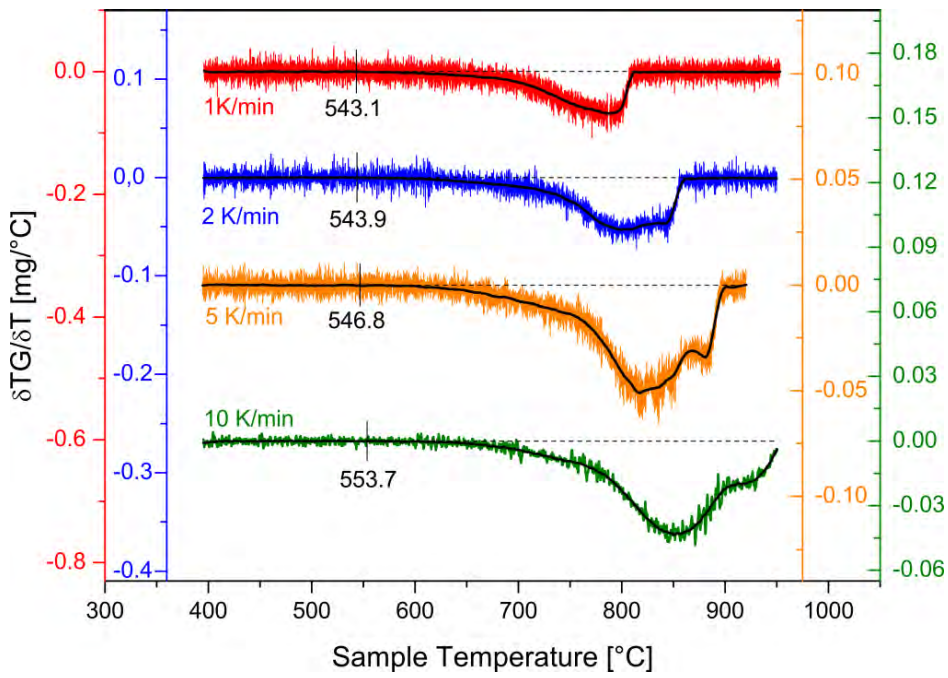

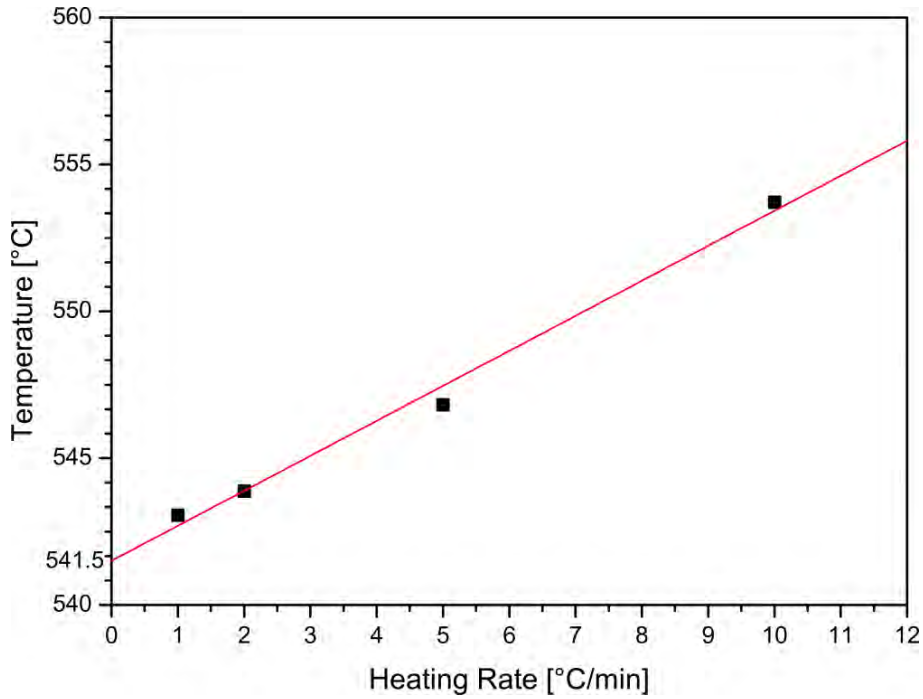

$$3LiMn_2O_4 \leftrightarrow 3LiMnO_2 + Mn_3O_4 + O_2$$

Karlsruhe Institute of Technology

Institute for Applied Materials

Thermodynamics of lithium ion batteries

Hans J. Seifert

Institute for Applied Materials – Applied Materials Physics (IAM-AWP)

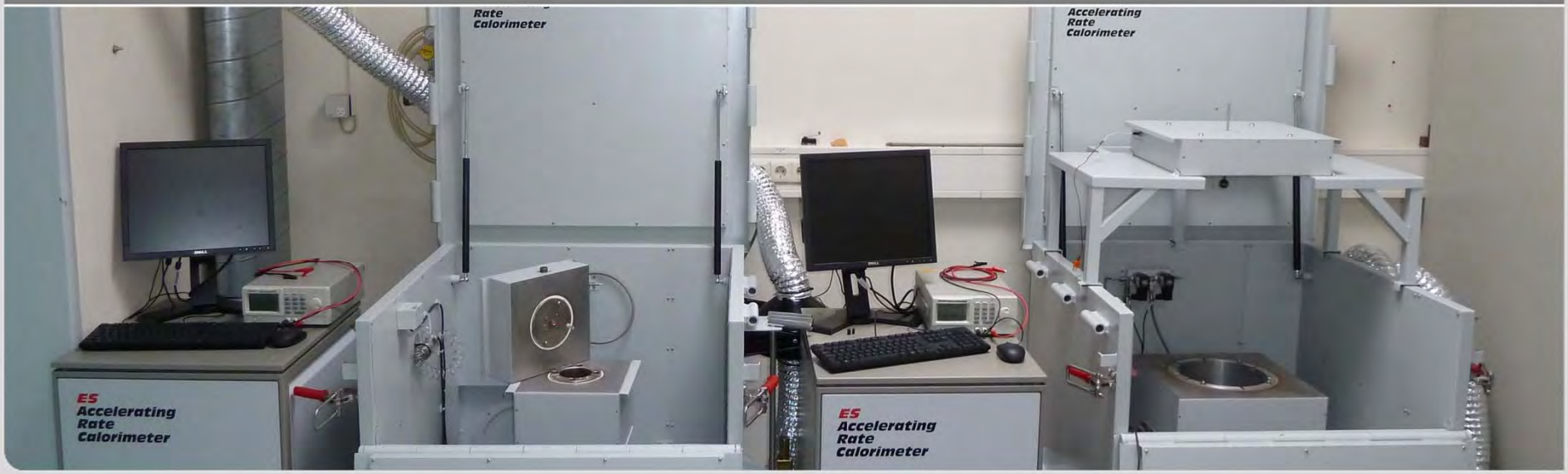

- SPP1473, Scientific Aims -

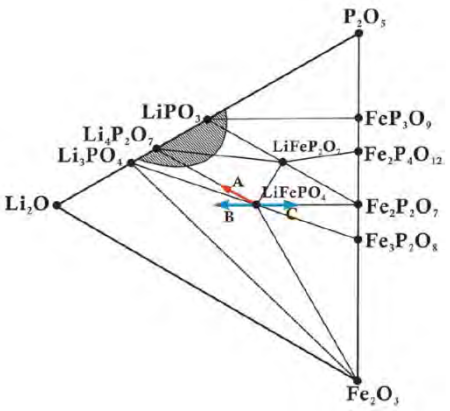

Materials
- Thermodynamics,
- Phase Diagrams,
- Kinetics

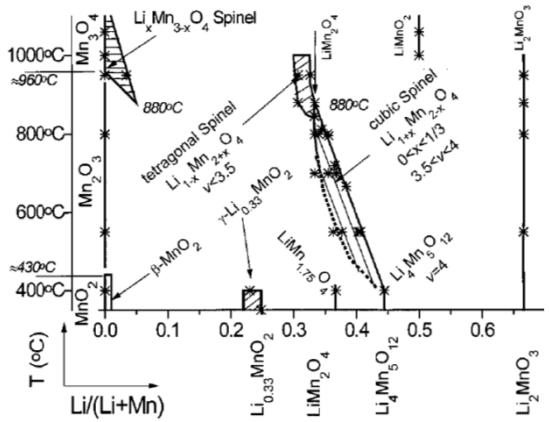

Micro- and Nanomaterials

Crystal structures,
Crystal chemistry,
Microstructure,
Reactivity

Electrochemical performance and safety of cells / batteries

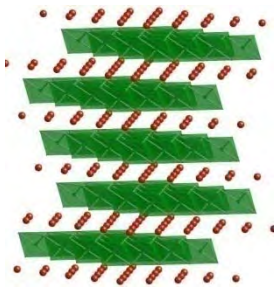

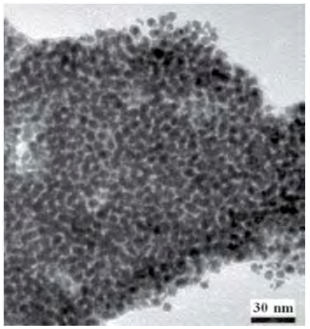

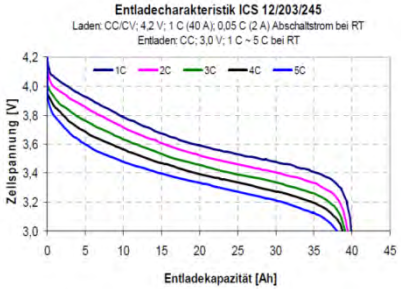

Li-Fe-P-O System

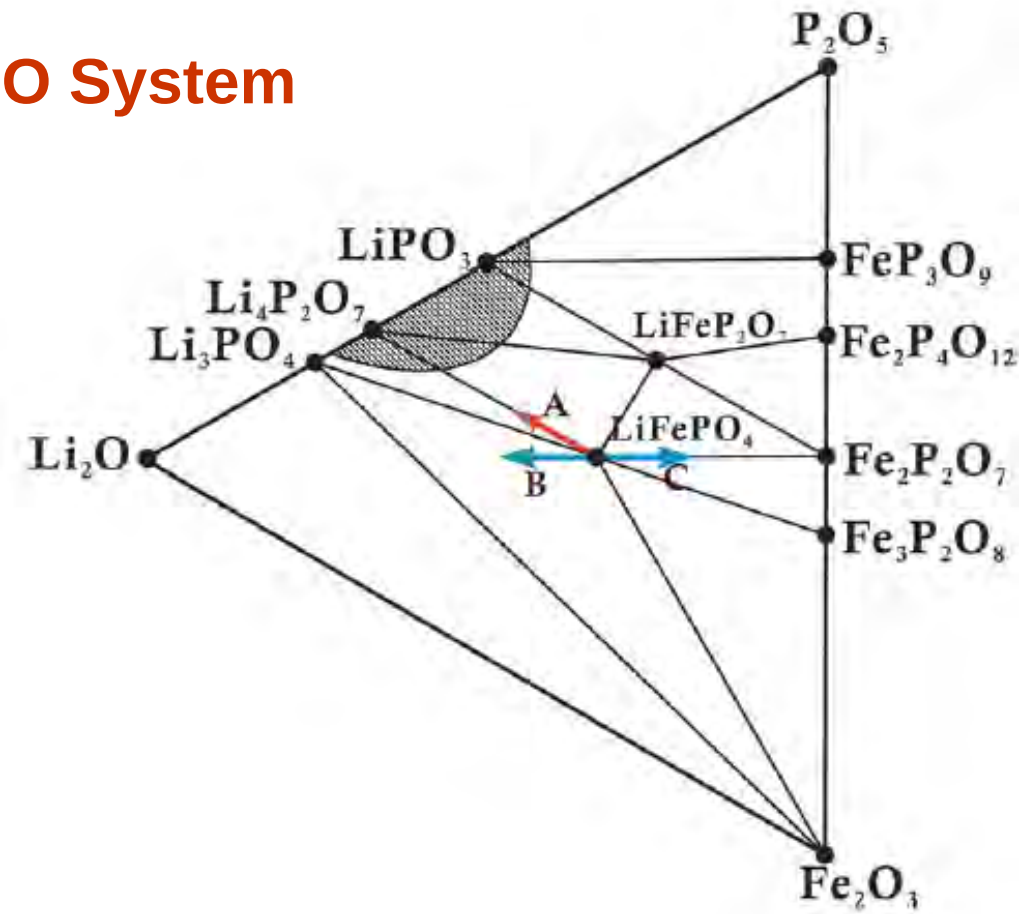

Figure S1. **Calculated Li-Fe-P ternary phase diagram equilibrated with an oxygen potential under reducing conditions.** The 'A' arrow indicates off-stoichiometry induced in the samples described in this Letter. The 'B' and 'C' arrow respectively indicate the more common one-to-one Fe/P deficiency and lithium deficiency. The shaded area in phase diagram indicates relevant coating compositions.

Kang and Ceder (2009)

Li-Fe-P-O System

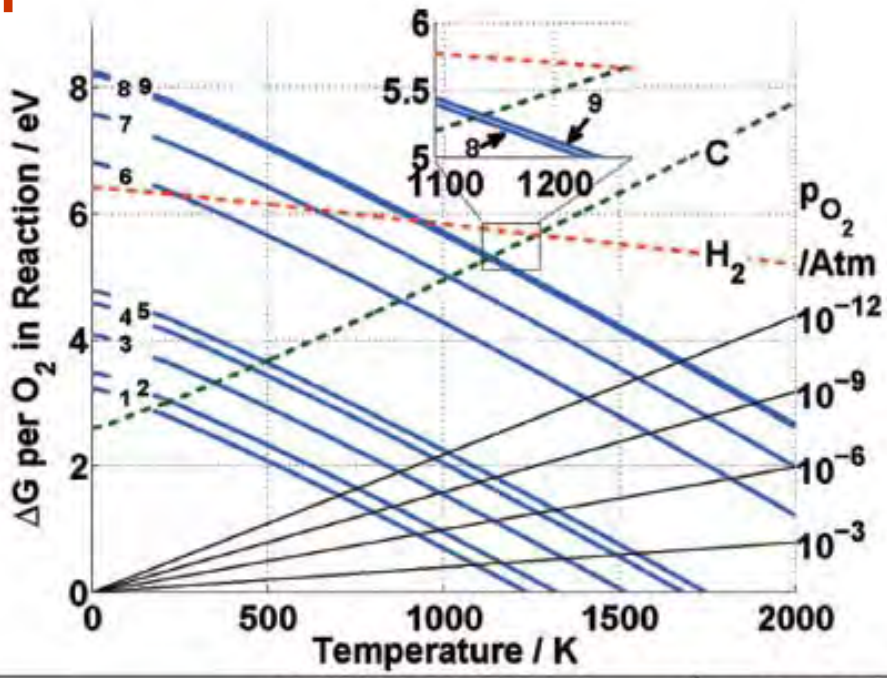

Reaction	Line Label
$3\ Li_3Fe_2(PO_4)_3 \rightleftharpoons 4\ LiFePO_4 + 2\ LiFeP_2O_7 + Li_3PO_4 + O_2$	1
$\frac{3}{2}\ Fe_7(PO_4)_6 \rightleftharpoons Fe_3(P_2O_7)_2 + \frac{5}{2}\ Fe_3(PO_4)_2 + O_2$	2
$2\ Fe_3(P_2O_7)_2 \rightleftharpoons 2\ Fe_2P_2O_7 + Fe_2P_4O_{12} + O_2$	3
$4\ LiFeP_2O_7 \rightleftharpoons 4\ LiPO_3 + 2\ Fe_2P_2O_7 + O_2$	4
$6\ Fe_2O_3 \rightleftharpoons 4\ Fe_3O_4 + O_2$	5
$2\ Fe_3O_4 \rightleftharpoons 6\ FeO + O_2$	6
$\frac{6}{5}\ Fe_2P_2O_7 \rightleftharpoons \frac{4}{5}\ Fe_3(PO_4)_2 + \frac{4}{5}\ P + O_2$	7
$2\ FeO \rightleftharpoons 2\ Fe + O_2$	} 8
$\frac{1}{4}\ Fe_3(PO_4)_2 \rightleftharpoons \frac{1}{28}\ FeP_4 + \frac{5}{14}\ Fe_2P + O_2$	
$\frac{3}{4}\ LiFePO_4 \rightleftharpoons \frac{1}{4}\ Li_3PO_4 + \frac{5}{14}\ Fe_2P + \frac{1}{28}\ FeP_4 + O_2$	9
$2CO \rightleftharpoons 2C + O_2$	C
$2H_2O \rightleftharpoons 2H_2 + O_2$	H_2

Figure 6. Modified Ellingham diagram for reduction reactions in the $Li-Fe-P-O_2$ system.

Ong et al. (2008)

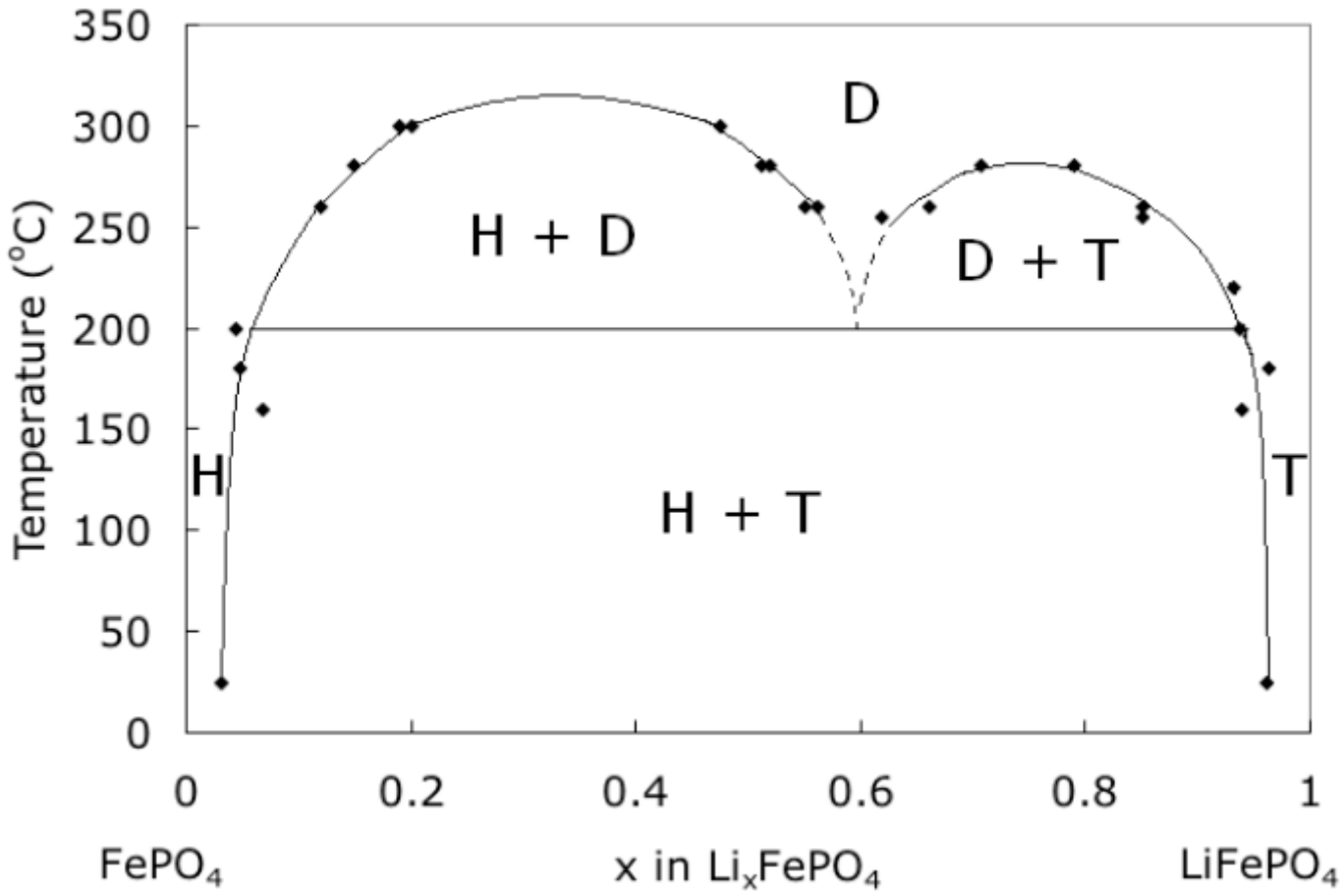

Figure 6. Phase diagram of $LiFePO_4$ (T, for triphylite) and $FePO_4$ (H, for heterosite) phases showing their merging to a solid solution (D, for disordered) in a eutectoid system. Data points at 25 °C are based on published work by Yamada [10]. The eutectoid point is around the composition x = 0.6 and temperature 200 °C. Above 200 °C, mixtures of heterosite or triphylite and the disordered phase were seen up to around 300 °C. Above 300 °C, the disordered phase dominates.

Li-Fe-P-O System

Dodd et al. (2006)

Li-Mn-O System

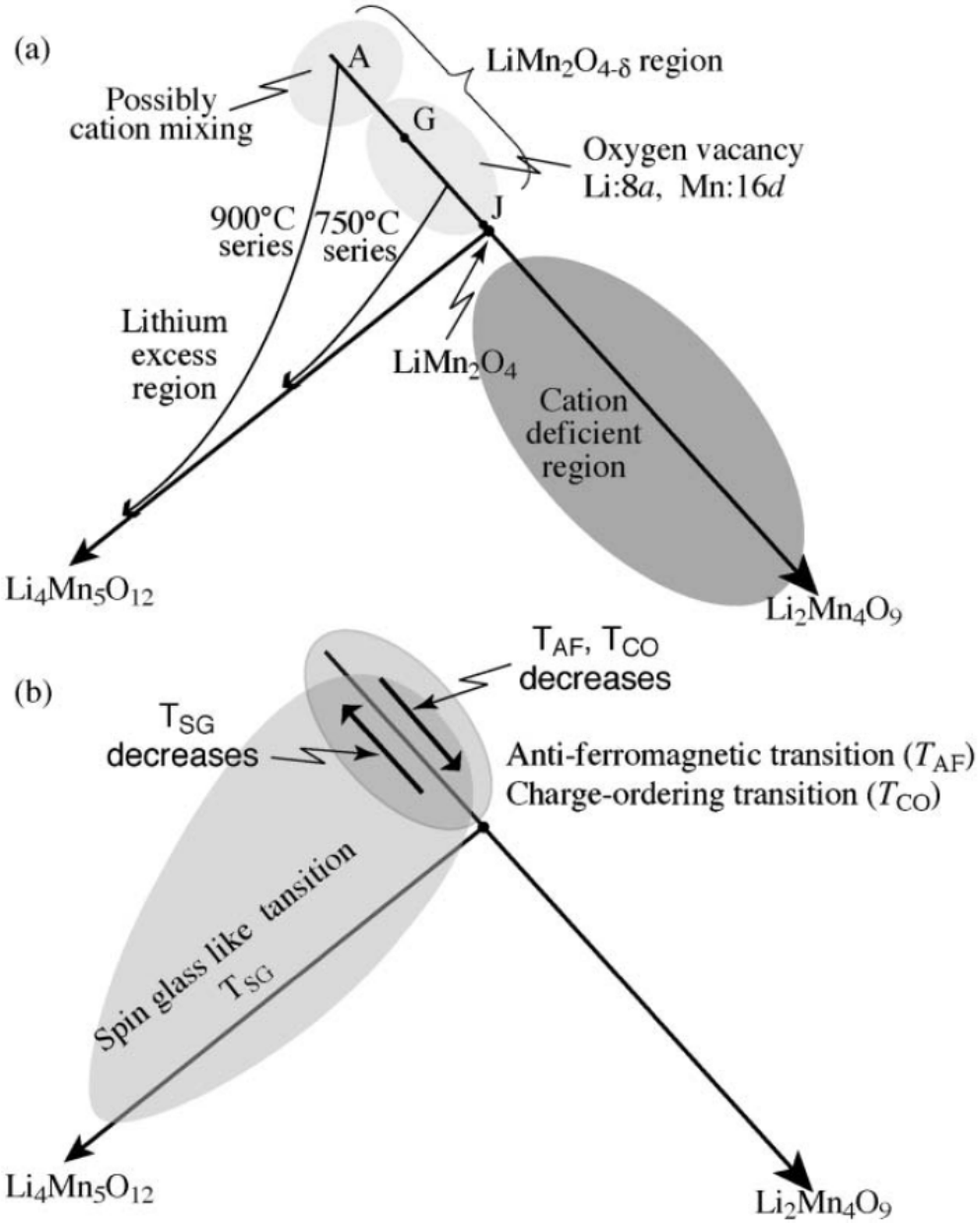

Detailed phase relationships in the subsystem
$LiMn_2O_4$ - $Li_4Mn_5O_{12}$ – $Li_2Mn_4O_9$ (Yonemura et al. 2004).

Li-Mn-O System

$p(O_2)$=0.21 atm

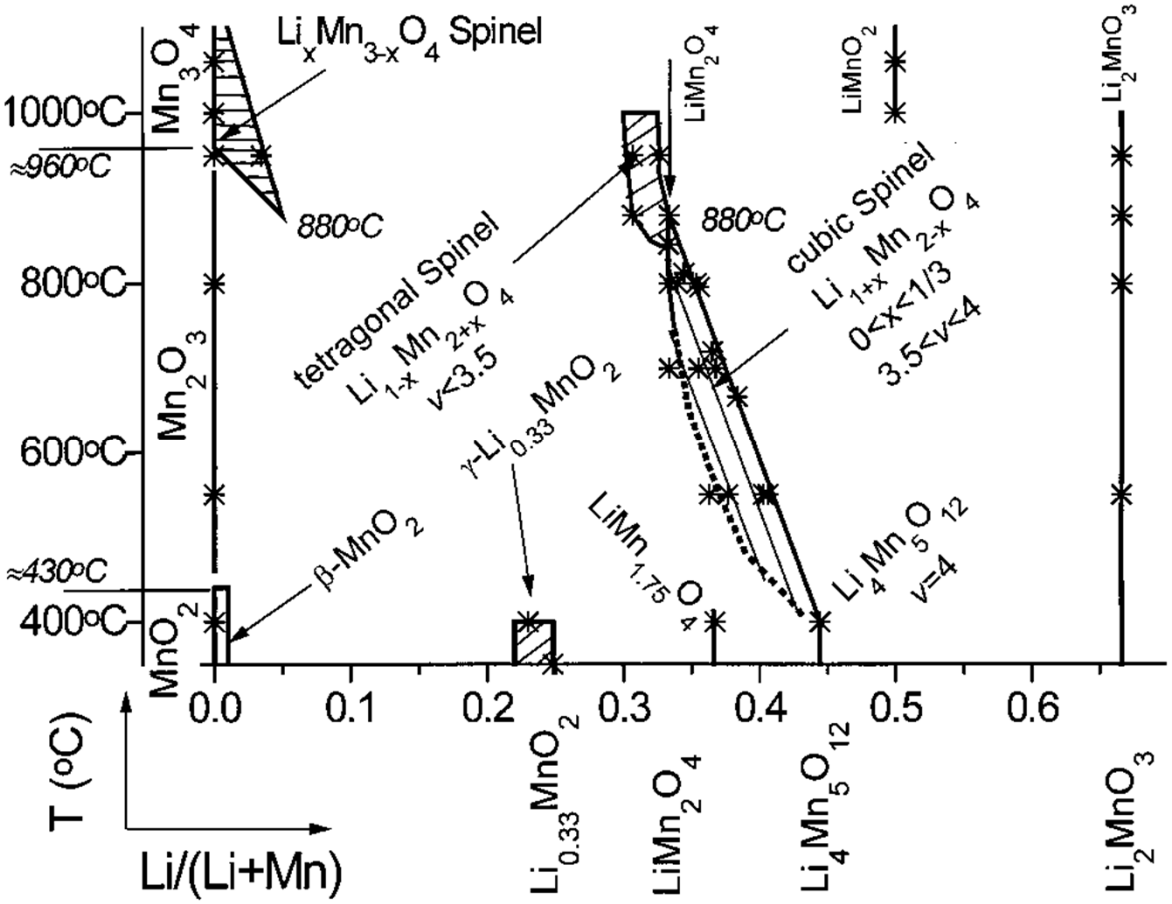

[1999Pau] Paulsen and Dahn, *Chem. Mater*., 11, 3065-3079, 1999

Lithium Ion Battery

discharging

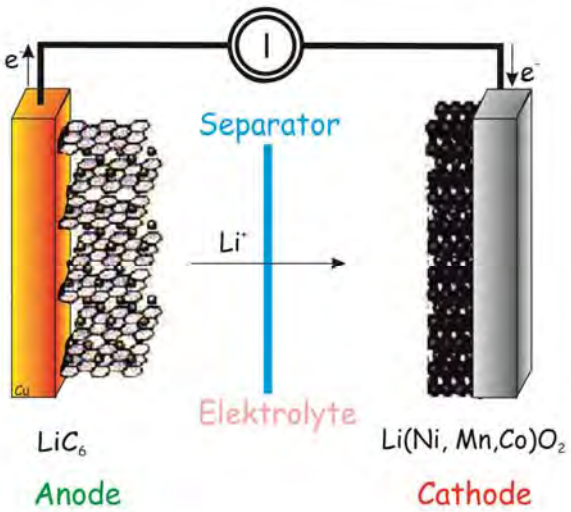

material of anode oxidized /
material of cathode reduced

$$LiC_6 \rightarrow Li_{1-x}C_6 + xLi^+ + xe^-$$

$$Li_{1-x}(Ni,Mn,Co)O_2 + xLi^+ + xe^- \rightarrow Li(Ni,Mn,Co)O_2$$

charging

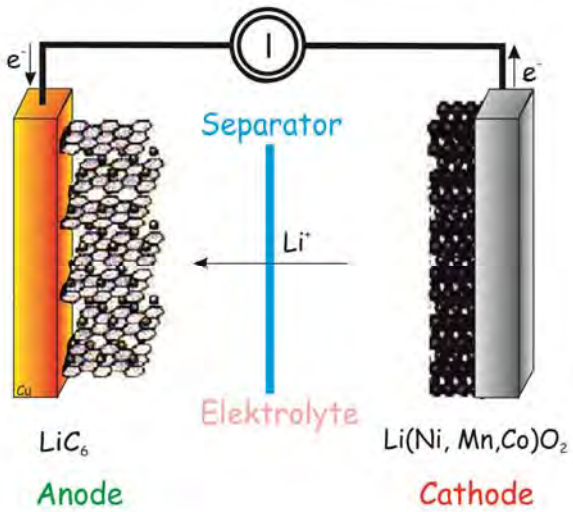

material of anode reduced /
material of cathode oxidized

$$Li_{1-x}C_6 + xLi^+ + xe^- \rightarrow LiC_6$$

$$Li(Ni,Mn,Co)O_2 \rightarrow Li_{1-x}(Ni,Mn,Co)O_2 + xLi^+ + xe^-$$

$$Li_{1-x}C_6 + Li(Ni,Mn,Co)O_2 \leftrightarrow Li_{1-x}(Ni,Mn,Co)O_2 + LiC_6$$

Li-Mn-O System

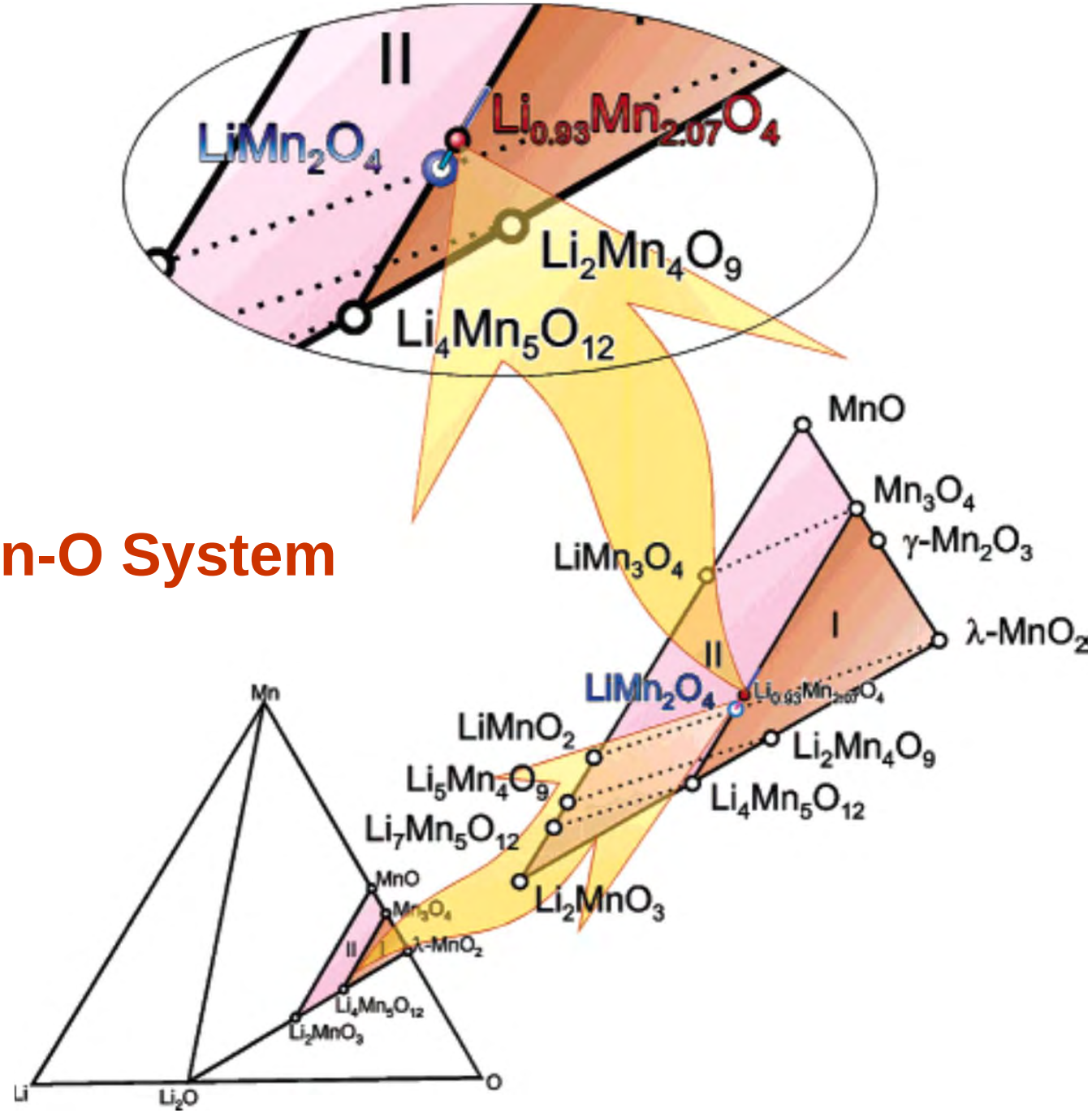

Li-Mn-O System

R. Huggins, Advanced Batteries

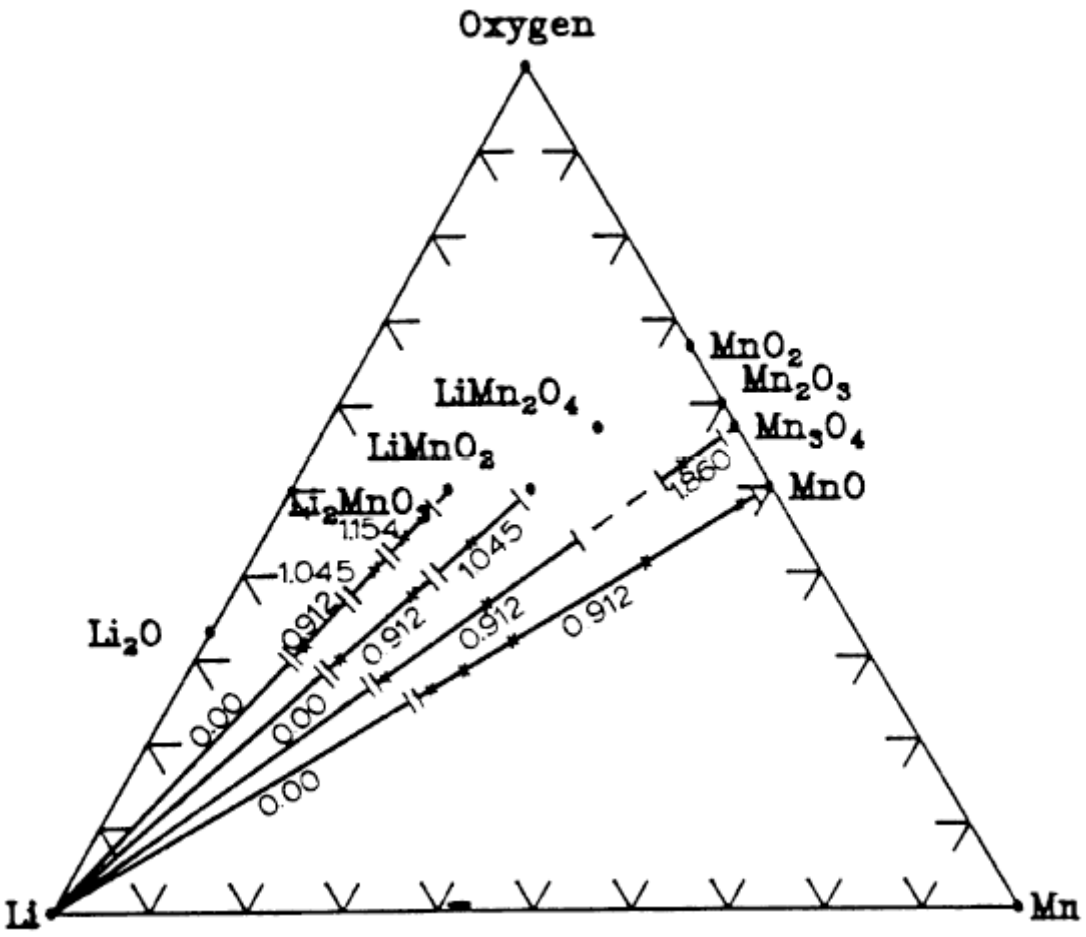

Heat generation rates

$$Q = \Delta G + T\Delta S + W_{el}$$

$$\Delta G = -nFE_{eq} \qquad \Delta S = nF\frac{dE_{eq}}{dT} \qquad W_{el} = -nFE$$

$$q = I\left[\left(E_{eq} - E\right) + T\frac{dE_{eq}}{dT}\right] + q_p$$

Sources of heat generation:

1. The "reversible" heat released (or absorbed) by the chemical reaction of the cell $q_{rev} = IT\frac{dE_{eq}}{dT}$
2. The "irreversible" heat generation by ohmic resistance and polarisation $q_{irrev} = I(E_{eq} - E)$
3. The heat generation by "side reactions", i.e. parasitic/corrosion reactions and "chemical shorts" q_p

S. Hallaj, H. Maleki, J.S. Hong, J.R. Selman, J. Power Source 83, p.1-8 (1999)

$C_{p,\ eff}$ measurement on a 40Ah pouch cell

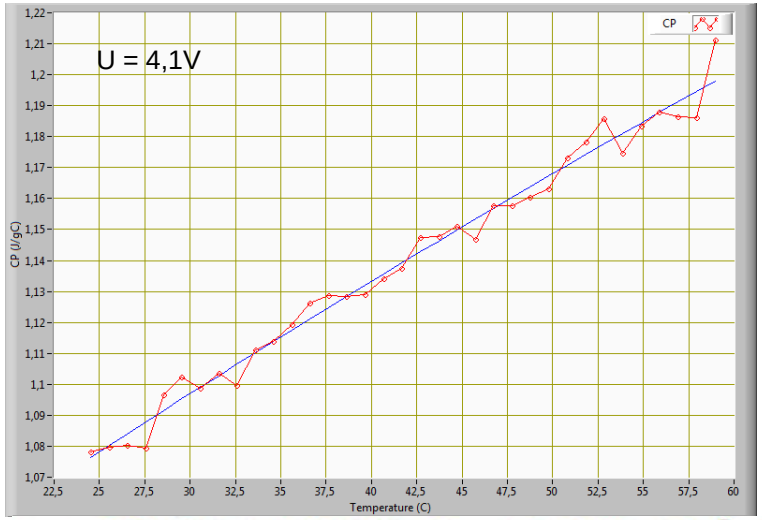

$$c_p = 0{,}96511 + 0{,}00491 \cdot T - 1{,}76899 \cdot 10^{-5} \cdot T^2$$

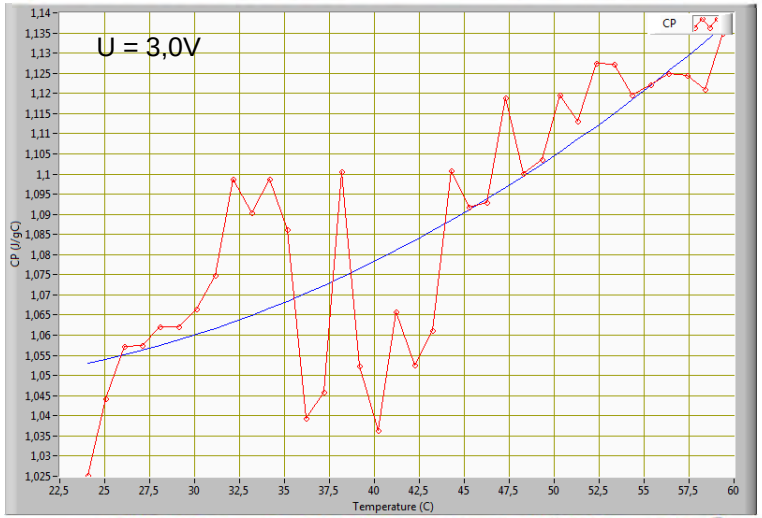

$$c_p = 1{,}05414 - 0{,}00102 \cdot T + 4{,}05094 \cdot 10^{-5} * T^2$$

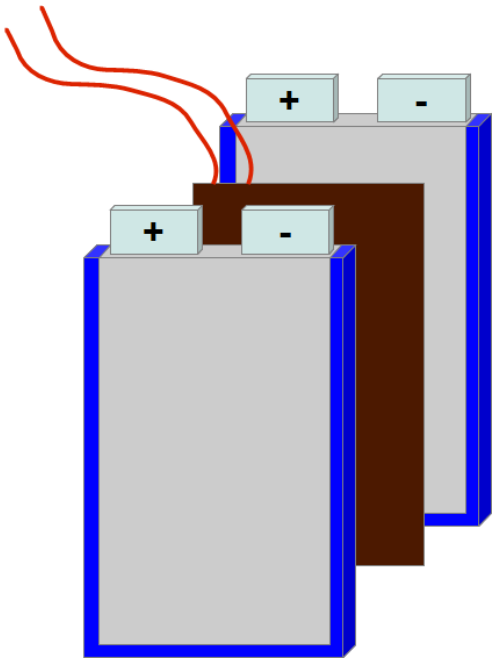

$$c_p = \frac{q}{m\Delta T} \qquad q = \int U \cdot I dt$$

Separation of reversible and irreversible parts

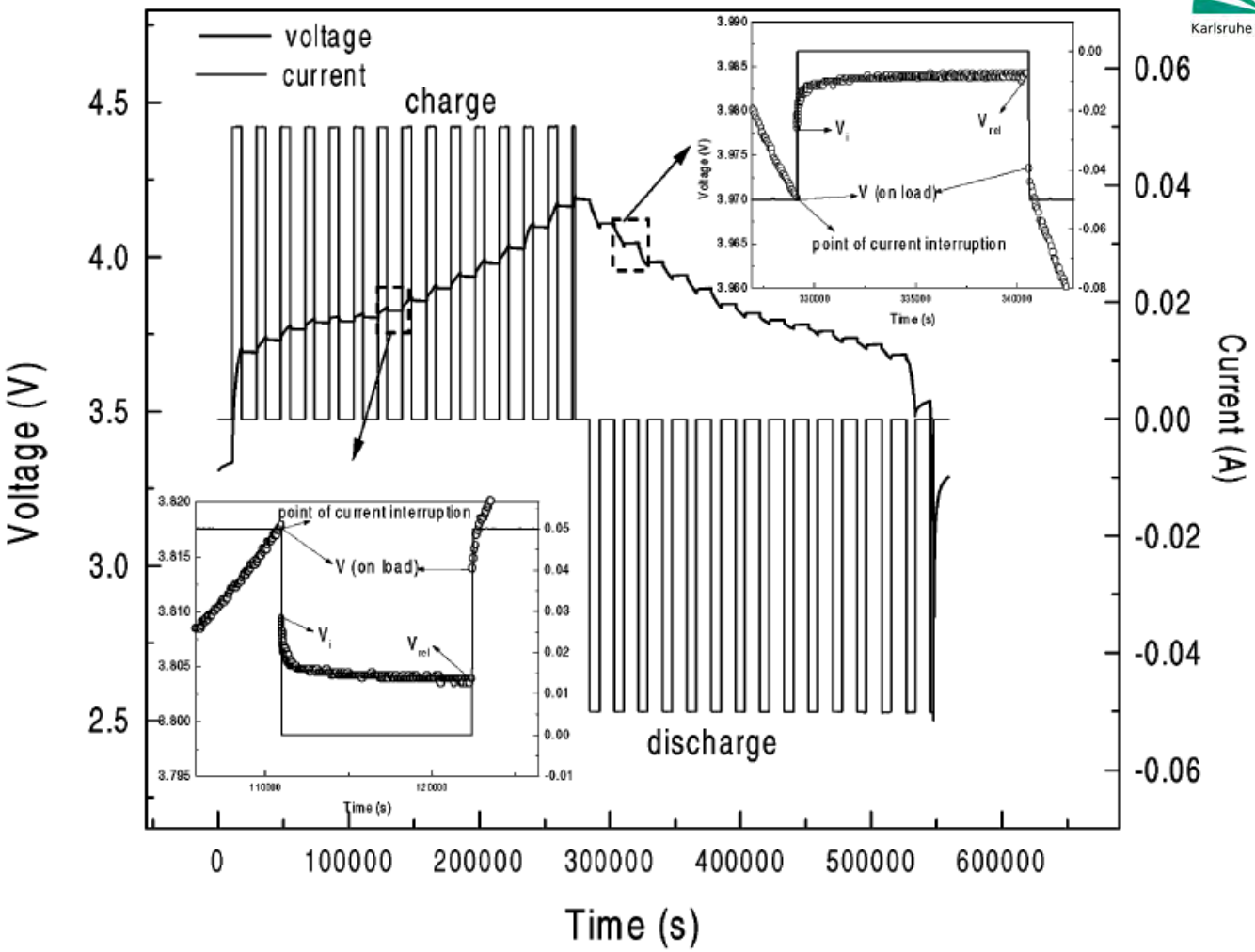

$$Q_{rev} = n_{Li} T \Delta S = T \left(\frac{\partial E_{eq}}{\partial T} \right) (It)_{dc}$$

J.R. Selman, S. Hallaj , J. Power Source 97-98, p.726-732 (2001)

Enthalpy of Drop Solution of $Li_{1+x}Mn_{2-x}O_{4-\delta}$

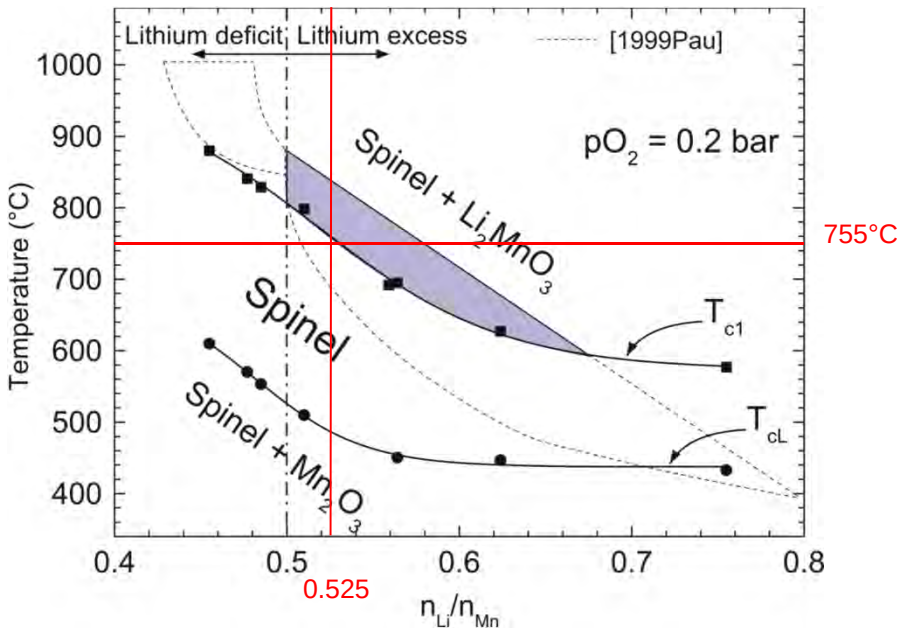

Li-Mn-O Temperature-Composition Ratio Section

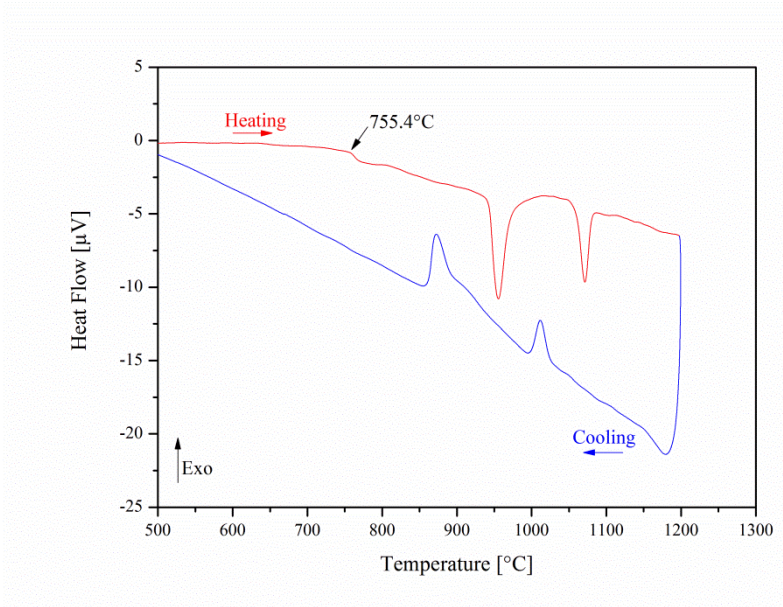

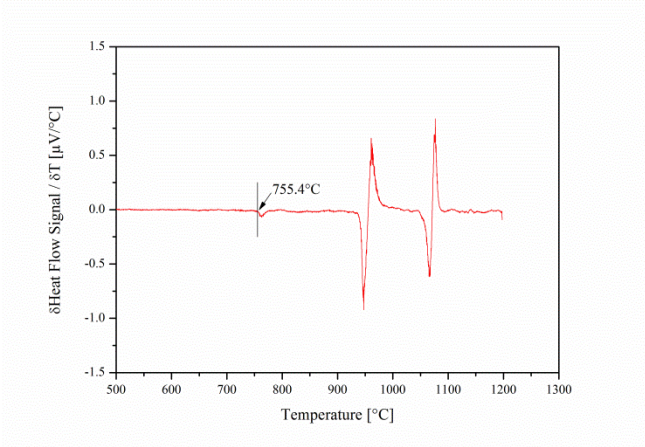

- Samples prepared using a modified Pechini method
- The homogeneity range of the spinel phase determined using thermogravimmetric analysis at po_2=0.2 atm

Li-rich boundary of the homogeneity range $Li_{1+x}Mn_{2-x}O_4$ should be refined

Li-Mn-O System

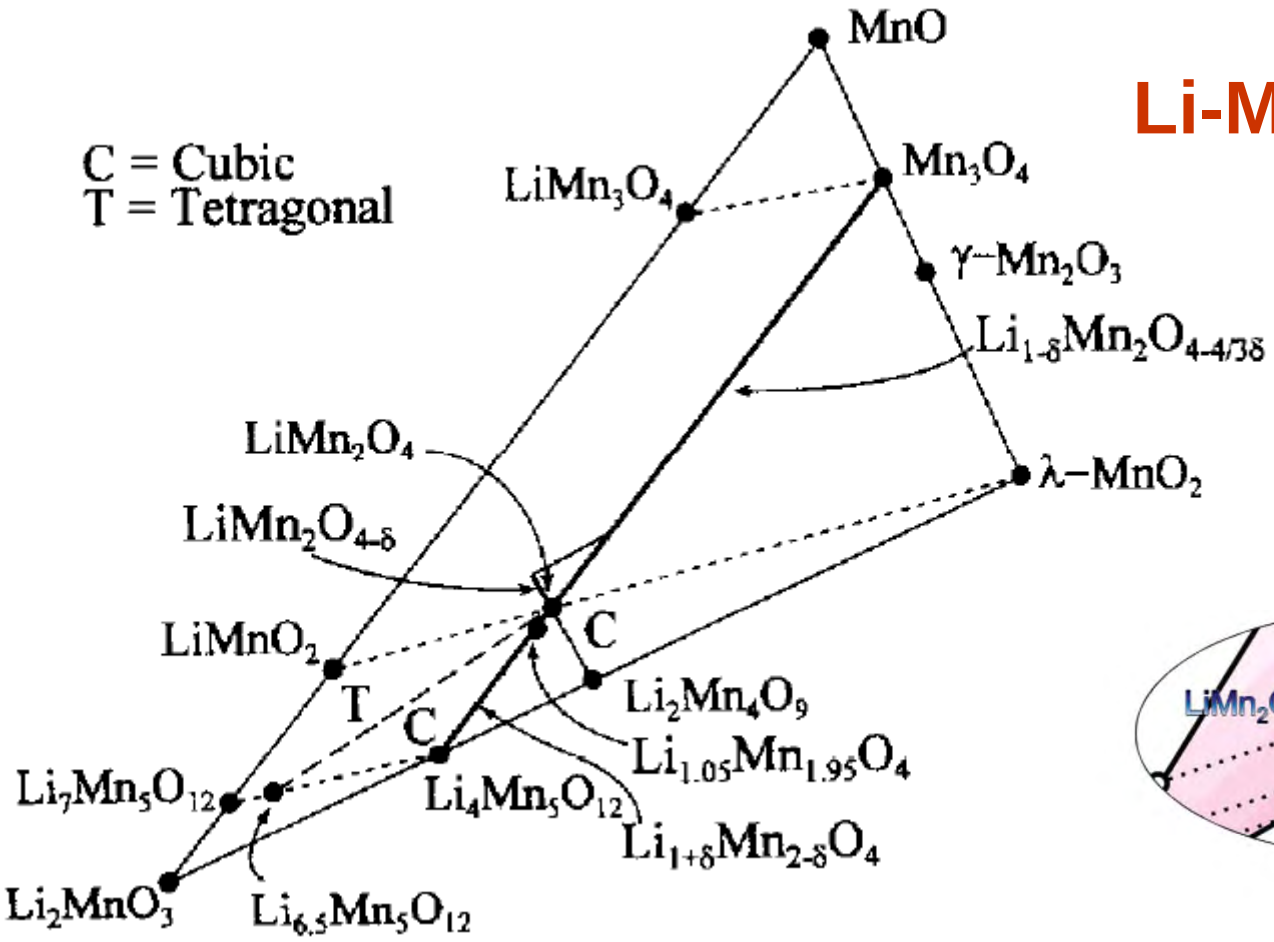

Section in the Li-Mn-O phase diagram (Thackeray et al., 1995).

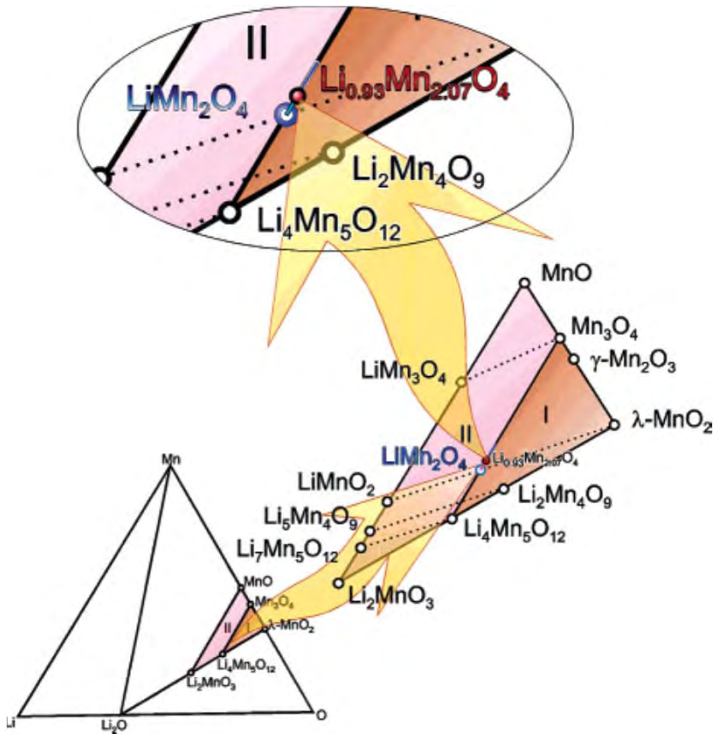

Li-Mn-O System, sample preparation

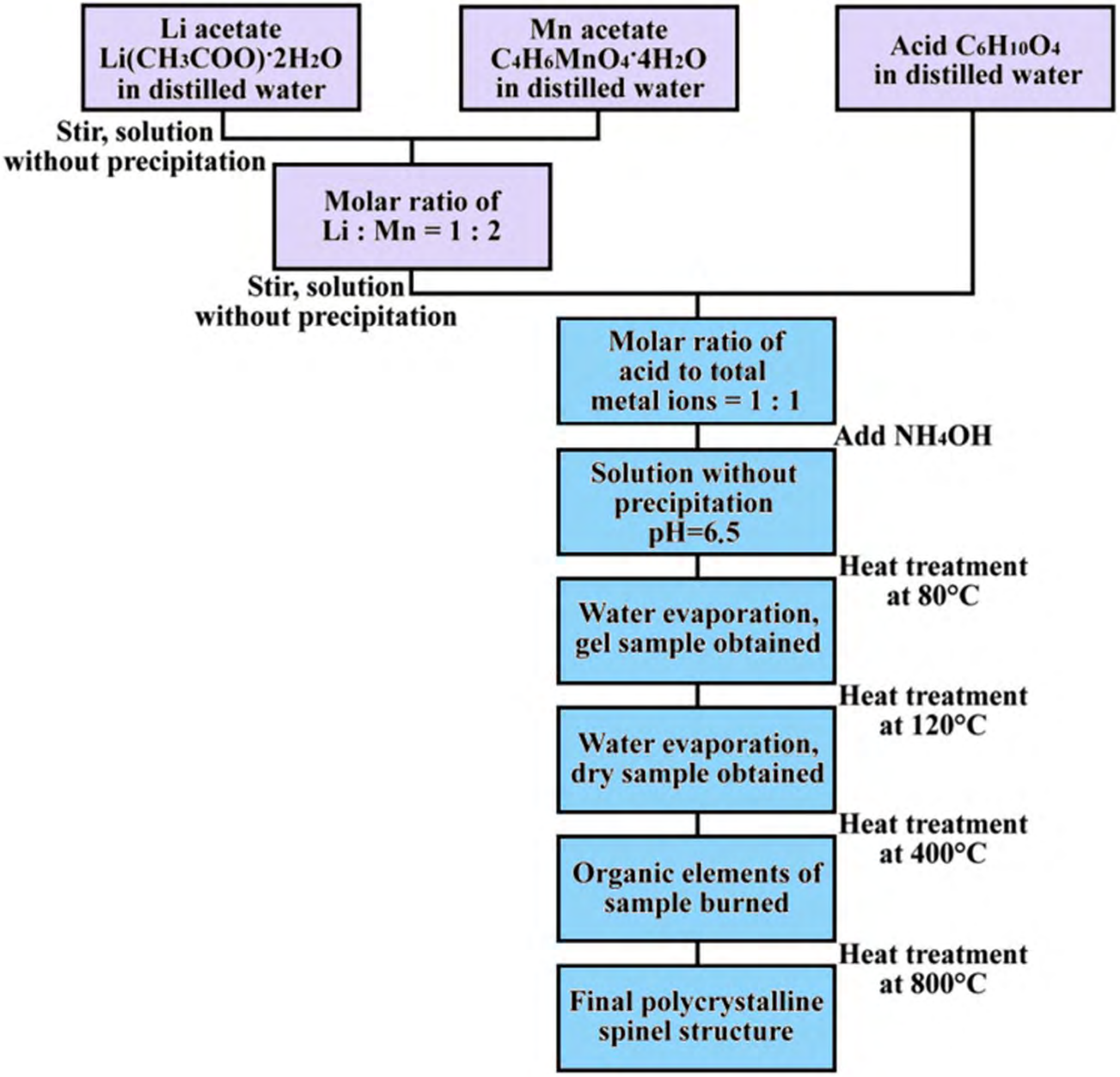

Li-Mn-O System

- Decomposition of $LiMn_2O_4$ in air
- Samples heat treated at 15 hours and quenched in liquid nitrogen

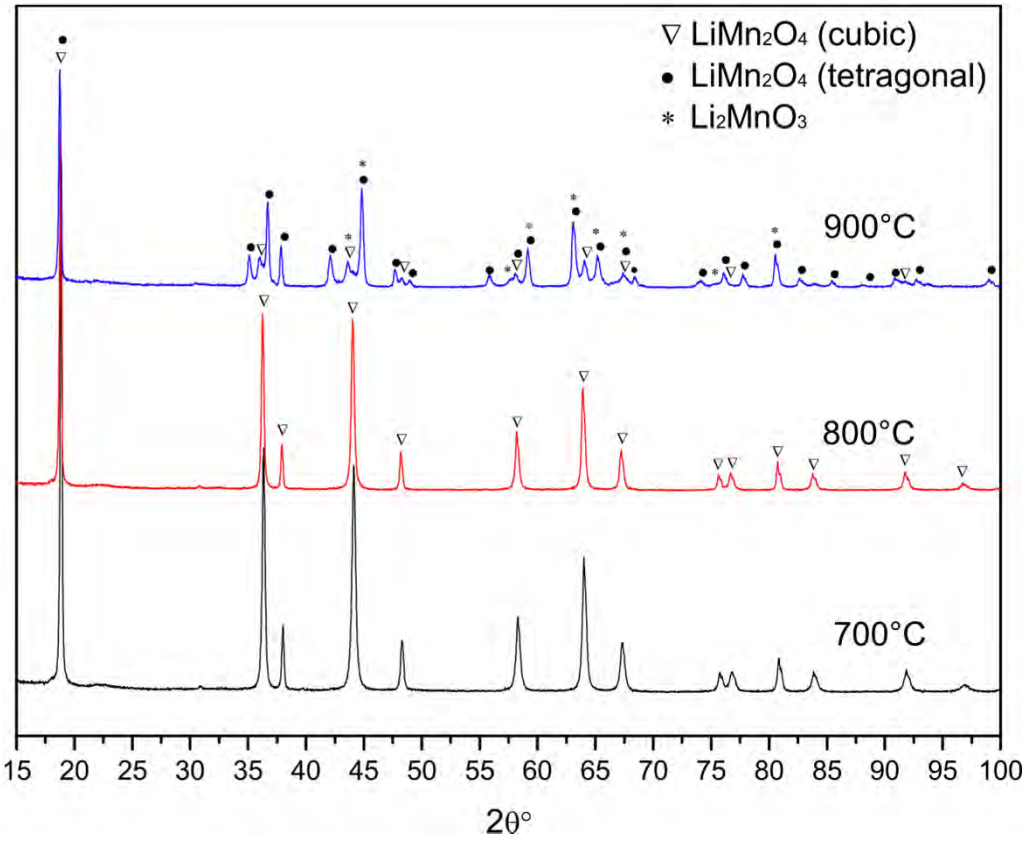

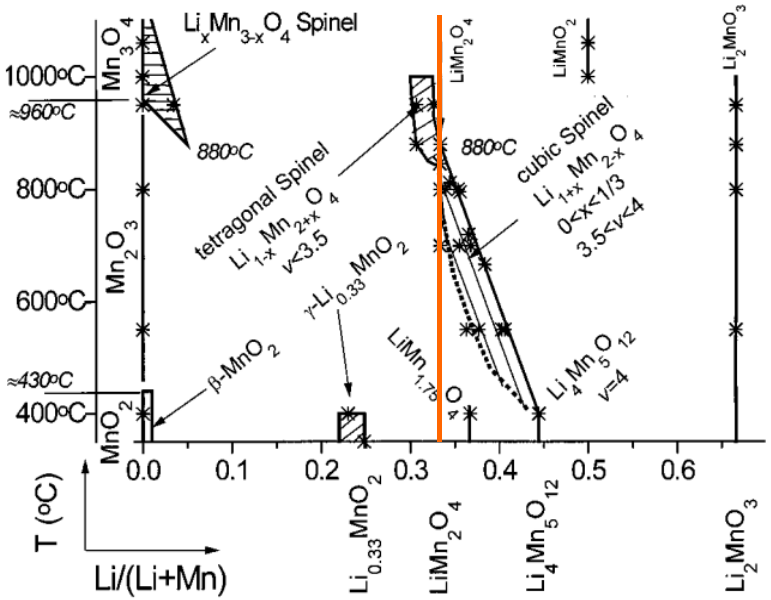

In-situ technique “entropymetry”

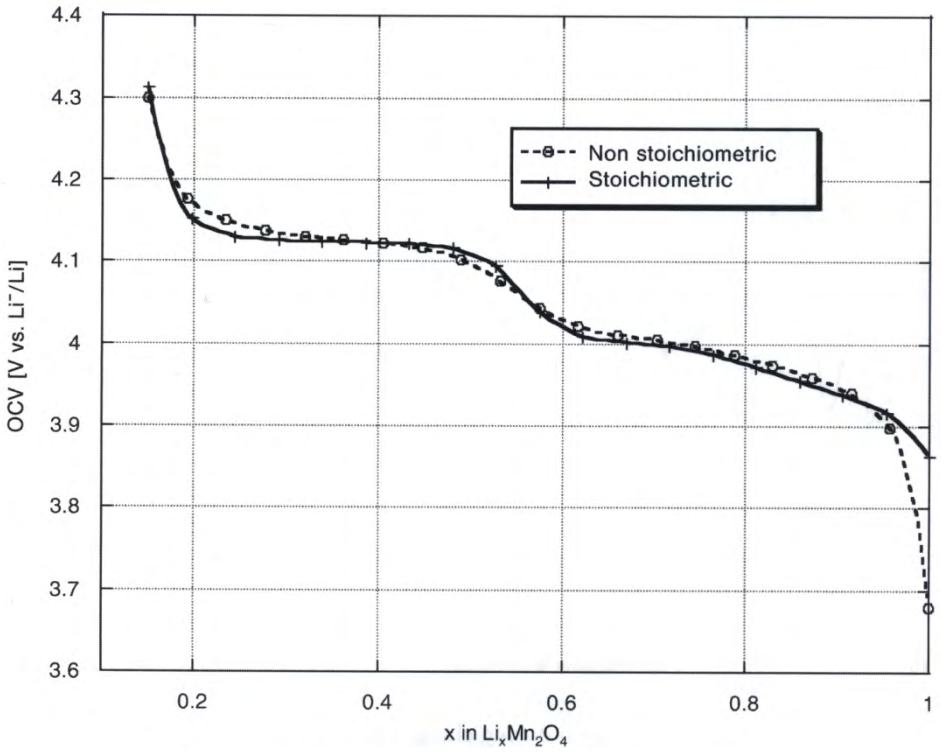

Open circuit voltage as a function of Li concentration in $LiMn_2O_4$

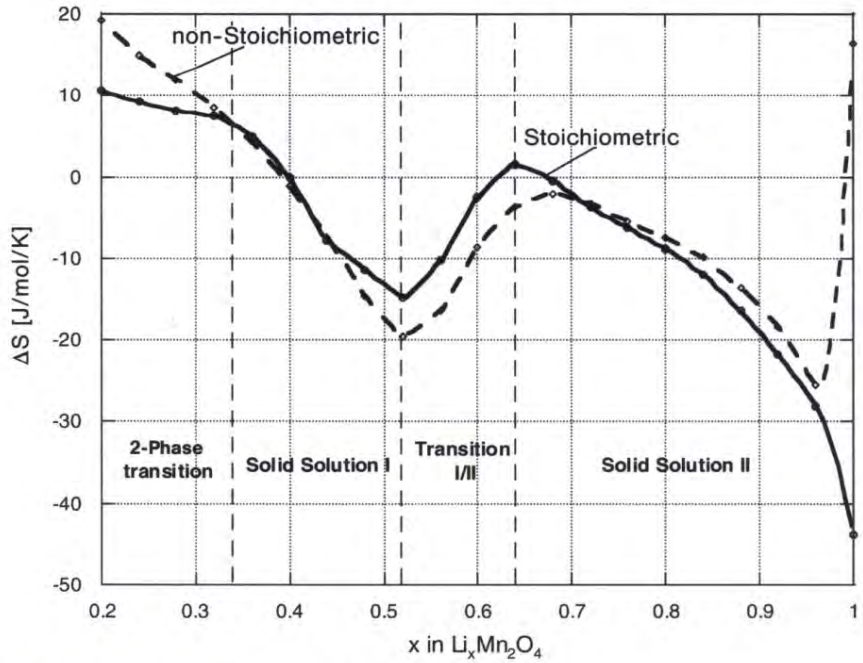

Entropy as a function of Li concentration in $LiMn_2O_4$

Note: Half cells measured

Yazami et al. in Lithium Ion Rechargeable Batteries, WILEY-VCH (2010)

2nd kind phase diagram in the Li-Mn-O system

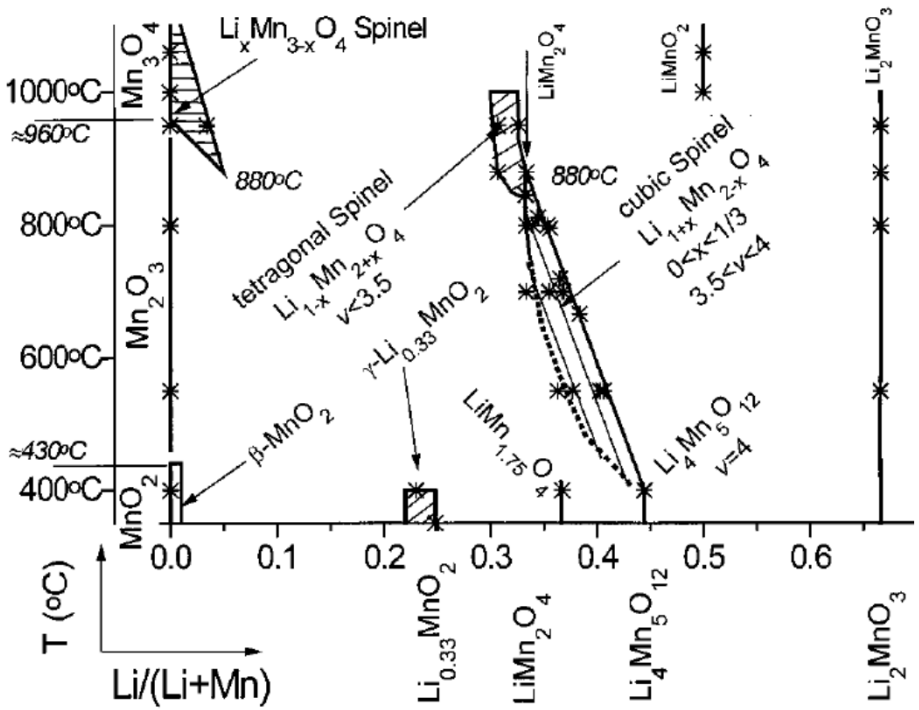

Paulsen and Dahn, 1999

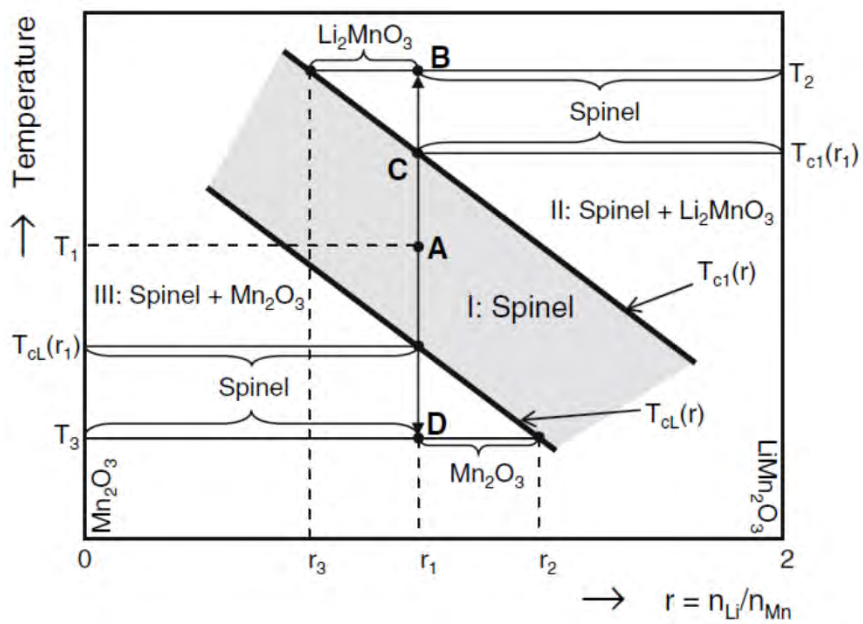

Luo and Martin, 2007

Li-Mn-O System

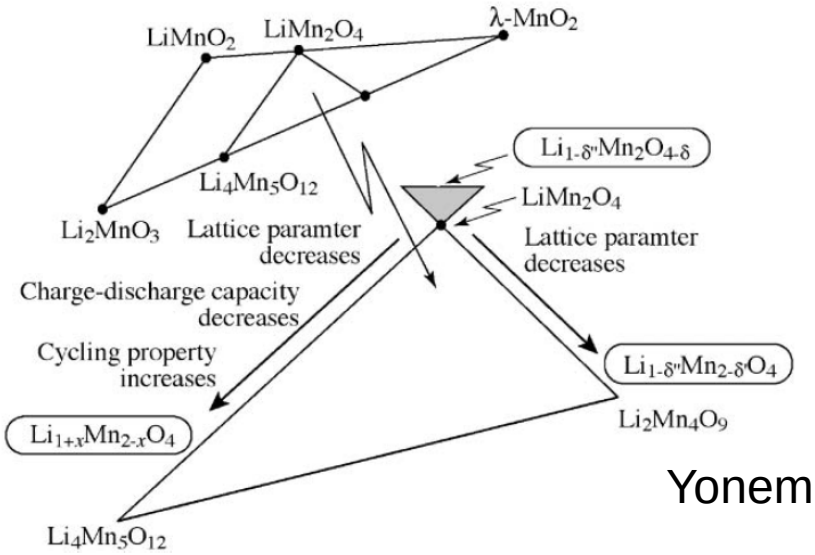

Yonemura et al. 2004

German Research Foundation, Priority Program 1473,
Materials with New Design for Improved Lithium Ion Batteries - WeNDeLIB

Battery Properties	Thermodynamics and Kinetics
Thermal runaway	Oxygen partial pressure, Gibbs free energies of reactions
Voltage, potential	Chemical potentials (of lithium)
Capacity, energy- and power density	Phase diagrams, Gibbs free energies
Life time	Stability of compounds in battery; Materials constitution
Power- and materials loss during first charge cycle	Formation of SEI; Relative thermochemical stabilities of materials for electrodes and electrolyte

Relationships Thermodynamics and Electrochemistry

Total change in enthalpy and entropy between two electrode compositions x_1 and x_2:

$$\overline{\Delta S}\Big|_{x1}^{x2} = F\left(\int_{x1}^{x2} \frac{\partial E_0(x,T)}{\partial T}\bigg|_x\right)$$

$$\overline{\Delta H}\Big|_{x1}^{x2} = F\int_{x1}^{x2}\left(-E_0(x,T) + T\frac{\partial E_0(x,T)}{\partial T}\bigg|_x dx\right)$$

… and with normalization $$y = \frac{x}{\Delta x_{\max}},\ 0 < y < 1$$

$$\overline{\Delta S}\Big|_{0}^{1} = F\left(\int_{0}^{1} \frac{\partial E_0(y,T)}{\partial T}\bigg|_y dy\right)$$

$$\overline{\Delta H}\Big|_{0}^{1} = F\int_{0}^{1}\left(-E_0(y,T) + T\frac{\partial E_0(y,T)}{\partial T}\bigg|_y dy\right)$$

Thermodynamic functions of active materials are needed

Battery technology spider chart (USABC) for electrical vehicles (EV)

Specific Power
Discharge: 300 W/kg

Operating temperature:
-40 to +50°C

Specific Energy at C/3:
150 Wh/kg

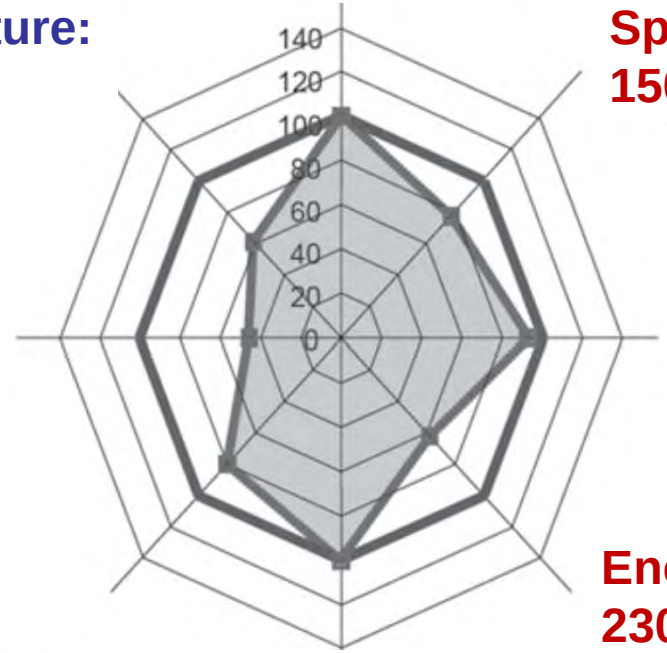

Selling price at
10k/Jahr: 150$/kWh

Power density:
460 W/l

Calendar life:
10 years

Energy density at C/3:
230 Wh/l

Cycle life at
80% DOD: 1000 Cycles

Sources:

(1) D. Howell, Energy Storage Research and Development, Annual Progress Report 2006 (Washington, D.C.: Office of FreedomCAR and Vehicle Technologies, U.S. Department of Energy, 2007)

(2) FreedomCAR and Fuel Partnership and United States Advanced Battery Consortium (USABC), Electrochemical Energy Storage Technical Team Technology Development Roadmap (Southfield, MI: USCAR, 2006)

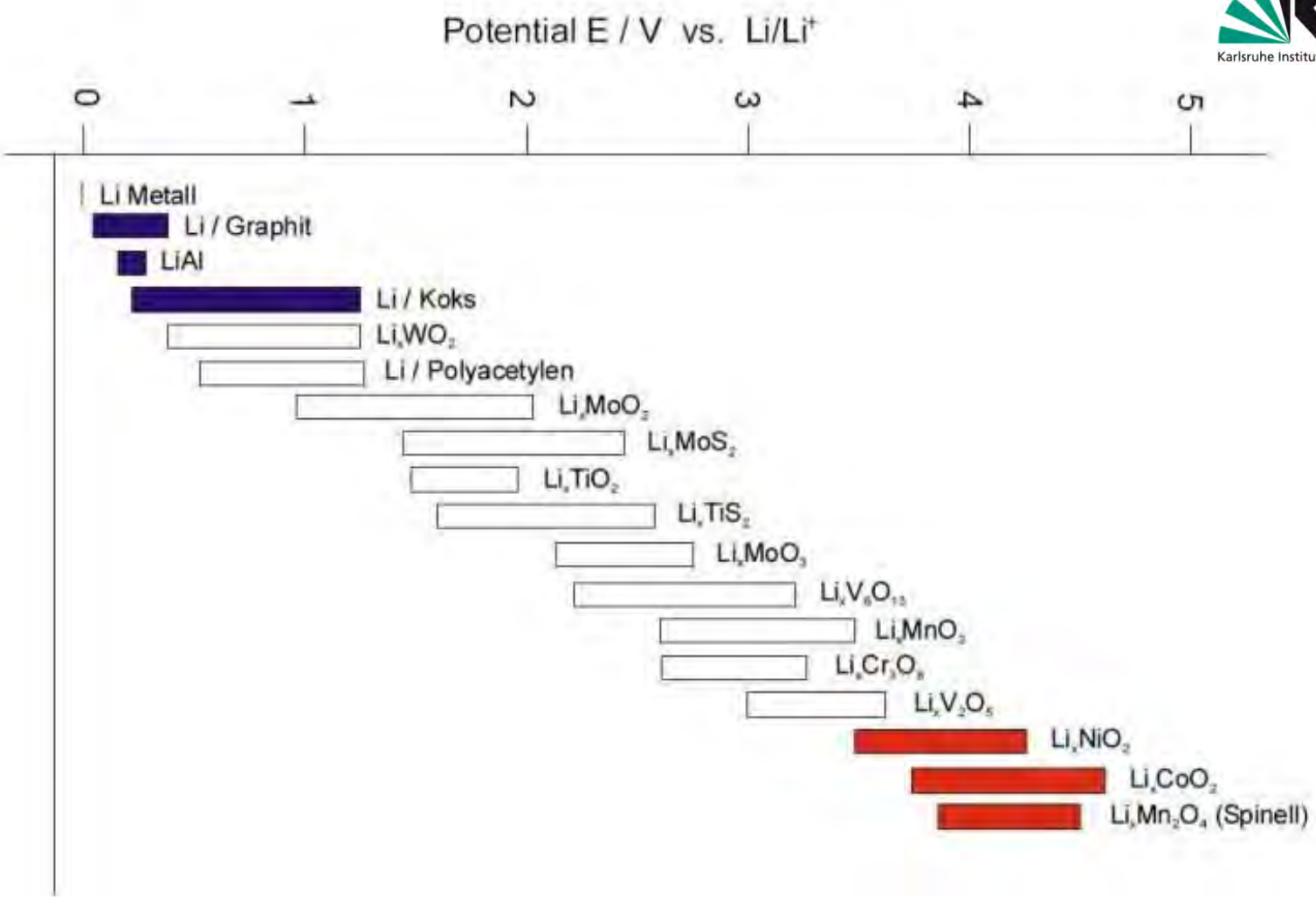

M Winter, J. O. Besenhard, Chem. uns. Zeit 33, p. 320-332 (1999)

Li-Cu-Fe-O System

- Thermodynamic calculations based on the CALPHAD method
  - predict battery performance

    equilibrium voltages (OCV)

    plateau capacities

- Database development for the **Li-Cu-Fe-O** System
  - The **Cu-Fe-O** ternary system assessed by Khvan et al.
  - First calculated phase diagrams in the **Li-Cu-O** system addressed in present work

N. Saunders, I. Ansara (Ed), Cost 507, Report,1994,168–169

B. Hallstedt,L.J. Gauckler CALPHAD, 2003, 27:177-191

K. Chang, B. Hallstedt, CALPHAD, 2011, 35:160-164

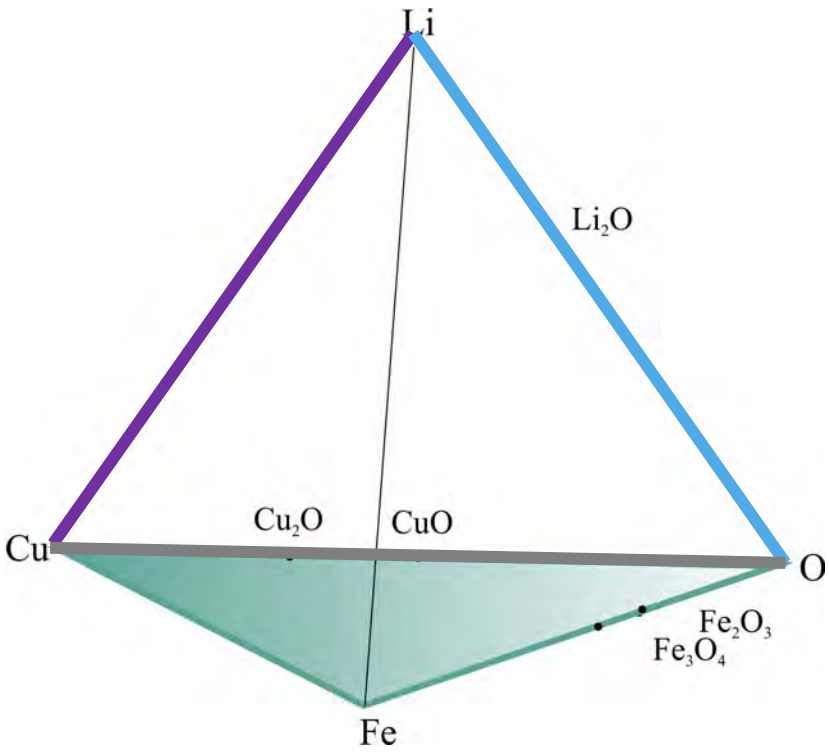

Isothermal calorimetric measurements on a 16 mAh Lithium ion coin cell

Discharge parameters:

- Method: constant current (CC)
- U_{min} = 2.75 V
- I = 16 mA → 1C-rate

Charge parameters:

- Method: constant current, constant voltage (CCCV)
- U_{max} = 4.25 V
- I = 16 mA → 1C-rate
- I_{min} = 1.6 mA

Isothermal Battery Calorimeter (IBC)

Cell type: coin cell LIR 2016,
Conrad energy (commercial)
Capacity: 20 ± 5 mAh; Working voltage: 3.6 V

Isothermal calorimetric measurements on a 16 mAh Lithium ion coin cell

Temperature T_{env} = 20 °C

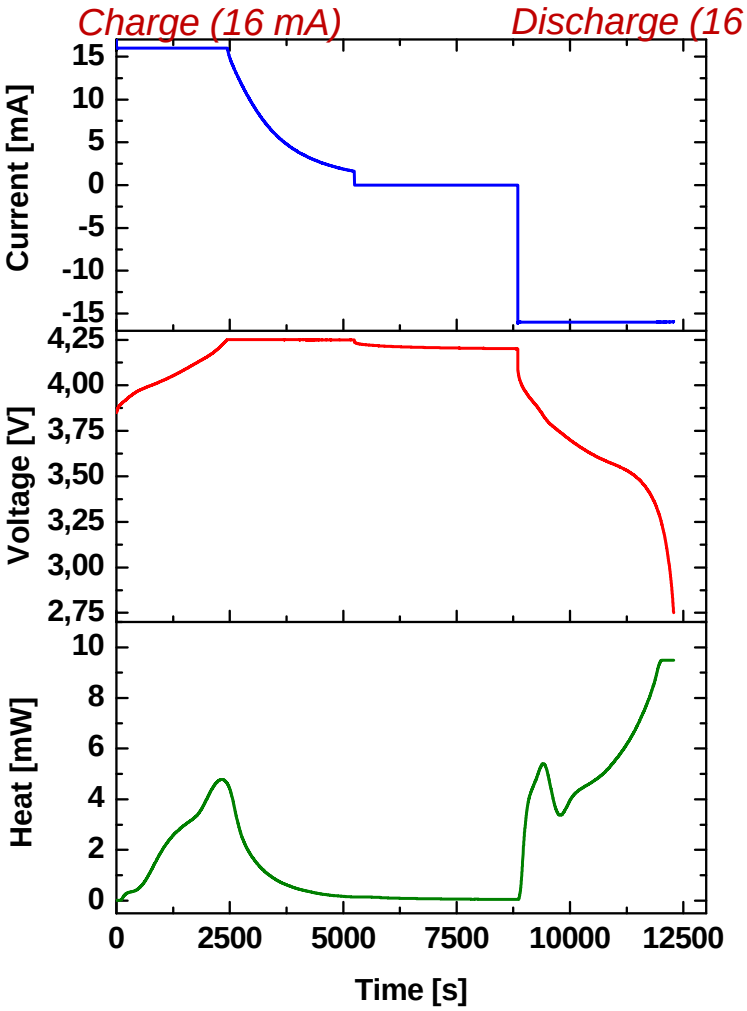

Temperature T_{env} = 40 °C

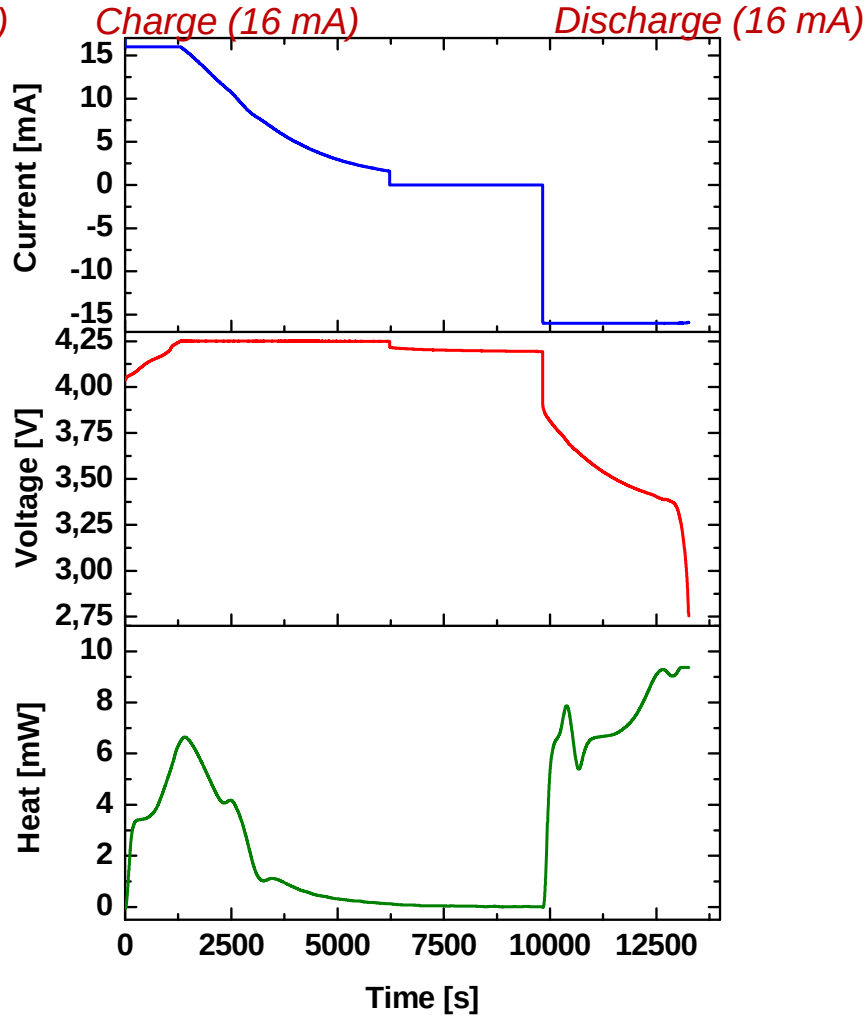

Accelerating Rate Calorimeter (ARC)

ARC provides an adiabatic environment in which a sample may be studied under conditions of negligible heat loss

heat of reaction: $\Delta H = \Delta T_{ad} c_p$

total heat generated: $Q_\Sigma = m\Delta H$

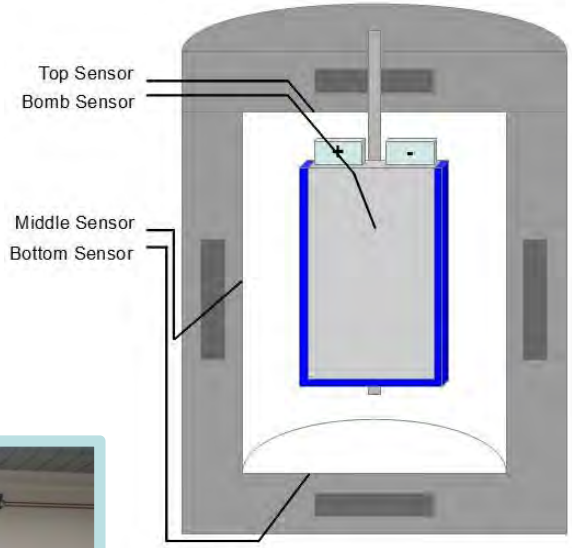

EVARC: Ø: 25cm
h: 50cm

ESARC: Ø: 10cm
h: 10cm

$$T = 20 \ldots 500°C$$

$$\Delta T_{det} = 0{,}005K$$

Thermodynamics of electrochemical reactions

Thermal Runaway

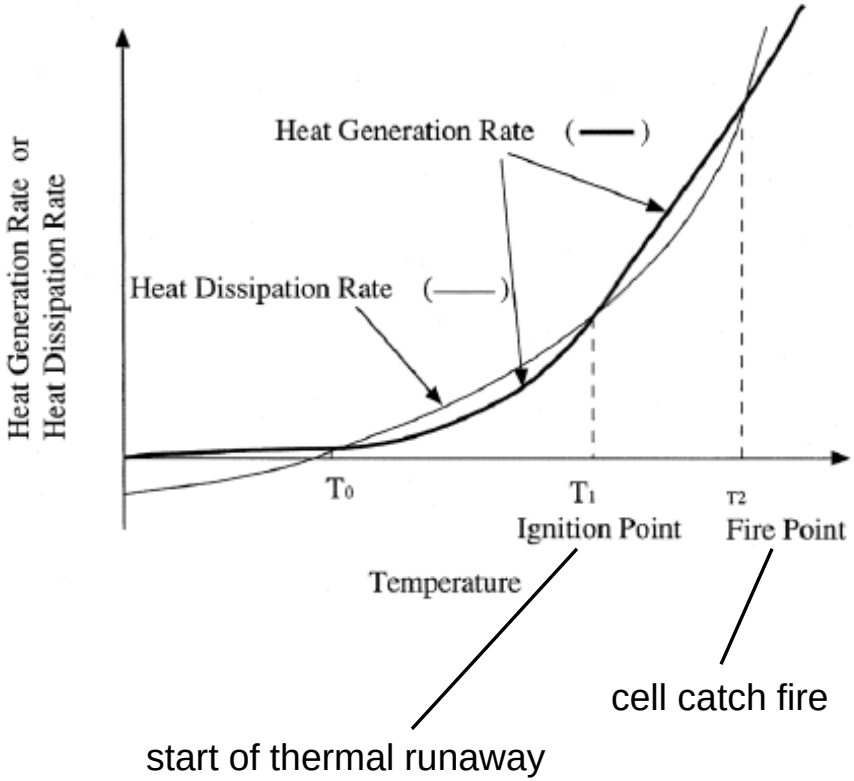

electrochemical reaction

$$\Delta G = -nFE$$

Gibbs-Helmholtz equation

$$\Delta S = -\left(\frac{\delta \Delta G}{\delta T}\right)$$

entropic change of electrochem. reaction

$$\Delta S = nF\left(\frac{\delta E}{\delta T}\right)$$

reversible heat

$$Q_{rev} = T\Delta S = nFT\left(\frac{\delta E}{\delta T}\right)$$

S. Tobishima, J.Yamaki, J. Power Source 81-82, p. 882–886 (1999)

A.K. Shukla, T.P. Kumar, Current Sci. 94, p. 314-331 (2008)

Enthalpy of Drop Solution of $Li_{1+x}Mn_{2-x}O_{4-\delta}$

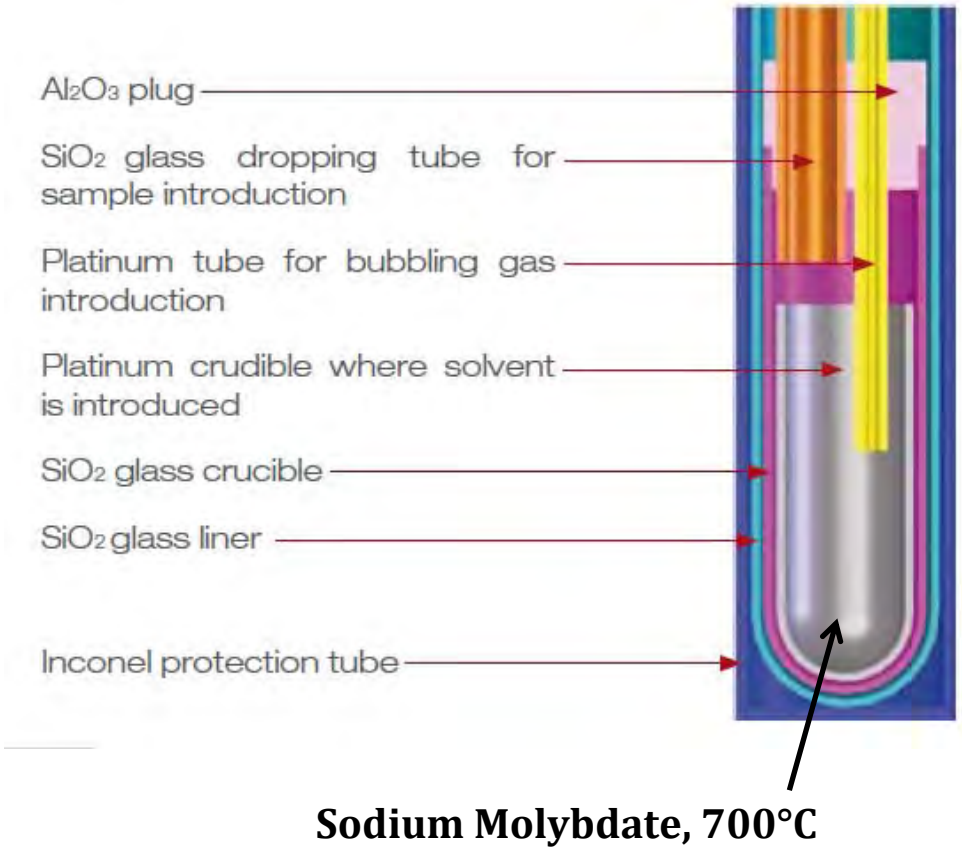

AlexSys 1000, SETARAM

High Temperature Calvet Calorimeter

Enthalpy of Drop Solution of $Li_{1+x}Mn_{2-x}O_{4-\delta}$

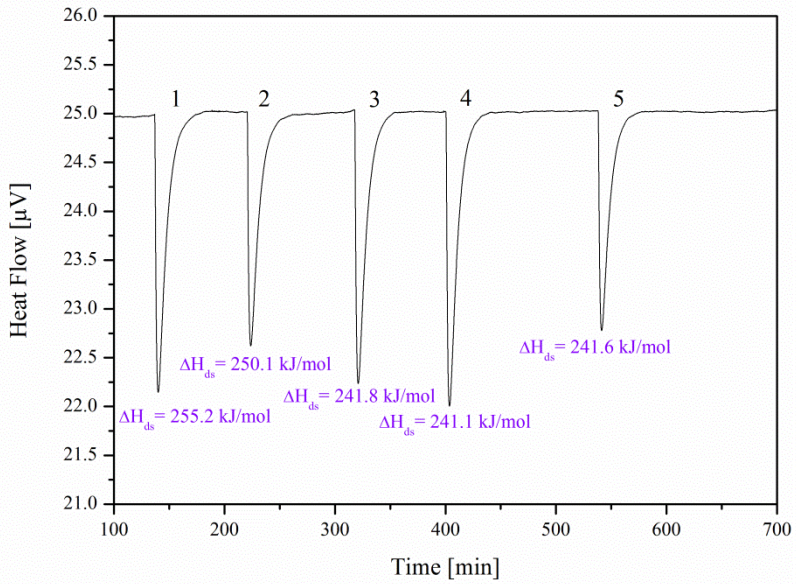

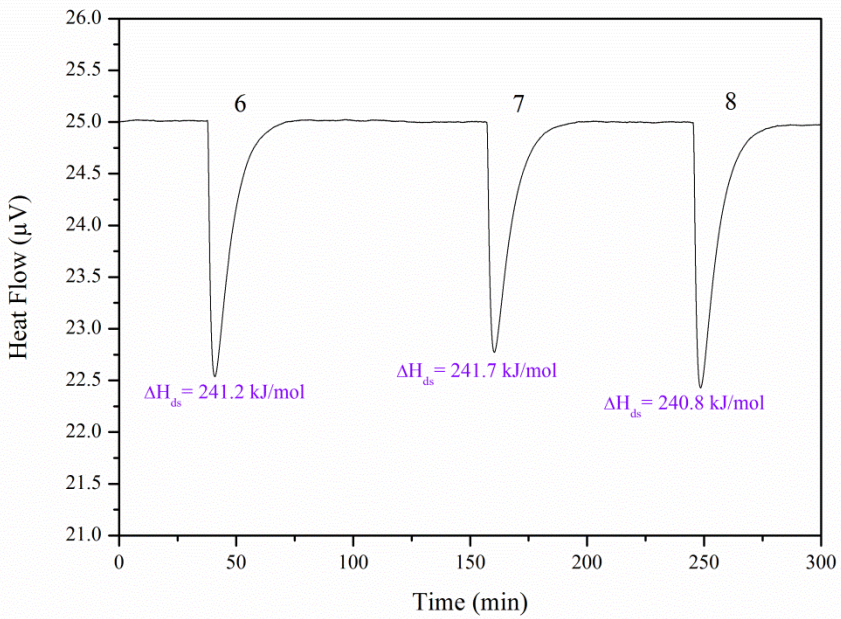

Sample Number	DROP 1	DROP 2	DROP 3	DROP 4	DROP 5	DROP 6	DROP 7	DROP 8
Date	08. Mai	08. Mai	08. Mai	08. Mai	08. Mai	09. Mai	09. Mai	09. Mai
Mass pellet (mg)	*6,00*	*5,14*	*6,10*	*6,62*	*4,85*	*5,35*	*4,83*	*5,59*
T(room) (°C)	*23,90*	*24,10*	*24,20*	*24,10*	*24,20*	*24,50*	*24,30*	*24,20*
T(cal.) (°C)	700,40	700,40	700,40	700,40	700,40	700,40	700,40	700,40
Formula weight (g/mol)	180,815	180,815	180,815	180,815	180,815	180,815	180,815	180,815
Moles of LiMn2O4 (mol)	0,0000332	0,0000284	0,0000337	0,0000366	0,0000268	0,0000296	0,0000267	0,0000309
Peak Area [µV.s]	1832,4170	1538,5640	1765,6030	1910,2030	1402,3320	1544,6110	1397,2290	1611,2630
Calibration factor from Al_2O_3 calibration[J/µV.s]	**0,00462077**	**0,00462077**	**0,00462077**	**0,00462077**	**0,00462077**	**0,00462077**	**0,00462077**	**0,00462077**
Measured Heat Effect (kJ/mol)	**255,1652**	**250,0926**	**241,8308**	**241,0849**	**241,5781**	**241,2203**	**241,6957**	**240,8258**
Accepted Measurement	0	0	1	1	1	1	1	1

2nd kind phase diagram in the Li-Mn-O system

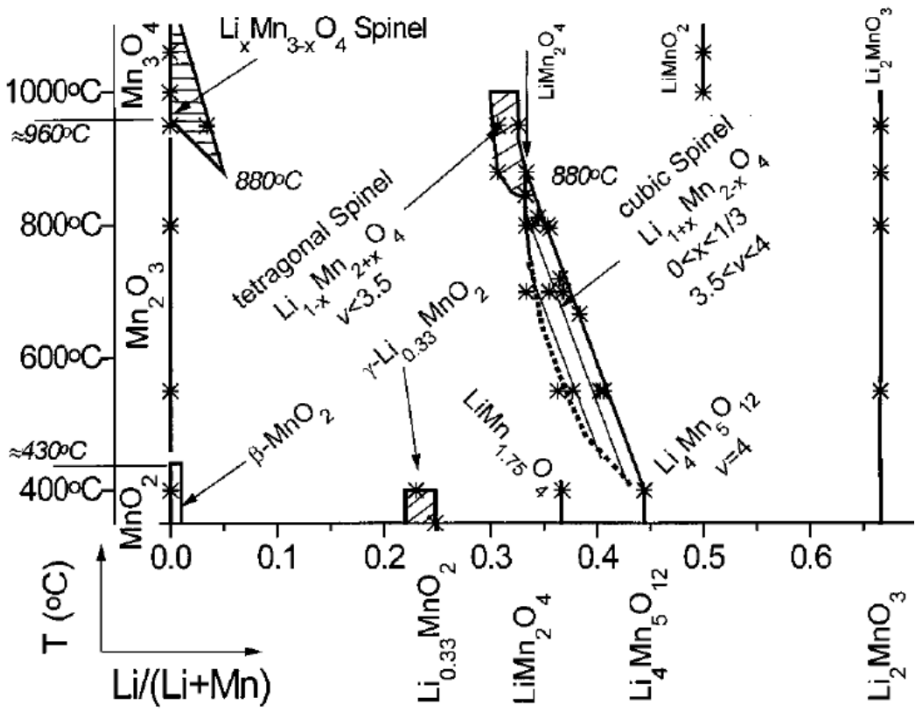

Paulsen and Dahn, 1999

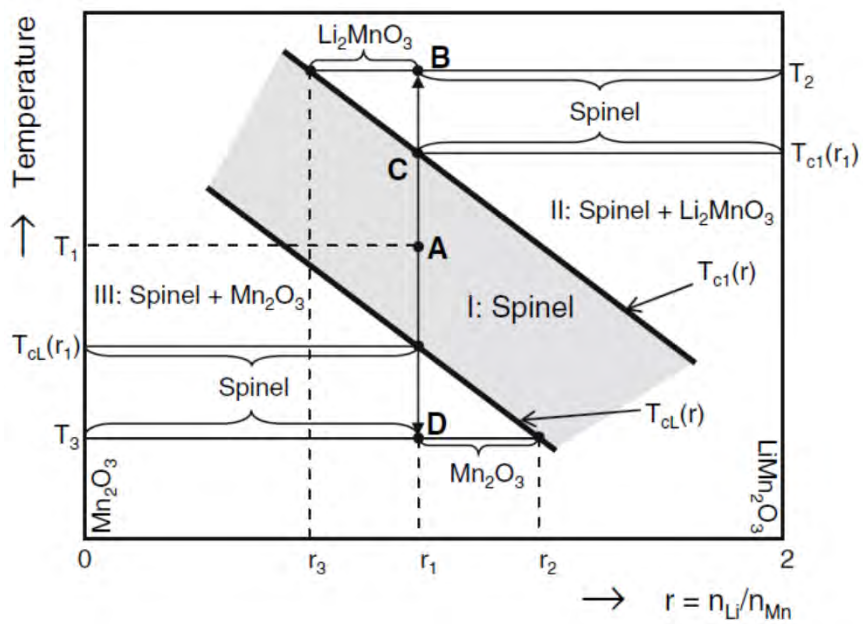

Luo and Martin, 2007

Li-Mn-O System

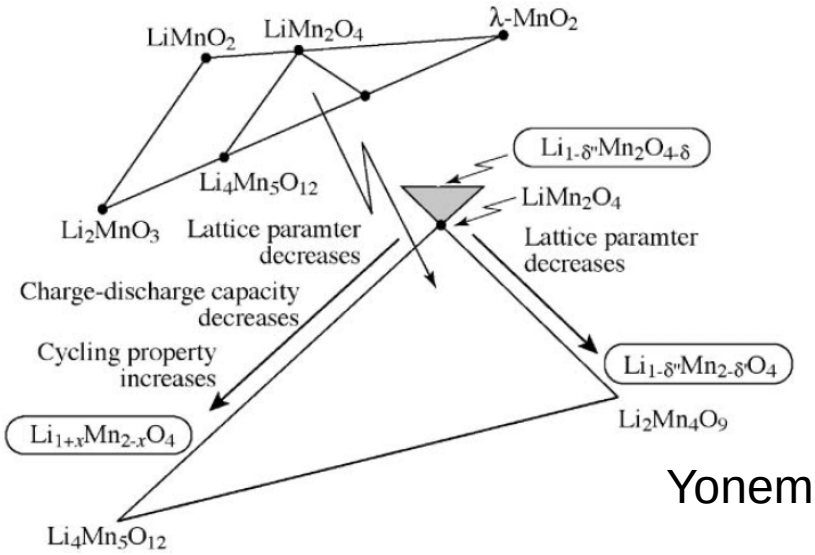

Yonemura et al. 2004

Li-Mn-O System

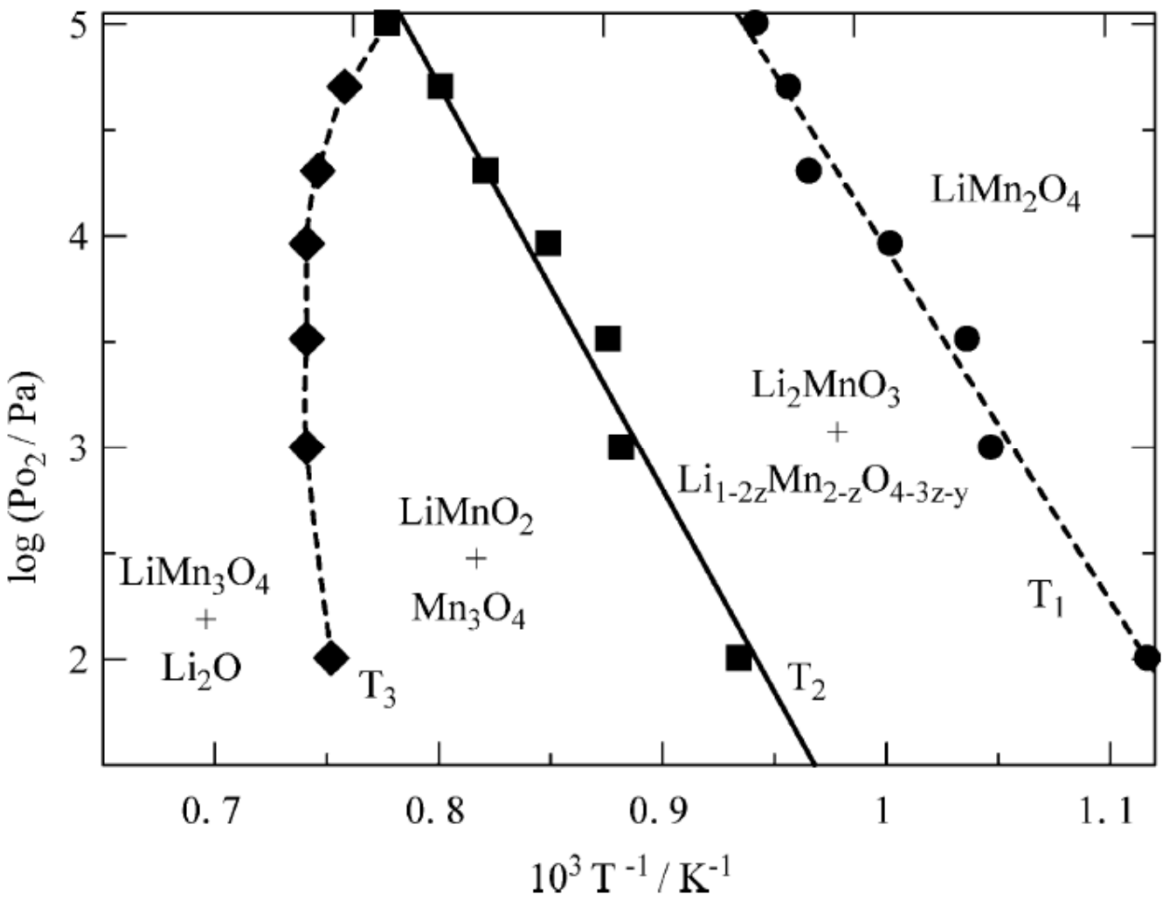

Chemical potential diagram in the Li-Mn-O system (Tsuji et al. 2005).

What to do next: (1) Evaluation; (2) Solution phase modeling; (3) Thermodynamic optimization

Li-Mn-O System

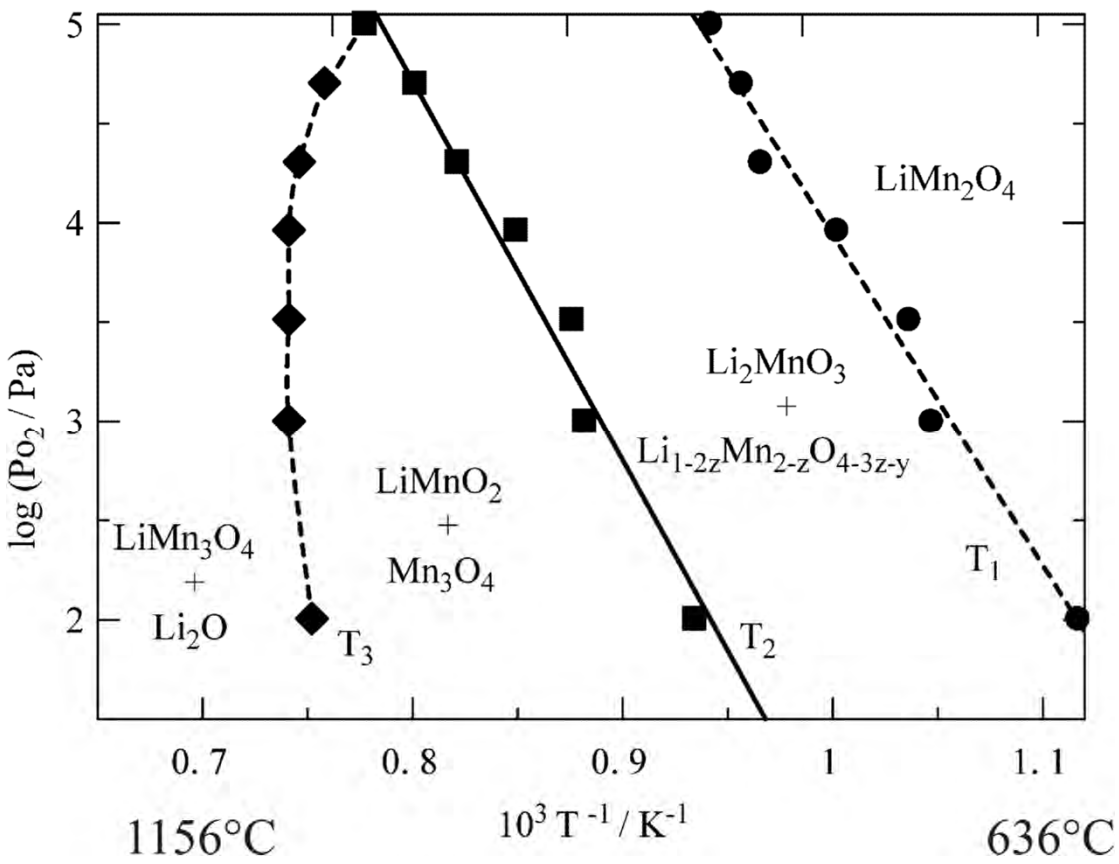

[2005Tsu] Tsuji et al., *J. Chem. Phys. Solids*, 66, 283-287, 2005

Li-Mn-O System

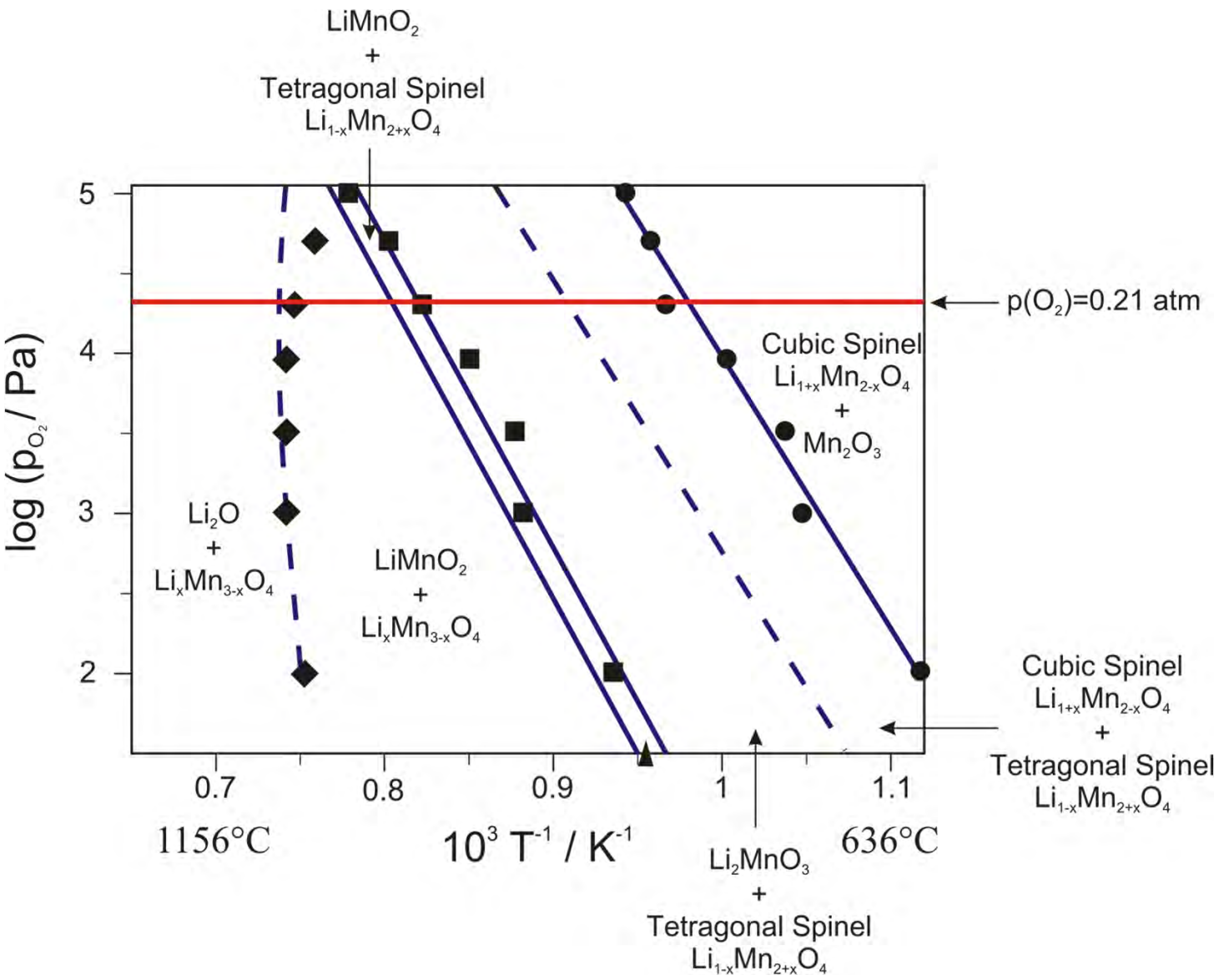

Li-Mn-O System

- $LiMn_2O_4$ composition is a vertical line in the temperature-composition ratio diagram
- $p(O_2)$=0.21 atm is a horizontal line in the potential diagram

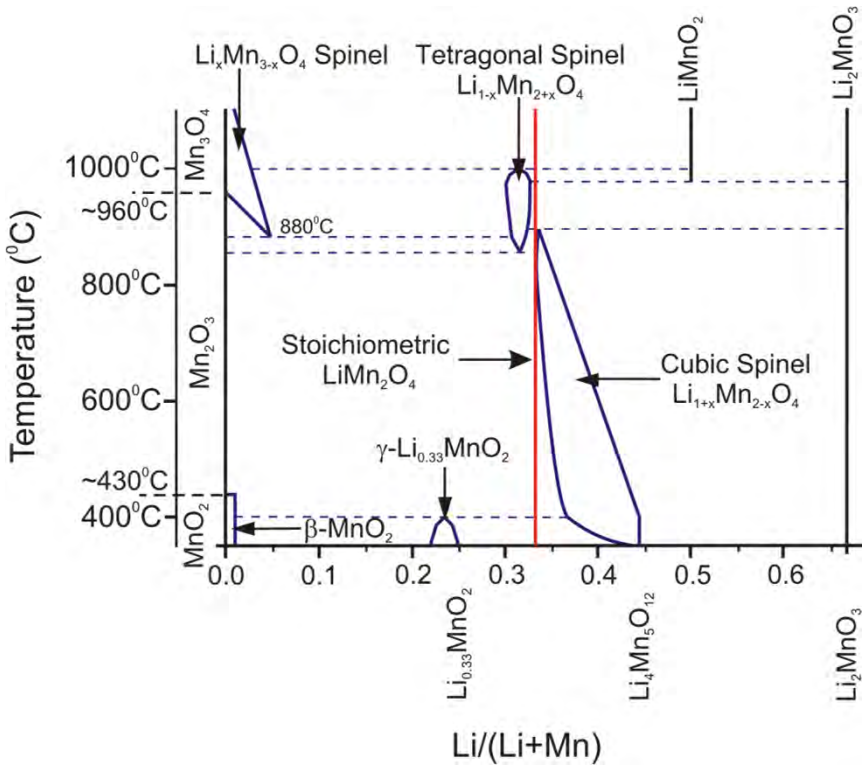

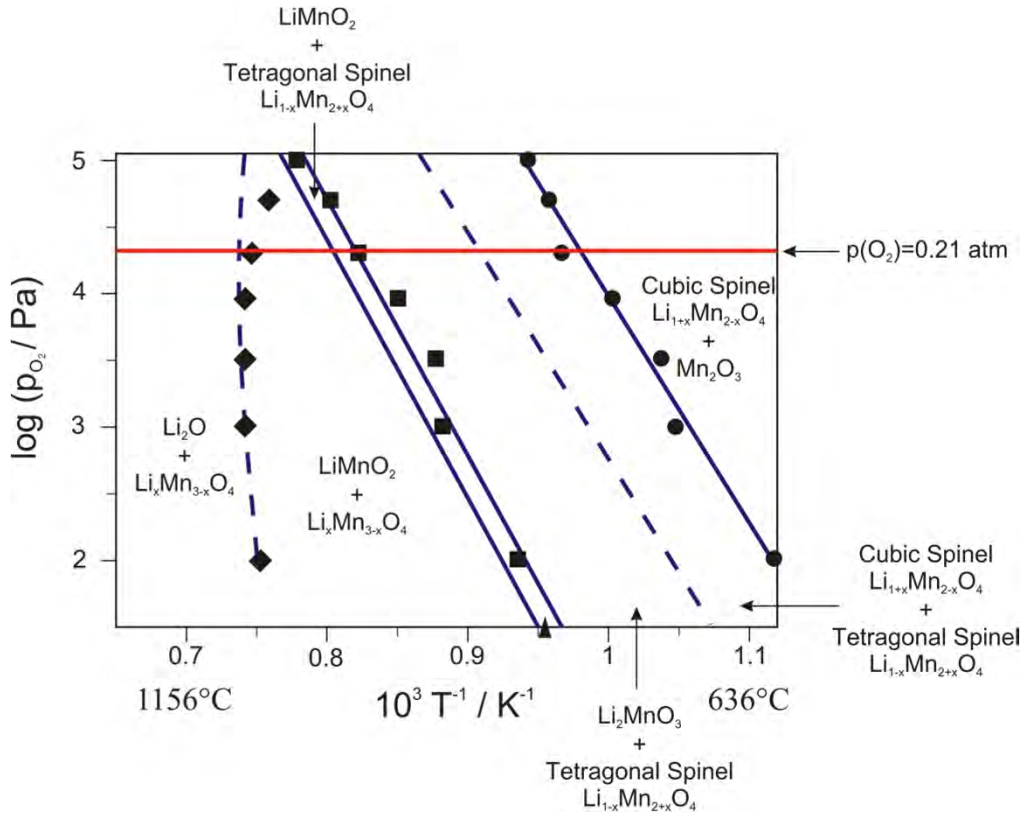

Li-Mn-O System

$p(O_2)$=0.21 atm

Li/Mn ratio for $LiMn_2O_4$

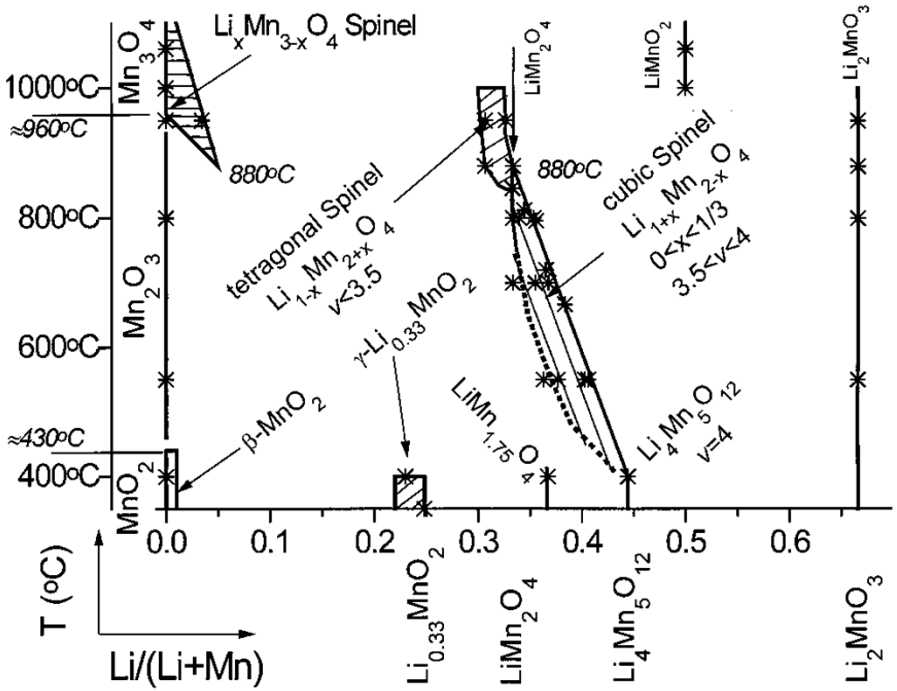

$$LiMn_2O_4 \leftrightarrow zLi_2MnO_3 + Li_{1-2z}Mn_{2-z}O_{4-3z-y}(tet) + (y/2)O_2$$

$$Li_{1-2z}Mn_{2-z}O_{4-3z-y}\ (tet) \leftrightarrow LiMnO_2 + (1/3)\ Mn_3O_4 + \{(1/3)-(y/2)\}O_2$$

[1999 Pau] *Chem. Mater.*, 11 (1999), 3065-3079.
[2005 Tsu] *J. Phys. Chem.*, Solids. 66 (2005), 283-287.

Commercial cathode material $LiMn_2O_4$

Spinel structure

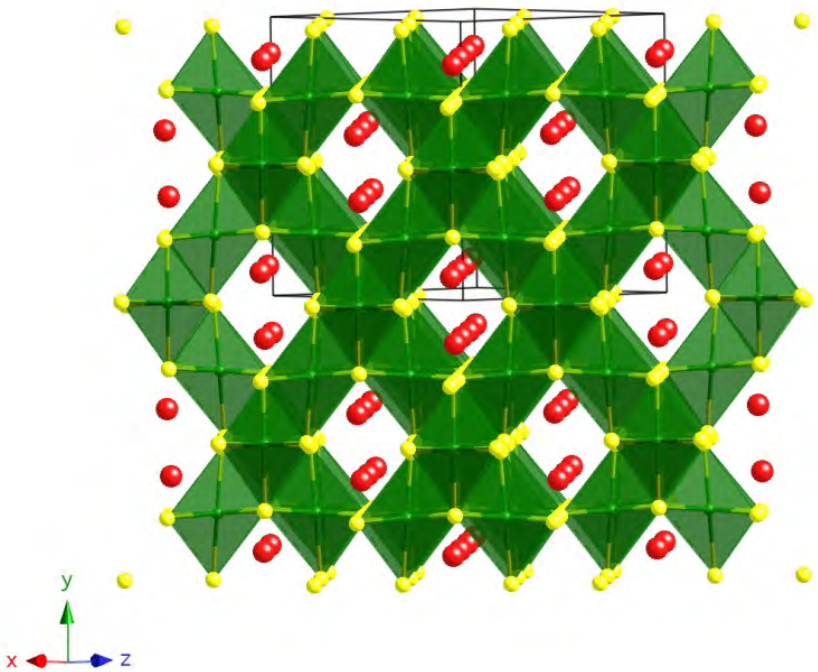

$LiMn_2O_4$: ≈ 100 mAh/g

Gravimetrical energy density (capacity)

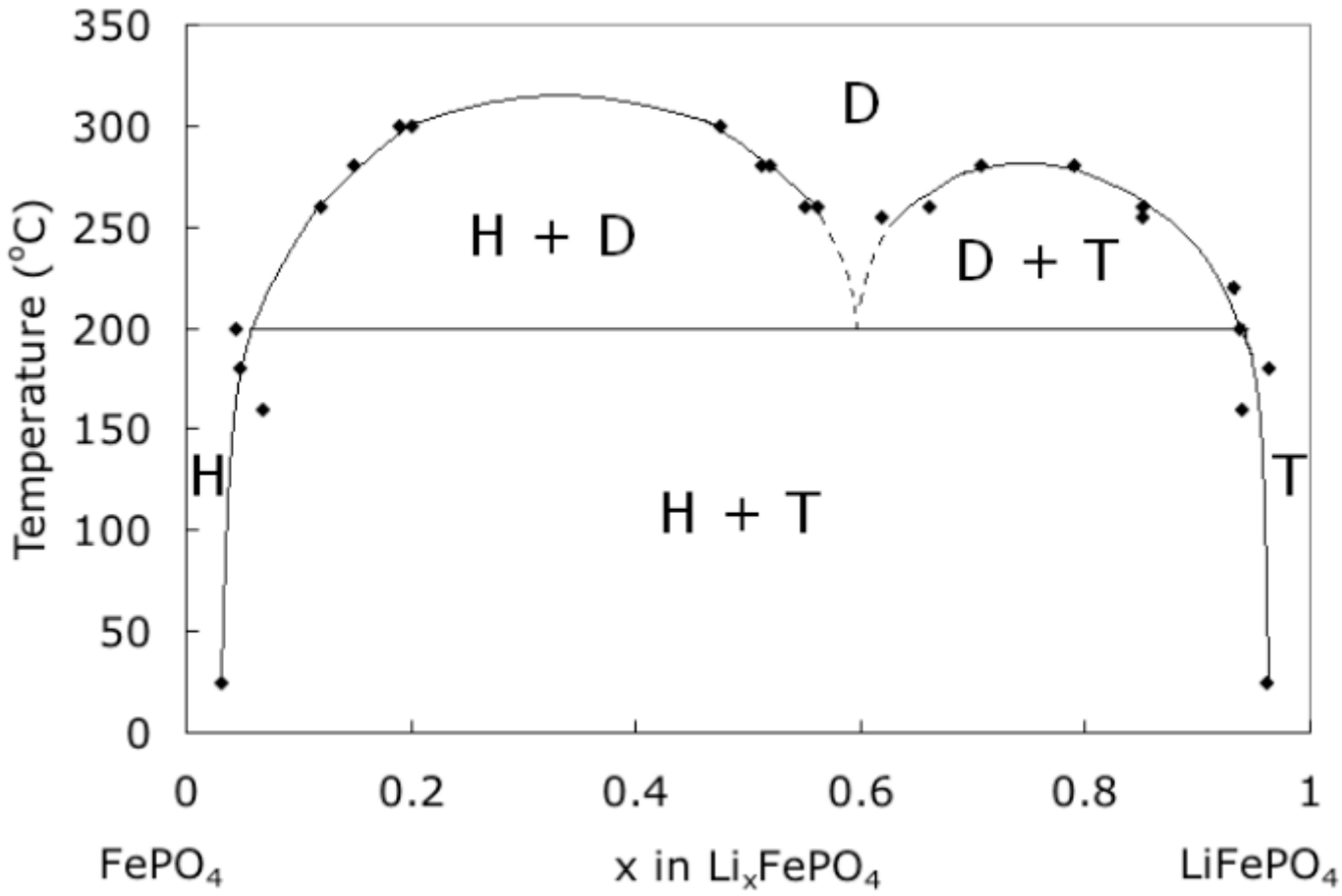

Figure 6. Phase diagram of $LiFePO_4$ (T, for triphylite) and $FePO_4$ (H, for heterosite) phases showing their merging to a solid solution (D, for disordered) in a eutectoid system. Data points at 25 °C are based on published work by Yamada [10]. The eutectoid point is around the composition x = 0.6 and temperature 200 °C. Above 200 °C, mixtures of heterosite or triphylite and the disordered phase were seen up to around 300 °C. Above 300 °C, the disordered phase dominates.

Dodd et al. (2006)

Li-Fe-P-O System

Lithium Ion Batteries – Operation

Solid Electrolyte Interface

Separator

Graphite

$LiCoO_2$

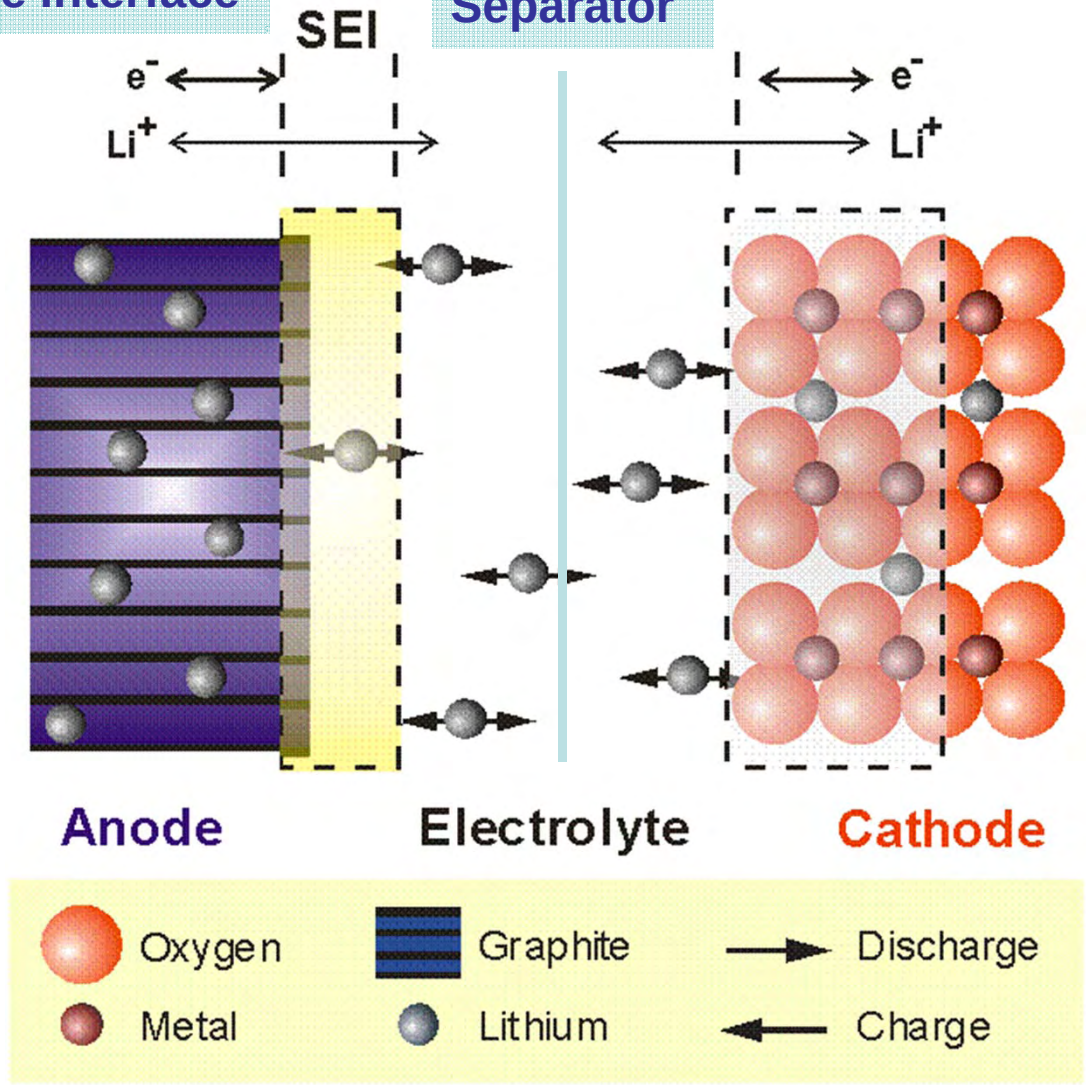

Li-Fe-P-O System

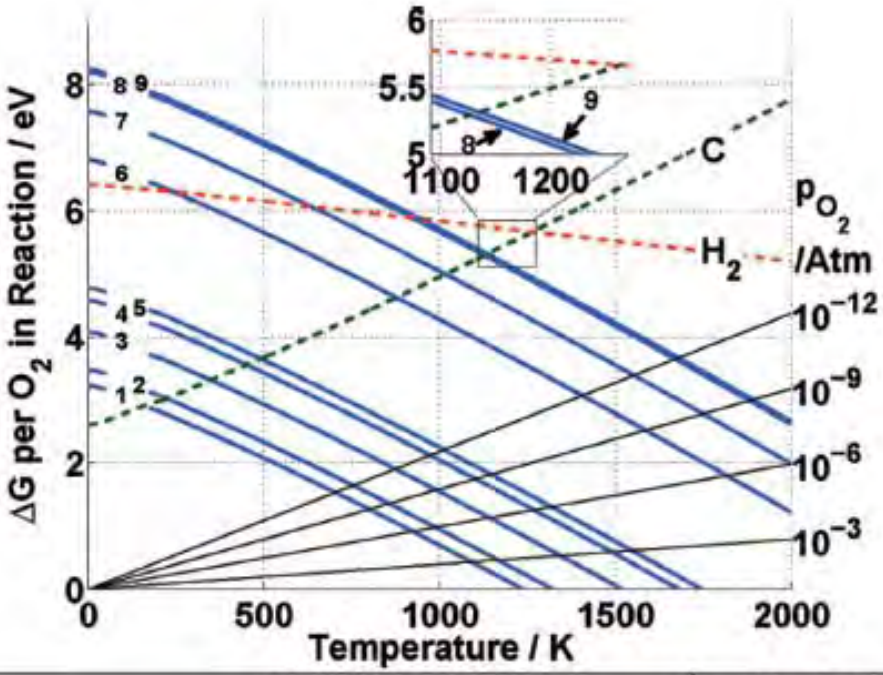

Reaction	Line Label
$3\ Li_3Fe_2(PO_4)_3 \rightleftharpoons 4\ LiFePO_4 + 2\ LiFeP_2O_7 + Li_3PO_4 + O_2$	1
$\frac{3}{2}\ Fe_7(PO_4)_6 \rightleftharpoons Fe_3(P_2O_7)_2 + \frac{5}{2}\ Fe_3(PO_4)_2 + O_2$	2
$2\ Fe_3(P_2O_7)_2 \rightleftharpoons 2\ Fe_2P_2O_7 + Fe_2P_4O_{12} + O_2$	3
$4\ LiFeP_2O_7 \rightleftharpoons 4\ LiPO_3 + 2\ Fe_2P_2O_7 + O_2$	4
$6\ Fe_2O_3 \rightleftharpoons 4\ Fe_3O_4 + O_2$	5
$2\ Fe_3O_4 \rightleftharpoons 6\ FeO + O_2$	6
$\frac{6}{5}\ Fe_2P_2O_7 \rightleftharpoons \frac{4}{5}\ Fe_3(PO_4)_2 + \frac{4}{5}\ P + O_2$	7
$2\ FeO \rightleftharpoons 2\ Fe + O_2$	} 8
$\frac{1}{4}\ Fe_3(PO_4)_2 \rightleftharpoons \frac{1}{28}\ FeP_4 + \frac{5}{14}\ Fe_2P + O_2$	
$\frac{3}{4}\ LiFePO_4 \rightleftharpoons \frac{1}{4}\ Li_3PO_4 + \frac{5}{14}\ Fe_2P + \frac{1}{28}\ FeP_4 + O_2$	9
$2CO \rightleftharpoons 2C + O_2$	C
$2H_2O \rightleftharpoons 2H_2 + O_2$	H_2

Figure 6. Modified Ellingham diagram for reduction reactions in the $Li-Fe-P-O_2$ system.

Ong et al. (2008)

Li-Fe-P-O System

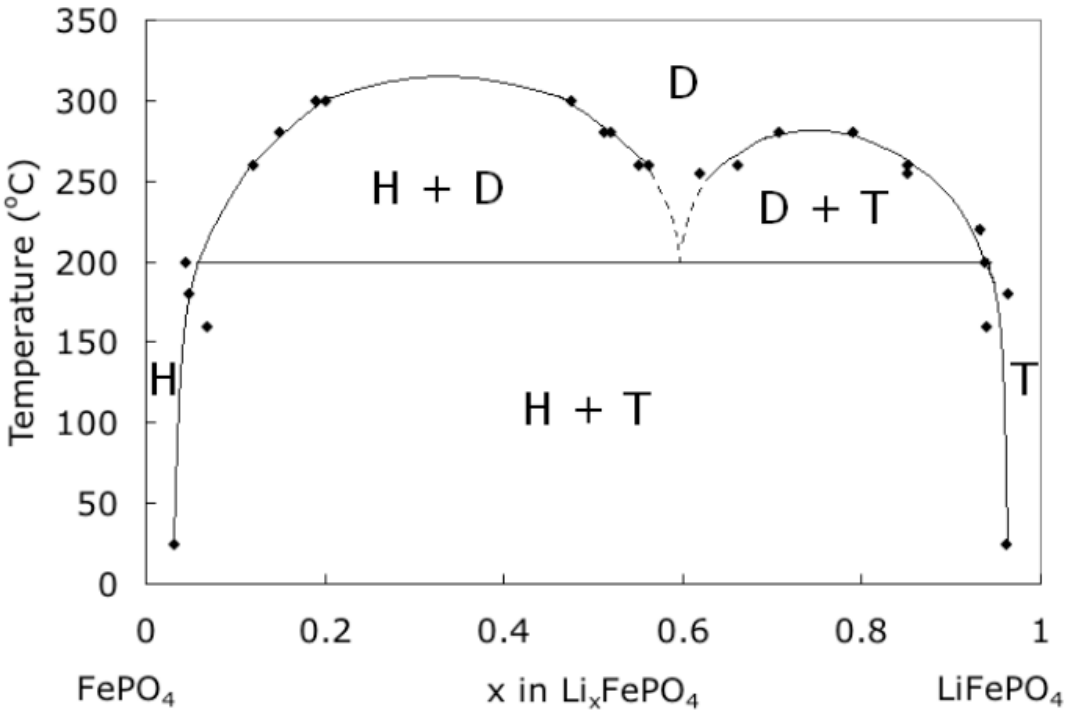

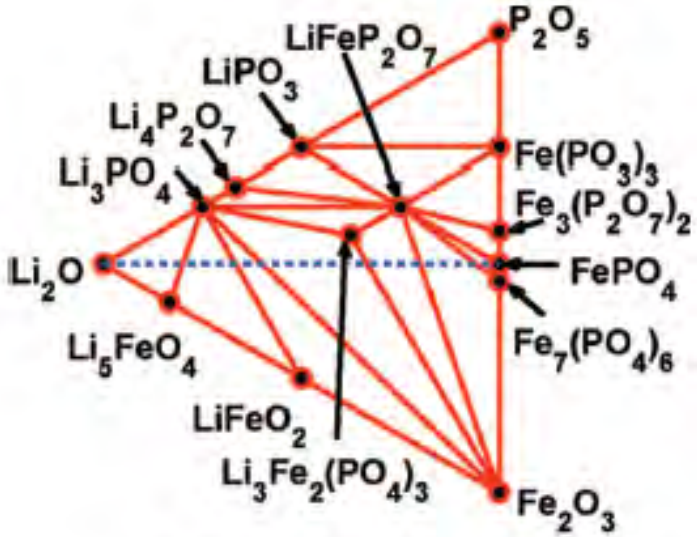

(a) $\mu_{O_2} = -10.50\ eV$, $Fe_7(PO_4)_6$ appears

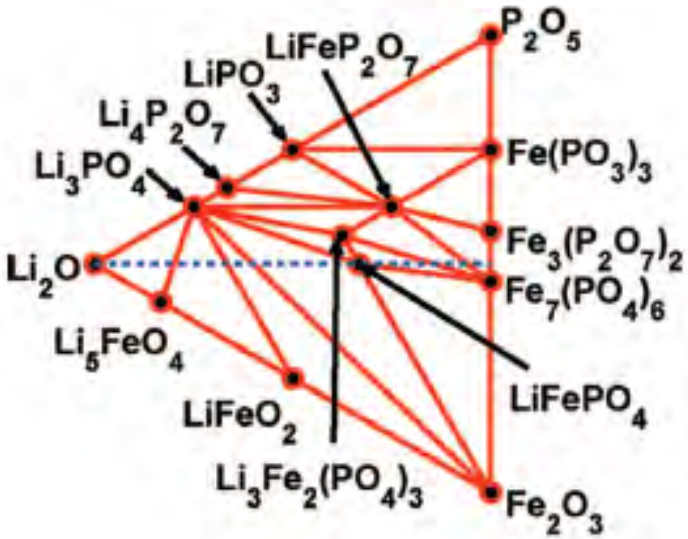

(b) $\mu_{O_2} = -11.52\ eV$, $LiFePO_4$ appears

Figure 2. Phase diagrams at less reducing environments.

Modelling and Simulation

CALPHAD

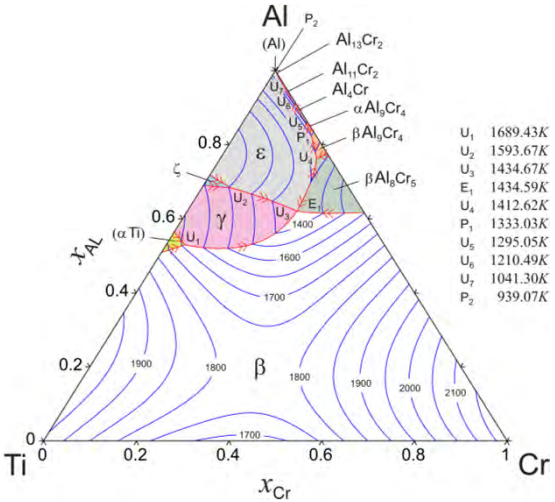

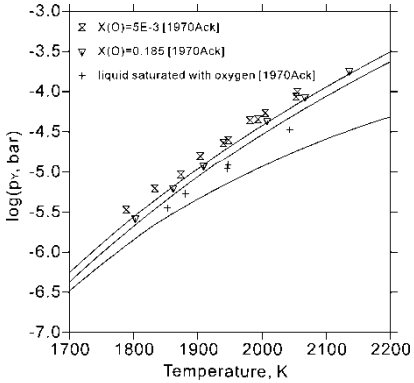

covalent

↓

ionic

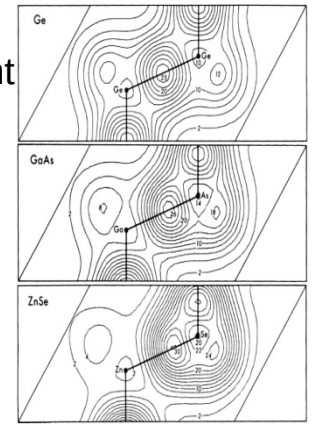

Kratzer et al.,
http://www.fhi-berlin.mpg.de

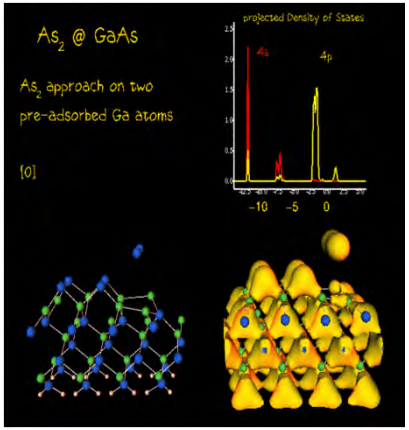

Chelikowsky et al.,
Phys. Rev. B 14, 556 (1976)

Ab-initio

Phase Field

interfaces
(length scale)

+

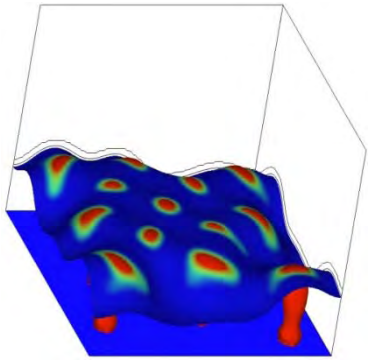

mechanical equilibrium
(energy scale)

+

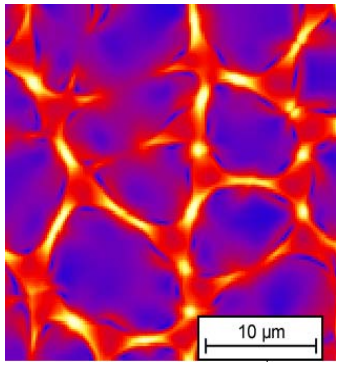

transport / diffusion
(time scale)

+

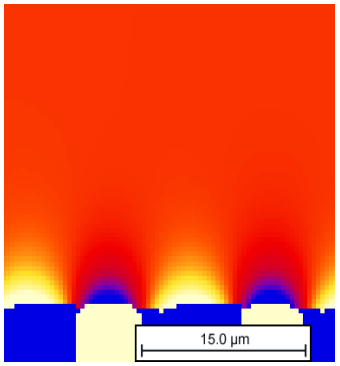

Accidents with lithium ion batteries

Rechargable battery of a laptop
– overheating or internal short circuit

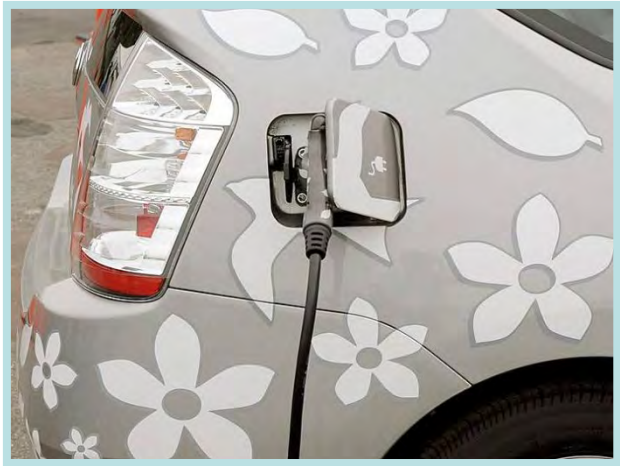

Fire 3 days after crashtest with EV
– mechanical impact

stationary energy storage
– overcharging